1-1-2016

Source Apportionment of Atmospheric Particulate Matter in Developing Countries Using Trace Elements and Stable Metal Isotope Ratios

Nitika Dewan
University of Denver

Source Apportionment of Atmospheric Particulate Matter in Developing Countries Using Trace Elements and Stable Metal Isotope Ratios

Abstract

The work presented herein details the source apportionment of atmospheric particulate matter in developing countries (Kyrgyzstan in Central Asia, metropolitan cities in Northern India, and Shenzhen in China) using trace elements and stable metal isotope ratios. The first study focused on the development of a novel method for the concomitant separation of rare-earth elements in environmental samples of any geological origin. The separation procedure is based on three extraction chromatographic materials, referred to as Sr.Spec, TRU.Spec, and Ln.Spec. This triple column arrangement enables the simultaneous isolation of pure Sr and Nd fractions in less than one day and with great reproducibility. This procedure greatly minimizes the consumption of acids necessary for the separation, allows high yields of Sr and Nd, and realizes very low blank levels.

Using the aforementioned method, the second study focused on if Aral Sea sediments are an important source of particulate matter in Central Asia. Central Asia is dominated by an arid climate and desert-like conditions, leading to the potential for long-range transport of desert dust within and out of the region. One potential source of dust within Central Asia is the Aral Sea, which has receded in size due to water diversion. As a result, newly exposed sediments and associated contaminants are resuspended by the wind and are a potential new source of particulate matter within in the region. Results from this study showed that Central Asia is impacted by yet unidentified regional and distant dust that requires additional measurements of desert sands in and around Central Asia.

The third study focused on the outcome of imposed pollution restrictions in Shenzhen during the 16th Universiade, an international multi-sport event, hosted in 2011. During this time, officials instituted several restrictions in the region in order to enhance the air quality of Shenzhen. The airborne $PM_{2.5}$ was collected during the controlled (when the restrictions were in place) and uncontrolled periods. Results from this study showed a significant increase in the elemental concentrations during the uncontrolled periods. These studies describe the transport of dust and identify some of the geological characteristics of important source areas.

Document Type

Dissertation

Degree Name

Ph.D.

Department

Chemistry and Biochemistry

First Advisor

Brian J. Majestic, Ph.D.

Second Advisor

Bryan J. Cowen

Third Advisor

Alex Huffman

Keywords

Fe speciation, Hybrid single particle Lagrangian integrated trajectory, Ion-exchange chromatography, MC-ICP-MS, Multi-collector inductively coupled plasma mass spectrometry, PCA, Principal component analysis, Strontium isotopes, Lead isotopes

Subject Categories

Atmospheric Sciences | Biochemistry | Chemistry | Geochemistry

Source apportionment of atmospheric particulate matter in developing countries using trace elements and stable metal isotope ratios

_____

A Dissertation

Presented to

the Faculty of Natural Sciences and Mathematics

University of Denver

_____

In Partial Fulfillment

of the Requirements for the Degree

Doctor of Philosophy

_____

by

Nitika Dewan

August 2016

Advisor: Dr. Brian J. Majestic

Author: Nitika Dewan
Title: Source apportionment of atmospheric particulate matter in developing countries using trace elements and stable metal isotope ratios
Advisor: Dr. Brian J. Majestic
Degree Date: August 2016

Abstract

The work presented herein details the source apportionment of atmospheric particulate matter in developing countries (Kyrgyzstan in Central Asia, metropolitan cities in Northern India, and Shenzhen in China) using trace elements and stable metal isotope ratios. The first study focused on the development of a novel method for the concomitant separation of rare-earth elements in environmental samples of any geological origin. The separation procedure is based on three extraction chromatographic materials, referred to as Sr.Spec, TRU.Spec, and Ln.Spec. This triple column arrangement enables the simultaneous isolation of pure Sr and Nd fractions in less than one day and with great reproducibility. This procedure greatly minimizes the consumption of acids necessary for the separation, allows high yields of Sr and Nd, and realizes very low blank levels.

Using the aforementioned method, the second study focused on if Aral Sea sediments are an important source of particulate matter in Central Asia. Central Asia is dominated by an arid climate and desert-like conditions, leading to the potential for long-range transport of desert dust within and out of the region. One potential source of dust within Central Asia is the Aral Sea, which has receded in size due to water diversion. As a result, newly exposed sediments and associated contaminants are resuspended by the wind and are a potential new source of particulate matter within in the region. Results from this study showed that Central Asia is impacted by yet unidentified regional and

distant dust that requires additional measurements of desert sands in and around Central Asia.

The third study focused on the outcome of imposed pollution restrictions in Shenzhen during the 16th Universiade, an international multi-sport event, hosted in 2011. During this time, officials instituted several restrictions in the region in order to enhance the air quality of Shenzhen. The airborne $PM_{2.5}$ was collected during the controlled (when the restrictions were in place) and uncontrolled periods. Results from this study showed a significant increase in the elemental concentrations during the uncontrolled periods. These studies describe the transport of dust and identify some of the geological characteristics of important source areas.

Acknowledgments

I emphatically express my sincere gratitude to my advisor, Dr. Brian J. Majestic for his invaluable guidance, patience, wisdom, and encouragement. The legacy of scientific temperament, which I have inherited, working with him, will remain with me as an everlasting treasure for the rest of my life.

Special thanks to my thesis defense committee: Dr. Bryan Cowen, Dr. Alex J. Huffman, Dr. Martin Margittai, and Dr. Rebecca L. Powell.

I express my heartfelt regards to Dr. Balasingam Murugaverl for his continuing source of encouragement and inspiration.

Thanks to the University of Denver Phillipson Grant for financial support and aid for carrying out this research.

Thanks to Dr. Benton Cartledge, Christine Fukami, Urvija Gupta, John Haynes, Eric Jones, Joe Salazar, Dr. Anju Sharma, and Dr. Vanshi Uniyal for their friendship and well wishes.

Thanks to my father (Mr. Ramesh Dewan), mother (Mrs. Navneeta Dewan), brother (Kartik Dewan), sister-in-law (Sonia Dewan), elder father (Mr. Vijay Dewan), elder mother (Mrs. Suman Dewan), father-in-law (Mr. Rob Mishler), and mother-in- law (Mrs. Marlene Mishler), brother-in-law (Cole Mishler) for their love, blessings, inseparable support and prayers.

Thanks to the love of my life, my husband (Clay Mishler) for his patience, love, and encouragement which has been the driving force in finishing my Ph.D. and keeping me energized in all my endeavors.

Table of contents

List of figures

List of abbreviations and common terms

APHL:	Association of Public Health Laboratories
AQ:	air quality
AQI:	air quality index
ARL:	Air Resources Laboratory
CMPO:	carbamoyl phosphine oxide
CMB:	chemical mass balance
CNG:	compressed natural gas
CPCB:	Central Pollution Control Board
Crown ether:	4,4' (5')-di-t-butyl cyclohexane-18-crown-6
CV:	coefficient of variation
EC:	elemental carbon
EF:	enrichment factor
EPA:	Environmental Protection Agency
ESE:	east-southeast
HDEHP:	di (2-ethyl hexyl) orthophosphoric acid
HYSPLIT:	Hybrid Single Particle Lagrangian Integrated Trajectory
ICP-MS:	inductively coupled plasma mass spectrometry
IIT:	Indian Institute of Technology
ISTC:	International Science and Technology Center
LIDAR:	light detection and ranging
LREE:	light rare-earth elements
MC-ICP-MS:	multi-collector inductively coupled plasma mass spectrometry

MDL: method detection limit

MNIT: Malaviya National Institute of Technology

MQ: high purity water (>18 MΩcm)

NIST: National Institute of Standards and Technology

NIOSH: National Institute for Occupational Safety and Health

OC: organic carbon

PCA: principal component analysis

PMF: positive matrix factorization

PM: particulate matter

$PM_{2.5}$: particulate matter with aerodynamic diameter less than 2.5 μm

PM_{10}: particulate matter with aerodynamic diameter less than 10 μm

PRD: Pearl River Delta

REE: Rare-earth elements

RH: relative humidity

ROS: reactive oxygen species

SF-ICP-MS: sector field inductively coupled plasma mass spectrometry

SRM: standard reference materials

$t_{1/2}$: half-life

TBP: tri-n-butyl phosphate

TIMS: thermal ionization mass spectrometry

TRU.Spec: Trans Uranic-element Specific

UCC: upper continental crust

USGS: United States Geological Survey

VOCs:	volatile organic compounds
WHO:	World Health Organization

Chapter One: Introduction

1.1 Metals in the environment

Metals are an intrinsic component of the environment. Their presence is considered unique in the sense as they are essential to life, but can be lethal [1]. For instance, zinc (Zn) is required for prenatal and postnatal development, but excess of Zn can cause ataxia and lethargy [1]. Therefore, quantification and identification of trace elements in the environment are of increasing importance in the biosphere, lithosphere (earth), hydrosphere (water), and atmosphere (air).

1.2 Sources of metals

Atmospheric particulate matter (PM) is a complex mixture of particles, which includes organic carbon (OC), elemental carbon (EC), inorganic ions, and major and trace elements. The United States Environmental Protection Agency (EPA) regulates PM in two categories based on sizes: (i) $PM_{2.5}$, particles which are less than 2.5 μm in aerodynamic diameter and (ii) PM_{10}, particles which are less than 10 μm in aerodynamic diameter [2].

Metals originate from both natural and anthropogenic sources in the environment. Most environmental contamination and human exposure results from a large list of possible anthropogenic activities such as mining and smelting, industrial emissions,

vehicular exhaust, power plants, waste deposition in landfills, and nuclear weapons [1, 3]. Natural phenomena such as weathering, erosion of surface deposits of minerals, forest fires, sea salt sprays, and volcanic activity have also been reported to contribute to heavy metal atmospheric pollution [3, 4, 5].

1.3 Health effects of metals

The size of the particle and elemental composition are source indicators of emissions in the atmosphere. Previous studies have shown that exposure to $PM_{2.5}$ can lead to asthma and other respiratory illness and mortality [6, 7, 8]. Increased PM_{10} is associated with mortality, exacerbation of airway diseases, decrement in lung function, and formation of reactive oxygen species (ROS) leading to lung cancer [9, 10, 11]. Several studies have found out the involvement of transition redox metals such as iron (Fe), manganese (Mn), and chromium (Cr) from the soluble fraction of PM and particle size is linked with the formation of ROS [12, 13, 14].

Soluble metals are more often associated with the adverse health effects as they are mobile, bioavailable, and toxic [15, 16]. Fe is the most abundant transition metal in the atmosphere [3, 17] and is involved in ROS formation through Fenton chemistry [18, 19]. The redox activity of Fe and its ability to form ROS is related to the amount of Fe in the soluble fraction and the Fe speciation [soluble Fe (II) or Fe (III)] [18, 19, 20]. The Fe speciation is one major motivation of our study and is discussed in Chapter 4. In addition, these metals are proven to be useful tracers and are used extensively to identify the sources of emissions [21, 22, 23].

1.4 Metals in the atmosphere

Atmospheric transport of particles has been recognized as an important factor affecting ecosystems and human populations [1, 24]. Smaller particles have a lower deposition velocity in the air than larger particles. Their residence time in the atmosphere is, therefore, longer, and they may travel thousands of kilometers before deposition [1, 24, 25]. As particles can travel great distances and their effects can be observed downwind [1, 25], it is important to elucidate their source of emission in order to understand their behavior [1, 26]. This so-called "source apportionment" can be attained using several different inputs to source apportionment models like analysis of organic tracer compounds [27, 28], trace elements, stable metal isotope ratios [29], and speciation of water-soluble components [30]. An ideal tracer is detectable, non-degradable, and unique to only one source. However, finding tracers with all of these attributes is very challenging.

1.5 Source apportionment with receptor models

Source apportionment is the practice of identification and quantification of sources responsible for the observed PM in the atmosphere [31]. Source apportionment is important in order to make air quality (AQ) policies, and assessment of the effectiveness of abatement measures. Different approaches are used to determine the sources of air pollution such as (i) explorative methods, (ii) emission inventories, (iii) inverse modelling, (iv) artificial neural networks, (v) Lagrangian models, (vi) Gaussian models, (vii) Eulerian models, and (viii) receptor models [32, 33]. We have employed receptor models as the basis of source apportionment in this dissertation, as discussed in Chapters

3 and 4. Receptor models are based on the principle of mass conservation between the emission source and the study site [32]. In order to find a solution, a large data set consisting of chemical constituents (elemental concentrations) and a number of observations (samples) are required and a factor analysis method such as chemical mass balance (CMB), principal component analysis (PCA), or positive matrix factorization (PMF) can be used to identify and apportion sources of atmospheric pollutants [32] . Recently, stable metal isotope ratios (e.g., strontium (Sr) and lead (Pb)), have shown promise in the apportionment of sources as the metals do not break down, nor do the ratios change during atmospheric transport [34, 35, 36].

1.6 The Pb isotopic system

Pb is a highly toxic and non-essential element does not have any beneficial biochemical role to play. It has been a pollutant of interest for decades as it may be released into the atmosphere from automobiles using leaded gasoline, lead-containing paint, and smelters [1]. There are four naturally occurring stable isotopes of Pb, three of which are radiogenic [35, 36]. ^{206}Pb, ^{207}Pb, and ^{208}Pb are the end products of the decay chains of ^{238}U ($t_{1/2}$ = 4.47 x 10^9 years), ^{235}U ($t_{1/2}$ = 0.407 x 10^{10} years) and ^{232}Th ($t_{1/2}$ = 14.0 x 10^9 years), respectively as shown in Figure 1.1. ^{204}Pb is the only stable non-radiogenic and stable isotope [35, 36]. The average modern natural abundances of ^{204}Pb, ^{206}Pb, ^{207}Pb, and ^{208}Pb are 1.4%, 24.1%, 22.1%, and 52.4%, respectively.

Pb isotope ratios were primarily used as a tool for dating the age of geological materials [37]. However, due to anthropogenic contamination (e.g., Pb-based fuels), this is no longer possible in modern soils. Pb isotope ratio analysis in atmospheric studies has

grown in prominence as Pb isotope ratios are not fractionated during physicochemical processes, weathering or atmospheric transport [35, 36, 38]. Therefore, Pb deposited in the environment has the same isotopic signature as the source in which it was originally formed, and can typically be traced back to its source [35, 36, 39]. The Pb isotopic composition of PM is influenced by local industrial emissions [40], natural sources [41], and long-range transport of pollutants [42]. In this context, the isotopic ratios are useful in distinguishing between natural and anthropogenic sources [35, 36, 43, 44].

The low abundance of ^{204}Pb can result in values affected by relatively poor precision especially for samples with low Pb content and therefore, the ^{204}Pb ratios are often normalized against ^{207}Pb [45]. ^{238}U has a relatively high abundance on earth whereas most of the ^{235}U has already decayed. As a result, the amount of ^{207}Pb has changed very little with time compared with ^{206}Pb, and Pb isotope ratios reported as ^{206}Pb/^{207}Pb can help in the determination of the age of the rocks [45].

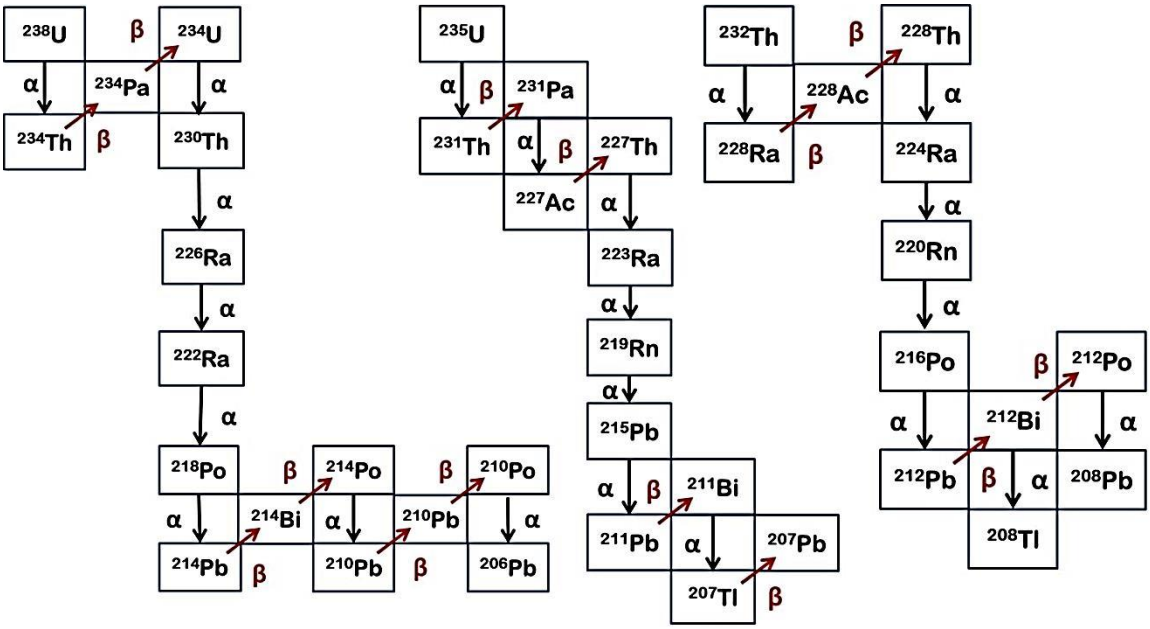

Figure 1.1: Decay chains of ^{238}U, ^{235}U, and ^{232}Th with ^{206}Pb, ^{207}Pb, and ^{208}Pb as stable end products.

1.7 The Sr isotopic system

Sr has four stable isotopes: ^{84}Sr, ^{86}Sr, ^{87}Sr, and ^{88}Sr. Only ^{87}Sr is radiogenic and is the β^- decay product of ^{87}Rb ($t_{1/2}$ = 48.8 x 10^9 years), as shown in equation *(1)*, where ϑ is anti-neutrino and Q is the energy released.

$$^{87}_{37}Rb \rightarrow {}^{87}_{38}Sr + \beta^- + \vartheta + Q \qquad (1)$$

The predominant source of Sr is the earth's crust. Sr is an abundant element in rocks and soils, contributing to 316 ppm of the crust [46]. The relative abundances for ^{88}Sr, ^{87}Sr, ^{86}Sr, and ^{84}Sr are 82.5%, 7.0%, 9.9%, and 0.6%, respectively.

Sr is released from rocks via weathering, cycled through soil and vegetation, and eventually entering the oceans. The mass-dependent fractionation of Sr isotopes is very small compared to the ^{87}Sr/^{86}Sr variability among different Sr sources. As a result, ^{87}Sr/^{86}Sr isotope ratio is associated with minimal fractionation thus, enabling its use for tracing purposes [47, 48, 49]. In this context, Sr isotopic ratio helps to identify geographical sources of dust [50].

1.8 Measurement techniques

The most sensitive and fastest growing method for detecting trace elements is quadrupole inductively coupled plasma mass spectrometry (Q-ICP-MS). Q-ICP-MS is used for rapid, precise, and accurate (<1000 ppm) trace element concentrations, isotope ratios, and speciation studies. The ICP torch generates the plasma which is used as an ion source. There are several advantages of using plasma such as (i) ionization occurs in a chemically inert environment, (ii) prevents oxide formation, and (iii) ionization is more

complete. The detection limit of Q-ICP-MS ranges from <0.1 to >10 ng L^{-1}, depending on an element's ionization energy and the presence of isobaric interferences [1].

The isotope ratios are typically measured either by thermal ionization mass spectrometry (TIMS) or multi-collector inductively coupled mass spectrometry (MC-ICP-MS). TIMS is a magnetic sector mass spectrometer offering the highest precision (~0.001%) and accuracy, however, it is hindered by extensive sample preparation and long measurement time [51]. Q-ICP-MS provides isotope ratios at low cost, however, it is typically at least two orders of magnitude less precise than TIMS (>0.1% *vs*. ~0.001%) because of several reasons: (i) less sensitivity and (ii) single amplifier detector making it less precise than Faraday cups detector used in TIMS [52, 53].

Recent development in MC-ICP-MS offers an alternative to TIMS. The MC-ICP-MS is a hybrid mass spectrometer that possesses advantages of superior ionization of an inductively coupled plasma source and the precise measurements and high resolution of a magnetic sector mass spectrometer. MC-ICP-MS instrumentation offers several advantages (i) simple and robust sample introduction, (ii) high mass resolution, (iii) higher ionization efficiency compared to TIMS, and (iv) use of Faraday cup detectors, allowing simultaneous analysis of multiple isotopes with high precision and accuracy [51, 54]. One of the foremost concerns with multi-collector is that MC-ICP-MS has larger mass fractionation than TIMS by an order of magnitude [52]. This is important to consider in order to produce accurate and precise measurements. Mass fractionation in TIMS is primarily due to evaporation of sample on the metal filament surface which causes lighter isotopes to preferentially evaporate [52, 55]. MC-ICP-MS mass fractionation is not fully understood but may result from a combination of factors,

including sampling of ions in the plasma as well as during the formation of the aerosol (from nebulizer). Instrumental mass fractionation in MC-ICP-MS can be accounted for by employing several methods such as sample-standard bracketing and double or triple spike techniques [56, 57, 58]. In addition, known isotopic standards are repeatedly used as reference materials.

1.9 Summary of subsequent chapters

The focus of this dissertation is using these various plasma techniques to assist in source apportionment of atmospheric PM. *Chapter 2* describes the method development of an ion exchange chromatographic technique as a precursor for precise and accurate determination of Sr and Nd isotope ratios. *Chapter 3* studies the elemental composition and Sr and Pb isotope ratios of PM_{10} collected in Kyrgyzstan. *Chapter 4* considers the results of chemical characterization and Pb isotope ratio measurements of $PM_{2.5}$ collected during 16^{th} Universiade held in Shenzhen, China. *Chapter 5* discusses the preliminary results of an ongoing study of source apportionment in Northern India. *Chapter 6* summarizes the main findings and makes some considerations about future work.

Chapter Two: Development of a chromatographic separation scheme for strontium and neodymium isotopic ratio analysis

2.1 Abstract

A novel method for the concomitant separation of rare-earth elements in environmental samples of any geological origin was developed and successfully tested using quadrupole inductively coupled plasma mass spectrometry. The separation scheme is based on combination and modification of methods published in papers by Christian Pin *et al.* and Jitka Mikova *et al*. The proposed separation procedure is based on three extraction chromatographic materials, referred to as Sr.Spec, TRU.Spec, and Ln.Spec. This triple column arrangement enables the simultaneous isolation of pure Sr and Nd fractions in 8 hours with great accuracy and reproducibility. This procedure greatly minimizes the consumption of acids from 160 mL to 67 mL necessary for the separation, allows high yields of Sr and Nd, and low blank levels. Feasibility of this separation procedure was confirmed by repeated measurements of $^{87}Sr/^{86}Sr$ and $^{143}Nd/^{144}Nd$ isotopic ratios using multi-collector inductively coupled mass spectrometry with three USGS reference rock materials: AGV-2, BCR-2, and BHVO-2.

2.2 Introduction

The ideal tracer is one which is easily detectable, non-degradable, and unique only to one source. However, finding tracers with all of these attributes is very challenging. Stable metal isotope ratios (e.g., strontium (Sr) and neodymium (Nd)), however, are very promising in that they do not break down, nor change during atmospheric transport. As such, these are powerful tools used extensively to determine the origin of geologic materials such as deep rocks and sediment cores [59, 60]. In addition, Sr and Nd stable isotope fingerprinting has been used to help identify the sources of airborne dust [49, 61]. Both rocks and minerals possess unique $^{87}Sr/^{86}Sr$ and $^{143}Nd/^{144}Nd$ ratios [60, 62]. ^{87}Sr is a stable decay product of ^{87}Rb ($t_{1/2}$ = 48.8 billion years) and ^{143}Nd is a stable decay product of ^{147}Sm ($t_{1/2}$ =106 billion years) [36]. The following equations *(1)* and *(2)* show the decay of ^{87}Rb and ^{147}Sm, respectively. The products, ^{87}Sr and ^{143}Nd, are radiogenic and non-radioactive isotopes; therefore, we would expect increased $^{87}Sr/^{86}Sr$ and $^{143}Nd/^{144}Nd$ ratios in older rocks and sediments [36].

$$^{87}_{37}Rb \rightarrow {}^{87}_{38}Sr + \beta^{-} + \vartheta + Q \qquad (1)$$

$$^{147}_{62}Sm \rightarrow {}^{143}_{60}Nd + {}^{4}_{2}He \qquad (2)$$

Isotopic composition and determination of elemental abundance measurements are commonly performed using thermal ionization mass spectrometry (TIMS) and multi-collector inductively coupled plasma mass spectrometry (MC-ICP-MS) [35, 36]. This requires chemical separation prior to mass spectrometric analysis as an impure sample will give a poor ion yield and cause beam instability, thereby resulting in the poor

analysis. In order to avoid isobaric interference of ^{87}Rb with ^{87}Sr, a Sr separation by extraction chromatography using Sr.Spec resin is performed [63].

Ion-exchange resins have proven to be the most effective for isolating the elements of interest from the sample matrix. However, these rarely offer high elemental selectivity [64]. Differences in distribution coefficients lay the basis of the chromatographic separation scheme (the larger the ratio of the coefficients of two different ions, the easier it is to separate them using ion-exchange) [63, 65]. Therefore, depending on the sample size, relatively large ion-exchange columns and elution volumes are required [63, 65].

A new generation of extraction chromatographic resin materials has been developed at the Argonne National Laboratory (U.S.A.) [66]. These resins were originally designed for separation of radioactive nuclides from nuclear waste solutions [67], but their high capacity and specificity make them appealing for environmental [66] and geological samples. These resins have solved difficulties of large amounts of reagents and long time required for separation of some of the elements. Here we present a chromatographic separation scheme for Sr and Nd isotopic analysis of environmental samples which is based on combination and modification of methods published in papers by Pin *et al.* and Mikova *et al.* [63, 65, 68].

2.3 Experimental

2.3.1 Reagents

All reagents (HNO_3, HCl, and HF) used were Optima grade (Fisher, U.S.A.). Optima grade nitric acid (Fisher, U.S.A.) was used for separation. The three chromatographic resins used in the procedure are Sr.Spec, TRU.Spec (TRansUranic-element Specific), and Ln.Spec (Eichrom, U.S.A.). The mesh size of both Sr.Spec and Ln.Spec resins are 50-100 μm whereas the mesh size of the TRU.Spec resin is 100-150 μm. Sr.Spec and TRU.Spec resin slurries were freshly prepared with 0.2 g of resin in 2 mL of 0.05 M HNO_3 and Ln.Spec resin slurry was freshly prepared with 0.2 g of resin in 2 mL 0.25 M HNO_3.

2.3.2 Columns

Modified 5 mL plastic Pasteur pipettes were used as columns. The tops of the pipette bulbs were cut off and to keep the resin in place, the bottom tip of the columns was closed by inserting glass wool. The Sr.Spec and TRU.Spec columns were made using 3 mL of the respective resins. The Ln.Spec columns were made using 4 mL of the resin. The Sr.Spec and TRU.Spec resins were discarded after each sample run but Ln.Spec resin was stored in 0.2 M HCl for future purification.

2.4 Procedure

2.4.1 Sample preparation

For method development, a stock solution was prepared in 2 M HNO_3 with desired absolute masses of the elements: Nd = 5 ng, Sm = 2 ng, Rb = 8 ng, and Sr = 20 ng based on method detection limit (MDL) of the respective isotope ratios [69, 70]. The US Geological Survey (USGS) standard reference materials (SRMs) AGV-2, BCR-2, and BHVO-2 were weighed up to approximately 200 and 300 mg and were digested in a 36-position microwave rotor (Milestone Ethos) with an acid matrix consisting of 0.75 mL nitric (16 M), 0.25 mL hydrochloric (12 M), 0.1 mL hydrofluoric (28 M) acids. These microwave digests were diluted to 15 mL with high purity water. The concentration of the procedural blank was 2 M optima grade HNO_3.

2.4.2 Separation of Sr and light rare-earth elements (LREEs)

Column preparation and conditioning: For Sr isotope analysis, the stock solution and SRM digests were evaporated and diluted to 1 mL using 2 M optima grade HNO_3. Figure 2.1 shows Sr and Nd chromatographic separation scheme. The Rb and Sr content of the digests ranged from 4-7 ng of Rb and 34-76 ng of Sr. The active component in the Sr.Spec resin is 4,4'(5')-di-t-butylcyclohexano 18-crown-6 (crown ether) in 1-octanol. The uptake of Sr by Sr.Spec resin increases with increasing HNO_3 concentration [67]. The active component of TRU.Spec resin is octylphenyl-N,N-di-isobutyl carbamoylphosphine oxide (CMPO) dissolved in tri-n-butyl phosphate (TBP), which complexes actinide elements and extracts them out of the aqueous solutions [66].

Sr was separated from other elements (particularly Rb) in the samples using Sr.Spec resin. The Sr.Spec and TRU.Spec resin slurries were prepared in 0.05 M HNO_3 and loaded into the modified 5 mL plastic Pasteur pipettes fitted with glass wool. The two columns were cleaned by passing through the column 15 mL of MQ water in three consecutive 5 mL portions, 2 mL of 0.05 M HNO_3, 5 mL of MQ water, and then conditioned by adding 2 mL of 2 M HNO_3 in four 0.5 mL portions.

Sample loading: The Sr.Spec column was physically placed above the TRU.Spec column so that the eluent from the Sr Spec can drain directly into the TRU. Following conditioning, the sample was loaded into the upper (Sr.Spec) column in two 0.5 mL aliquots. Sr was retained, in the Sr.Spec resin, while LREE were collected in the lower column filled with the TRU resin. Both columns were then rinsed with 1 mL of 2 M HNO_3 to remove the matrix elements. Following this step, the two columns were separated and used individually.

Sr elution: The sample loaded Sr.Spec column was washed with 1 mL of 2 M HNO_3, then 4 mL of 7 M HNO_3 in eight 0.5 mL portions, and 1 mL of 3 M HNO_3 to remove Ba and alkali and alkaline earth metals from the matrix, while Sr was retained. Sr was eluted from the column by passing 3 mL of 0.05 M HNO_3 in six 0.5 mL portions.

LREE elution: The TRU.Spec column containing sample was washed with 4 mL of 2 M HNO_3 in eight 0.5 mL portions and 1 mL of 0.05 M HNO_3 as shown in Figure 2.1.

2.4.3 Separation of individual LREE

Nd suffers isobaric interference from ^{144}Sm, ^{148}Sm, and ^{150}Sm, therefore, prior to MC-ICP-MS, a good chemical separation of Nd from Sm, as well as from other elements, is required to achieve precise and accurate isotope ratio measurements.

Column preparation and conditioning: The Ln.Spec column was conditioned by passing 15 mL of MQ water in three consecutive 5 mL portions and 3 mL of 2 M HNO_3 to remove Y, Hg, and Fe.

Sample loading: The LREEs are stripped with six of 1 mL of 0.05 M HNO_3 onto Ln.Spec resin column to sorb the LREEs. Following this step, the columns were decoupled and Ln.Spec column was prepared for separation and elution of Nd. The extractant used in Ln Resin is di (2-ethylhexyl) orthophosphoric acid (HDEHP).

Nd elution: The Ln.Spec column was washed with 3 mL of 0.20 M HNO_3. The Nd fraction was eluted using 10 mL of 0.25 M HNO_3 in eight 1 mL portions.

2.4.4 Inductively coupled plasma mass spectrometry (ICP-MS)

Separated samples were evaporated to dryness and dissolved in 2% optima grade HNO_3 prior to analysis to ensure the similar matrix conditions to the standards. Concentrations and elution profiles of Rb, Sr, Nd, and Sm were measured on quadrupole ICP-MS (Agilent 7700) with 1 ppb of ^{115}In as an internal standard.

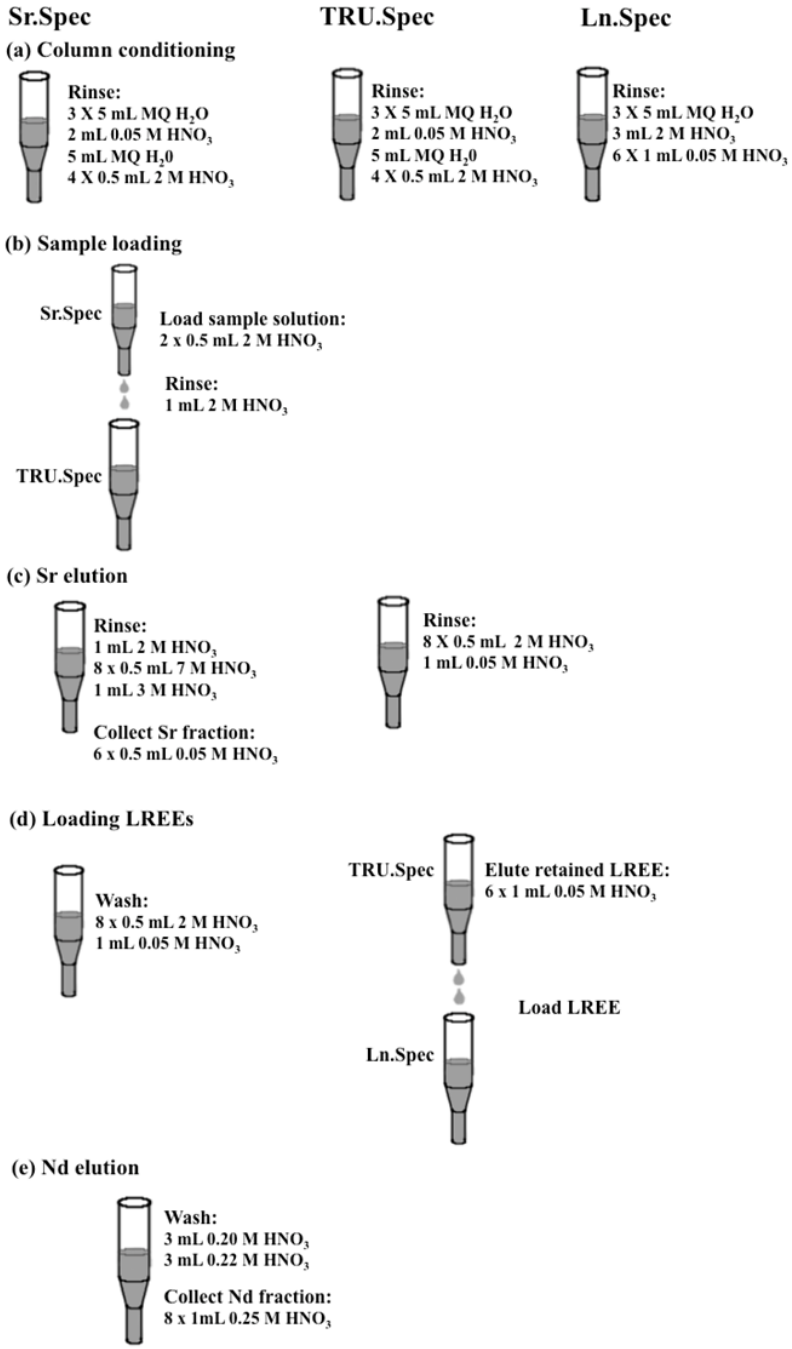

Figure 2.1: Sr and Nd chromatographic separation scheme (a) conditioning of columns, (b) coupling of Sr.Spec and TRU.Spec column and sample loading on Sr.Spec and TRU.Spec column, (c) decoupling of columns and Sr elution, (d) coupling of TRU.Spec and Ln.Spec columns and loading of LREEs from TRU.Spec to Ln.Spec, (e) decoupling of columns and Nd elution.

2.4.5 Method validation

The chromatographic separation scheme was further validated with the SRMs on MC-ICP-MS. The method was done ten times to check its reproducibility and the $^{87}Sr/^{86}Sr$ and $^{143}Nd/^{144}Nd$ isotope ratios were compared with the literature values of the SRMs. The percent recovery of pure Sr and Nd fractions from the column ranges from 90-110%.

2.5 Results and discussion

Procedural blank (contains no analyte but reagents) for Sr separation was 0.06 ng and for Nd separation was 0.03 ng. Three SRMs were analyzed using the method described above. The results are listed in Table 1 and compared with Sr and Nd reference values [71]. Our experiments are in good agreement with the published values (*t*-test, $p < 0.05$). All measured ratios fall within the range of the published values. The results of this study demonstrate that ion-exchange chromatography provides a simple and efficient method of separation of Sr and Nd from a wide variety of metal ions in nitric acid medium.

The separation of Sr from sample constituents such as Rb, Ca, Ba, and Pb is an essential step [66]. Pb, Ca, and Ba are found to be sorbed to crown ether. Both Ba and Ca are readily separated from the Sr by passing 7M and 3M nitric acid, respectively, thereby allowing Sr elution from the column, while Pb remains sorbed [66]. Prior to the separation of individual LREE, TRU.Spec resin is used because of two reasons: (1) it affords the extraction of pure LREE in a single pass and (2) LREEs are stripped using a

small volume (i.e., 3 mL) of dilute acid (0.05 M HNO_3) [68]. Fe is the only element that is sorbed to a significant extent with CMPO-TBP present in TRU.spec resin and therefore, a distinct color change of the resin from white to yellow is observed [68]. The yellow color disappeared with the acid rinses allowing the extraction of Fe^{3+}, while ensuring high distribution coefficients of LREEs. In the Ln.Spec system, the lightest lanthanides elute first and this tandem approach alleviates the need for time consuming step of evaporation and the redissolution of the REEs fraction. The results of separation scheme for a stock solution are shown in Figures 2.2 and 2.3.

Figure 2.2 shows the elution profile of Sr.Spec resin. No Sr was observed in the first fraction. Only ~1% in the second and over 90% Sr was eluted by the end of third fraction. Similarly, Figure 2.3 shows the elution profile of Ln. Spec resin. No Nd was observed in the first fraction and over 85% Nd was eluted in fifth fraction. Sm was not observed in any of the fractions exhibiting excellent selectivity for Nd.

Table 1: Average $^{87}Sr/^{86}Sr$ and $^{143}Nd/^{144}Nd$ isotopic ratios for USGS standard reference materials. Analytes were separated on Sr.Spec, TRU.Spec, and Ln.Spec columns. The uncertainty represents the coefficient of variation (CV) of the multiple measurements. The uncertainty is in the last digits. The previously published values of SRMs are from Raczek et al. 2003 [71].

Reference materials	**Sr ($\mu g\ g^{-1}$)**	**Nd ($\mu g\ g^{-1}$)**	**Measured $^{87}Sr/^{86}Sr$**	**Published $^{87}Sr/^{86}Sr$**	**Measured $^{143}Nd/^{144}Nd$**	**Published $^{143}Nd/^{144}Nd$**
AGV-2	658	30	0.7039 ± 0.0017	0.7039 ± 0.0010	0.5127 ± 0.0010	0.5127 ± 0.0006
BCR-2	364	28	0.7049 ± 0.0015	0.7049 ± 0.0010	0.5126 ± 0.0013	0.5126 ± 0.0007
BHVO-2	389	25	0.7034 ± 0.0019	0.7034 ± 0.0010	0.5129 ± 0.0011	0.5129 ± 0.0008

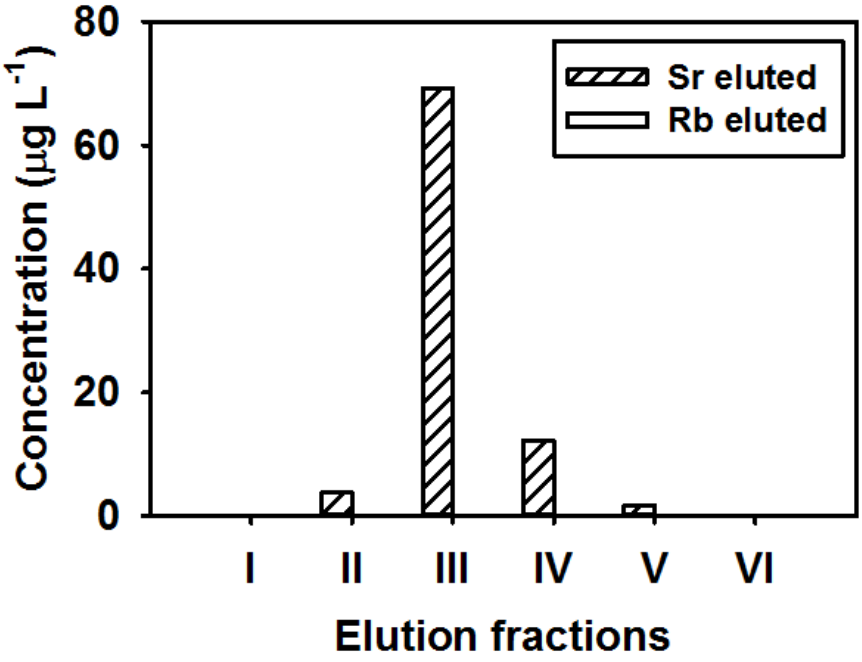

Figure 2.2: Plot showing elution profile of a Sr.Spec column of stock solution.

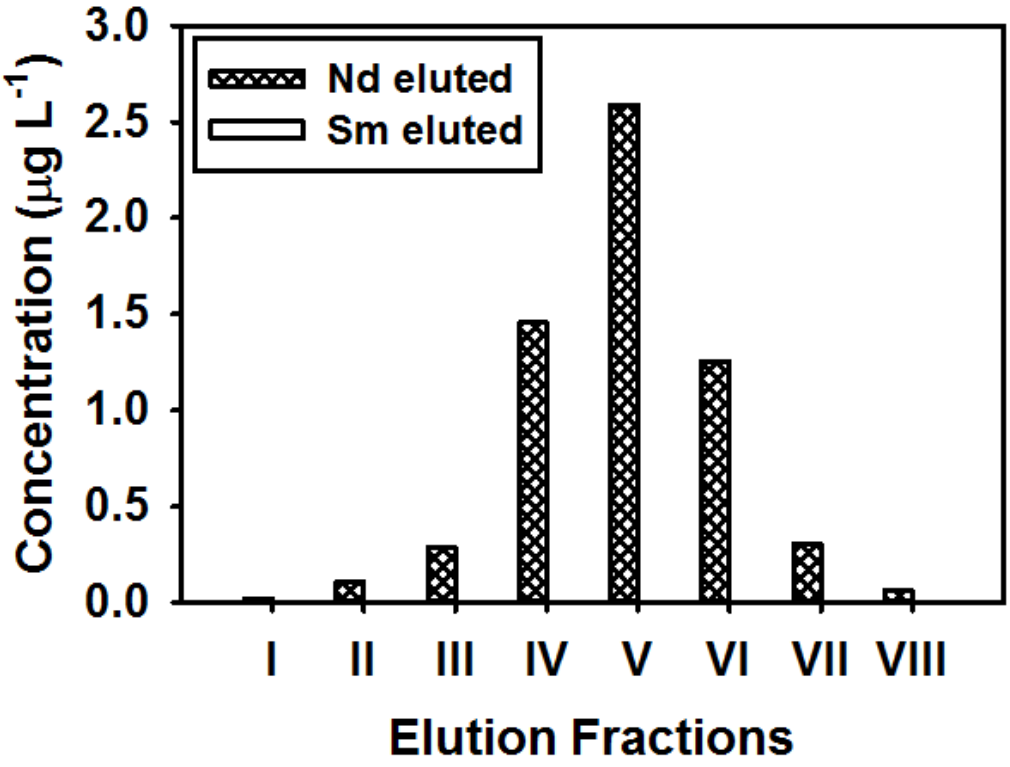

Figure 2.3: Plot showing elution profile of Ln.Spec column of stock solution.

2.6 Conclusions

The present chromatographic separation scheme has been optimized from previously published Sr and Nd separation procedures. This scheme offers a simple and rapid separation of REEs with high yields, good purity of the metal of interest, low blank levels, and better reproducibility by using small amounts of single acid. The quantities of acids required for separation was significantly reduced from 160 mL to 67 mL. The use of small amounts of dilute acids provides an environmental advantage. This method allows the separation in a single run thus, reducing separation times by 50% compared to conventional techniques. This method is suitable to use with any environmental, biological, and geological samples whose preparation requires digestion with nitric acid. The only significant drawback recognized yet is the fact that the resins are prone to memory effects. The Sr separation method was also successfully applied to Kyrgyzstan study presented in Chapter 3.

Chapter Three: Stable isotopes of lead and strontium as tracers of sources of airborne particulate matter in Kyrgyzstan

3.1 Abstract

Central Asia is dominated by an arid climate and desert-like conditions, leading to the potential for long-range transport of desert dust within and out of the region. Of particular interest is the Aral Sea, which has receded in size largely due to water diversion. As a result, newly exposed sediments are resuspended by the wind and thus, may be a potential new source of particulate matter within the region. Here, strontium and lead stable isotope ratios are employed along with detailed elemental composition, to explore the contribution of long-range transport of Aral Sea sediments, as well as other potential sources of dust, within Central Asia. Ambient PM_{10} samples were collected during dust and non-dust events from mid-2008 to mid-2009 at two sites in Kyrgyzstan located ~1,200 and 1,500 km ESE of the Aral Sea. Aral Sea sediments and local Kyrgyzstan soils were resuspended and sized to PM_{10}. The Aral Sea sediments have an average $^{87}Sr/^{86}Sr$ ratio of 0.70992. In contrast, the Sr isotope ratio in local soils exhibits an average ratio of 0.71579. Ambient PM_{10} collected in Kyrgyzstan has an average $^{87}Sr/^{86}Sr$ ratio of 0.71177, falling between the values of these two potential sources and indicating a complex mixture of contributing sources. At both sites, airborne Sr isotope ratios measured during dust events were similar, suggesting that the Aral Sea sediments

only minimally affect air quality in Kyrgyzstan. Elemental analysis and Pb isotope ratios supported this finding. While the Pb isotopes and elemental data both indicate an anthropogenic source, long-range dust transport from other deserts inside and outside the region cannot be ruled out as sources of PM_{10} in Central Asia.

3.2 Introduction

Atmospheric particulate matter (PM) is a complex mixture of particles of varying chemical composition and size both of which depends on their source of emissions, environmental factors (e.g. temperature, relative humidity), and atmospheric processing. Important chemical components include organic carbon, elemental carbon, inorganic ions, and major and trace elements. PM in the atmosphere is a major concern worldwide because of its impact on climate, human health, visibility, biogeochemical cycles, and atmospheric chemistry [2, 72, 73].

PM can travel up to thousands of km from the source location, affecting not only surrounding local areas but regions far downwind [25]. For instance, wind-blown dust from the Gobi Desert and Tarim Basin (Taklamakan Desert) in Western China travels more than 10,000 km, affecting air quality on the western coast of the United States [74]. West to east wind patterns transport Saharan and Arabian dust to Korea and Japan through the mountain ranges of Central Asia [75, 76, 77] and east to west patterns bring Saharan dust to Bermuda [78], the Amazon rain forest [79] and the eastern United States [80].

Dust originating from various sources in Central Asia not only influences the seasonal cycles of PM but also is an important constituent of airborne PM within the region and regions affected by long-range transport. Due to the lack of air pollution observations within Central Asia, the magnitude and impact of this transport on PM levels in the region is highly uncertain. Previous studies have illustrated the long-range transport of PM sources using forward trajectories as well as transport into Central Asia using backward trajectories. The major trajectory of pollution to eastern Asia is from Europe while passing through Central Asia [81]. Air mass transport within and into Central Asia is associated with regional dust sources (e.g. Aral Sea basin and surrounding deserts and Taklamakan desert, respectively) and long-range transport from North Africa, the Middle East, and Southwest Asia [82, 83].

The Aral Sea, formerly one of the largest freshwater lakes in the world, is located in Central Asia and straddles the boundary between Uzbekistan and Kazakhstan (45° 01' 18 N 59° 36' 38 E). The Aral Sea is an endorheic basin, which endures an arid climate characterized by low precipitation (an annual average of 101 mm) and high evapotranspiration. The Aral Sea's surface area has receded in size from 68,000 km^2 to 8,444 km^2 between 1960 and 2014, largely due to water diversion, and may be an increasingly important dust source in Central Asia [84]. In addition to being a relatively new source of dust in the region, the Aral Sea basin is also a trap for wind-blown dust originating from surrounding deserts: Circum-Aral Karakum to the north, Kyzylkum to the east, Karakum to the south and Ustyurt to the west. Subsequently, dust storms originating in the Aral Sea likely contain a mixture of dust from the surrounding deserts,

in addition to the native sediments [85]. The Aral Sea's desiccation has led to various ecological problems like soils salinization, groundwater table reduction, and an increase in frequency and intensity of dust storms [86]. The quantitative contribution of dust from the Aral Sea region to regions to the east remains largely uncharacterized.

Stable metal isotopes (e.g. Sr and Pb) are powerful tools used extensively to determine the origin of geologic materials and solutions in contact with rocks and sediments [59, 60, 62]. More recently Sr and Pb stable isotope fingerprinting have been used to help identify the sources of airborne dust [29, 49, 61, 87]. ^{87}Sr is a stable product of ^{87}Rb radiogenic decay. The $^{87}Sr/^{86}Sr$ ratio increases in older rocks and sediments allowing distinction between older and younger geologic materials [36]. Phase changes, chemical reactions, and biological processes do not fractionate the Sr isotopes [34], and therefore, the Sr isotope ratios measured at a receptor site provide clues to the source of the Sr or a mixing ratio if multiple sources impact the PM in the ambient sample.

Like Sr, Pb stable isotope ratio changes are insignificant during chemical processing and transport of source materials and therefore, the isotope ratios in airborne Pb will only depend on the isotope ratio fingerprint of the source materials. Lead has three naturally occurring radiogenic and stable isotopes; ^{206}Pb, ^{207}Pb, and ^{208}Pb produced from the radioactive decay chain of ^{238}U, ^{235}U, and ^{232}Th respectively.

The only stable non-radiogenic isotope is ^{204}Pb. Lead isotopic ratios can vary considerably depending on their origin [35, 88, 89]. $^{207}Pb/^{206}Pb$ and $^{208}Pb/^{206}Pb$ isotope values are commonly analyzed in environmental samples [35] and are useful in differentiating anthropogenic Pb from natural Pb [90, 91]. Stable Pb isotope ratios

($^{207}Pb/^{206}Pb$) in the range 0.7952– 0.8405 can be used as a tracer species to identify natural sources of PM, such as aeolian dust resulting from weathering, whereas, Pb isotope ratios ($^{207}Pb/^{206}Pb$) in the range of 0.8604–0.9651 can be used to identify anthropogenic sources contributing to PM concentrations in air [92].

In this study, we use stable Sr and Pb isotope ratios and elemental composition to characterize sources of PM_{10} in Central Asia at two sampling sites in Kyrgyzstan, with a focus on the Aral Sea basin as a potential source region. We test the hypothesis that the PM sampled in Kyrgyzstan, ~1200 – 1,500 km ESE of Aral Sea, is influenced by long-range transport of resuspended Aral Sea sediments. The specific goals of the study were to determine (a) if the metal content of PM collected at the sampling sites during dust events differs from non-dust event periods; (b) whether the isotopic composition of the Aral Sea sediments and the soils collected in the vicinity of the air sampling sites are distinguishable from each other and those of soils from Western and Central China; and (c) if long-range transport of resuspended Aral Sea sediments is an important source of PM to Central Asia.

3.3 Experimental

3.3.1 Sample collection

The Kyrgyz Republic (Kyrgyzstan), located in Central Asia, is bordered by Kazakhstan to the north, Tajikistan to the south, China to the east, and Uzbekistan to the west. It is a mountainous country bisected by the Tien-Shan mountain range. PM_{10} was collected at two sites ((Bishkek and light detection and ranging (LIDAR)) from 14th July

2008 to 10th July 2009. Soil samples were also collected in the vicinity of the PM sampling sites along with sediments collected in the dry areas of the Aral Sea basin. The soil and sediment samples were suspended in a sealed chamber, where dried and filtered air was forced through it. The resuspended particles were collected on 47 mm Teflon filters at 16.7 L min^{-1} after passing through PM_{10} cyclone to obtain the PM_{10} size-cut.

Bishkek is the capital and the largest city in Kyrgyzstan with a population of ~854,000. The Bishkek site is 23 km south of the Bishkek city center and ~1200 km ESE of the Aral Sea at an elevation of 1250 m, at 42° 40' 47.80" N, 74° 31' 44.30" E. The LIDAR sampling site is located in Teploklyuchenka, 30 km north-east of Karakol and 380 km east of Bishkek at an elevation of 1920 m, at 42° 27' 49.30" N, 78° 31' 49.30" E. Integrated 24-hour samples were collected on pre-cleaned Teflon filters (Teflo, Pall-Gelman) using URG 3000ABC samplers (URG Corporation, U.S.A). PM_{10} was collected using a PM_{10} inlet followed by a cyclone at 32 L min^{-1} with 8 L min^{-1} passing through each of 4 PM_{10} filters. Using primarily PM mass as a guide, multiple dust and non-dust events dates were selected, along with bi-weekly composites for chemical and isotopic analysis. Additional details of the sample collection can be found in a previous manuscript [93]. The map of the region showing the two sampling sites is shown in Figure 3.1.

Figure 3.1: Map of Central Asia and geographical location of the sampling sites (shown as stars) and surrounding deserts (1-Kyzylkum, 2-Aral Karakum, 3-Karakum, 4-Ustyurt and Mangyshlak, 5-Betpak Dala, 6-Saryesik-Atyrau, 7-Taukum, 8-Qaratal and Lepsy, 9-Moinkum, 10-Aralkum) relative to Aral Sea location.

All sample preparation was performed under positive pressure HEPA filtered air. A microbalance (MX5, Mettler-Toledo, U.S.A.) was used for determination of mass (estimated total uncertainty of < 7% or ± 4 μg). Prior to weighing, the filters were equilibrated in a constant humidity (35 ± 3% RH) and temperature (21 ± 2 °C) dedicated weighing room for 24 hours. Static charge on the filters was removed using a Po-ionization source.

3.3.2 Elemental analysis

The PM_{10} resuspended Aral Sea sediments and Kyrgyzstan soils, and the airborne PM_{10} were solubilized in a 36-position Microwave Rotor (Milestone Ethos) with an acid matrix consisting of 1 mL nitric (16 M), 0.25 mL hydrochloric (12 M), and 0.1 mL hydrofluoric (28 M) acids. The microwave digests were diluted to 15 mL with high purity water (>18 MΩcm, MQ) and elemental (Al, As, Ba, Ca, Cd, Ce, Co, Cr, Cu, Fe, K, La, Mg, Mn, Na, Nd, Ni, P, Pb, Rb, S, Sb, Sc, Sm, Sr, Th, Ti, U, V, and Zn) concentrations were determined using magnetic sector inductively coupled plasma mass spectrometry (SF-ICPMS, Element 2, Thermo-Fisher). Recoveries of all elements from the standard reference materials (SRMs), San Joaquin Soil (NIST 2706) and Urban Dust (NIST 1649a) were between 80-120%. Data were blank-corrected using the average of multiple field filter blanks. The uncertainty associated with each element in every sample was estimated from an error propagation analysis, which included uncertainty components from the triplicate SF-ICPMS analysis, uncertainty in the field blanks, uncertainty in the

air flow rates, and uncertainty in the microwave digestion element recovery. Uncertainty for total Sr and Pb for PM_{10} were in the range of ± 0.2-1.0 ng m^{-3}.

3.3.3 Analysis of Sr and Pb stable isotope composition

For Sr isotope analysis, the digests were evaporated and diluted to 1 mL using 2 M optima grade HNO_3 (Fisher, U.S.A.). The Rb and Sr content of the digests ranged from 4 to 178 ng of Rb and 18 to 682 ng of Sr. Some PM_{10} samples were composited to achieve a total Sr mass of at least 18 ng (the MDL). Sr was separated from the other elements (particularly Rb) in the digest using Sr.Spec resin (Eichrom, U.S.A.). The separation technique is detailed in [63], with some modifications. The Sr.Spec resin slurry was prepared in 0.05 M HNO_3 and loaded into modified 5 mL plastic Pasteur pipettes fitted with glass wool. This column was cleaned by passing through the column 15 mL of MQ water in three consecutive 5 mL portions, 2 mL of 0.05 M HNO_3, 5 mL of MQ water, and then conditioned by adding 2 mL of 2 M HNO_3 in four 0.5 mL portions. Following conditioning, the sample was loaded onto the column in two 0.5 mL aliquots. The loaded column was washed with 1 mL of 2 M HNO_3, then 4 mL of 7 M HNO_3 in eight 0.5 mL portions, and 1 mL of 3 M HNO_3 to remove the matrix, while Sr was retained. Sr was eluted from the column by passing 3 mL of 0.05 M HNO_3 in six 0.5 mL portions. Separated samples were then analyzed by quadrupole ICP-MS (Agilent 7700) to determine total Sr and Rb levels. The Sr recoveries and Rb removal efficiencies for all sample types were between 90 - 115% and 90 – 99.7%, respectively. The chemical separation was validated by analyzing certified reference materials (NBS 987 and NIST

981). $^{87}Sr/^{86}Sr$ ratios of the Aral Sea sediments were measured by a Nu Plasma II multi-collector (MC)-ICP-MS and PM_{10} and Kyrgyzstan soils by a Thermo-Finnigan Neptune MC-ICP-MS. Pb stable isotope ratios in all samples were determined by MC-ICP-MS (Thermo-Finnigan Neptune Plus). The uncertainty for $^{87}Sr/^{86}Sr$ and Pb isotope ratios are in the range of ± 0.0002 and ± 0.0125, respectively. Analysis of the NBS 987 yielded $^{87}Sr/^{86}Sr = 0.71030 \pm 0.00001$ (n = 17) by Neptune and $^{87}Sr/^{86}Sr = 0.71023 \pm 0.00003$ (n = 17) by Nu Plasma vs. the certified value of 0.71024 ± 0.00007. Analysis of the NIST 981 yielded $^{208}Pb/^{206}Pb = 2.1656 \pm 0.0014$ (n = 16) and $^{207}Pb/^{206}Pb = 0.9144 \pm 0.0001$ (n = 16) *vs.* the certified values of 2.1681 ± 0.0008 and 0.9146 ± 0.0003, respectively.

3.4 Results and discussion

3.4.1 Site-dependent elemental compositions

A summary of the major and trace elemental concentrations quantified in the resuspended Kyrgyzstan soils and Aral sediments, and PM_{10} collected at the Bishkek and LIDAR sites during dust and non-dust events, is presented in Table 2. The concentrations (μg g^{-1}) of major elements in the LIDAR and Bishkek soils were similar: LIDAR; Al (~67000 ± 6000), Fe (~50000 ± 3500), and Ca (~29000 ± 2500); Bishkek; Al (~63000 ± 6000), Fe (~40000 ± 3000), and Ca (~22000 ± 2500). In contrast, Ca (~50000 ± 3500) was the dominant element in the Aral Sea sediments, followed by Fe (~20000 ± 1500), and Al (~23000 ± 1500). An approximate two-fold difference was observed in the concentrations of Ca, Cr, Fe, Nd, Ni, and Ti and a three-fold difference for Al, Sc, and Sr for Aral Sea sediments compared to Kyrgyzstan soils, (Table 2).

Table 2: Mean elemental concentrations (μg g^{-1}) of resuspended local Kyrgyzstan soils, Aral Sea sediments, and of airborne PM_{10} (ng m^{-3}) at the Bishkek and LIDAR sites.

Element	Bishkek soils (n =4) (μg g^{-1})	LIDAR soils (n = 4) (μg g^{-1})	Aral Sea sediments (n = 5) (μg g^{-1})	Bishkek dust events PM_{10} (n = 8) (ng m^{-3})	Bishkek non-dust events PM_{10} (n = 21) (ng m^{-3})	LIDAR dust events PM_{10} (n = 7) (ng m^{-3})	LIDAR non-dust events PM_{10} (n =18) (ng m^{-3})
Al	63000 ± 6000	67000 ± 6000	23000 ± 1500	440 ± 40	200 ± 20	750 ± 60	180 ± 20
K	19000 ± 6000	21000 ± 7000	16000 ± 3000	400 ± 50	150 ± 20	560 ± 80	250 ± 50
Ca	22000 ± 2000	29000 ± 2500	50000 ± 3500	900 ± 90	300 ± 30	990 ± 85	250 ± 30
Mg	10000 ± 1000	15000 ± 1100	6000 ± 500	160 ± 10	60 ± 5	330 ± 25	60 ± 5
Na	12000 ± 1100	16000 ± 1500	9500 ± 750	170 ± 17	70 ± 7	300 ± 20	70 ± 7
Cr	90 ± 6	100 ± 6	250 ± 40	1.0 ± 0.5	0.70 ± 0.09	1.0 ± 0.2	1.0 ± 0.1
P	600 ± 50	1100 ± 60	500 ± 30	25 ± 2	10 ± 1	15 ± 1	10 ± 1
Mn	800 ± 60	960 ± 60	650 ± 30	15 ± 1	6.4 ± 0.5	10 ± 1	5.0 ± 0.3
S	370 ± 30	480 ± 40	11000 ± 1000	530 ± 50	300 ± 30	350 ± 35	280 ± 30
Fe	40000 ± 3000	50000 ± 3500	20000 ± 1500	470 ± 35	200 ± 10	700 ± 30	200 ± 15
Ni	42 ± 3	43 ± 4	60 ± 6	1.0 ± 0.2	0.5 ± 0.1	1.0 ± 0.1	0.50 ± 0.20
V	120 ± 7	130 ± 8	100 ± 5	2.0 ± 0.2	1.0 ± 0.1	2.0 ± 0.1	1.0 ± 0.1
Sc	12 ± 1	14 ± 1	4.5 ± 0.3	0.080 ±0.008	0.037 ± 0.004	0.13 ± 0.01	0.037± 0.004
Zn	56 ± 6	60 ± 7	73 ± 9	8 ± 1	6.2 ± 0.7	5 ± 1	4 ± 1
Co	16 ± 1	17 ± 1	11 ± 1	0.30 ± 0.01	0.11 ± 0.01	0.37 ± 0.02	0.120 ±0.009
Cu	32 ± 2	34 ± 2	21 ± 1	1.5 ± 0.3	1.11 ± 0.13	1.8 ± 0.2	2.2 ± 0.1
Ti	4600 ± 360	5300 ± 400	1800 ± 120	55 ± 5	20 ± 2	80 ± 6	25 ± 2
As	11 ± 3	9 ± 2	15 ± 3	1.4 ± 0.1	0.40 ± 0.08	1.2 ± 0.1	0.37 ± 0.07
Rb	60 ± 5	81 ± 6	46 ± 5	0.6 ± 0.1	0.50 ± 0.04	2.0 ± 0.2	0.540 ±0.036
Sr	160 ± 15	250 ± 20	630 ± 50	8 ± 1	2.0 ± 0.2	5 ± 1	3.0 ± 0.2
Mo	1.0 ± 0.1	2.0 ± 0.2	8 ± 1	0.088±0.009	0.050 ± 0.006	0.080 ± 0.009	0.072 ±0.008
Sb	1.5 ± 0.1	1.2 ± 0.1	25 ± 2	0.5 ± 0.3	0.20 ± 0.01	0.23 ± 0.02	0.20 ± 0.01
Ba	500 ± 40	530 ± 40	400 ± 20	7 ± 1	3.0 ± 0.2	11 ± 1	3.4 ± 0.3
La	20 ± 1	30 ± 2	15 ± 1	0.30 ± 0.02	0.10 ± 0.01	0.50 ± 0.03	0.10 ± 0.01
Ce	40 ± 3	61 ± 4	28 ± 3	0.66 ± 0.03	0.20 ± 0.02	0.60 ± 0.04	0.30 ± 0.02
Nd	21 ± 1	28 ± 2	11 ± 1	0.15 ± 0.01	0.10 ± 0.01	0.25 ± 0.02	0.10 ± 0.01
Pb	24 ± 2	25 ± 2	18 ± 2	7 ± 1	4 ± 1	5.0 ± 0.4	3.0 ± 0.2
Sm	5 ± 1	6 ± 1	2.0 ± 0.3	0.045± 0.003	0.020 ± 0.002	0.060 ± 0.004	0.018 ±0.001
Th	8 ± 1	9 ± 2	5.0 ± 0.7	0.07 ± 0.01	0.050 ± 0.002	0.10 ± 0.02	0.040 ±0.006
U	4.0± 0.3	9 ± 1	3.0 ± 0.3	0.05 ± 0.01	0.040 ± 0.003	0.060 ± 0.005	0.030 ±0.003
K/Pb	775	86	842	57	46	112	76

Most elements measured in PM_{10}; in particular, Al, Ca, Fe, K, Mg, Na, P, S, and Ti had significantly higher concentrations during dust events at both sampling sites as shown in Figure 3.2 (a-d). At the Bishkek site, Ca and Al concentrations (in ng m^{-3}) were ~900 and ~440, respectively, during dust events and ~300 and ~200 during non-dust events. Similarly, at the LIDAR site, Ca and Al concentrations (in ng m^{-3}) were ~650 and ~500 respectively, during dust events and ~250 and ~180 during non-dust events. The elemental concentrations for PM_{10} at both sites showed that the dominant elements were Ca, Fe and Al. Also, toxic elements (As, Ba, Co, Cr, Ni, Pb, V, and Zn) and rare-earth elements (REEs) (Ce and La) were measured in PM_{10} and had higher concentrations during dust events at both sites.

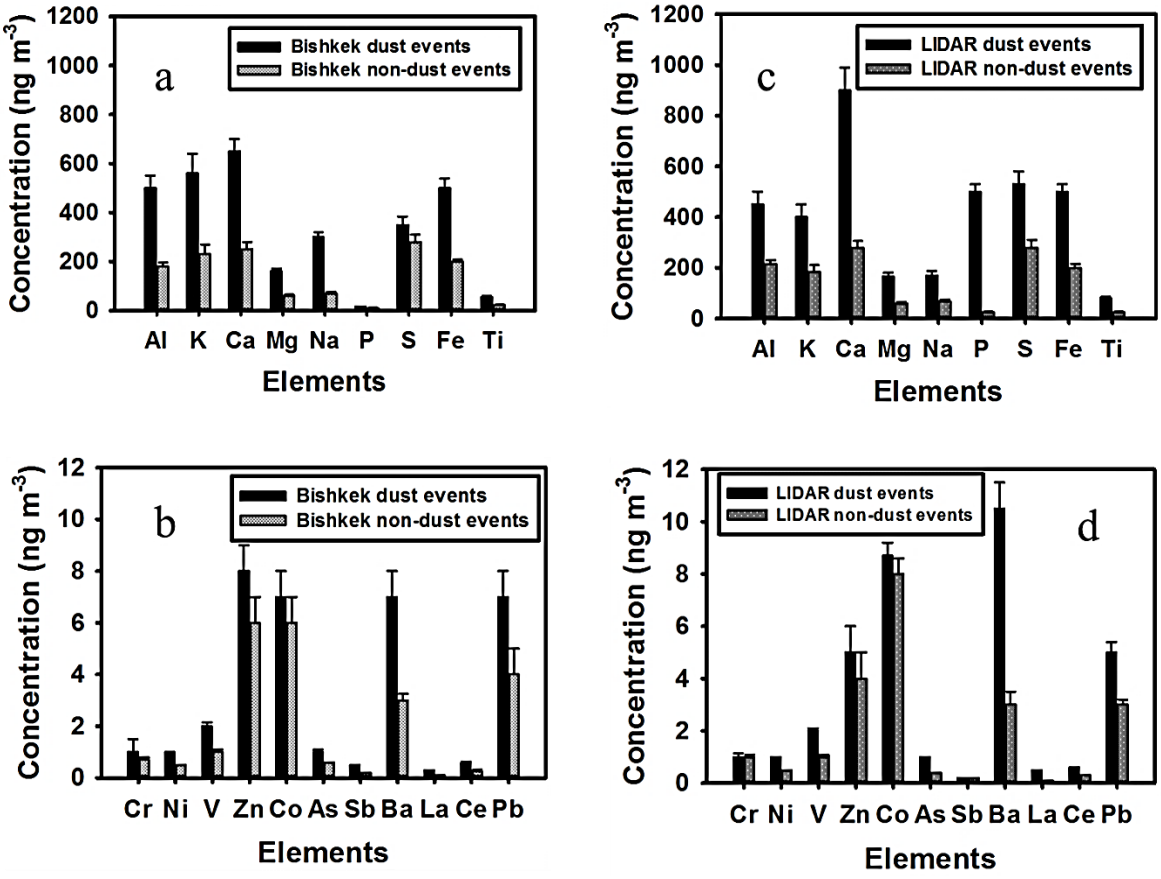

Figure 3.2: Average (ng m^{-3}) crustal and toxic and rare-earth elements observed in PM_{10} at the Bishkek (a and b) and LIDAR sites (c and d) during dust and non-dust events. The uncertainties in the elemental concentrations are represented by the error bars.

A seasonal dependence also was observed in the ambient PM_{10} elemental concentrations at both sampling sites as shown in Appendix A (Figure A1 (a,b)). Higher crustal related elemental concentrations were observed in the spring at both sites with a secondary peak in the fall. The peak in the spring is attributed to the higher frequency of dust storms during this period. It is consistent with the intensity of dust storms observed in a previous manuscript [83].

3.4.2 Sources of lead in PM_{10}

Since ^{208}Pb is produced through the radioactive decay chain of ^{232}Th, the concentrations of total Pb against total Th is presented to help understand the sources of Pb (i.e. natural or anthropogenic) in the Kyrgyzstan soils, Aral Sea sediments, and airborne PM_{10} (Figure 3.3).

In Figure 3.3 (a), Pb correlates linearly with Th in the Aral Sea sediments and Kyrgyzstan soils, indicating that the Pb in the soils and sediments is primarily from natural sources. The low upper continental crust enrichment factor (UCC EF) for Pb in soils (EF_{Pb} = 1.54) and the Aral Sea sediments (EF_{Pb} = 3.09) is also consistent with a low anthropogenic contribution [94]. In Figure 3.3 (b), no relationship is observed between total Pb and Th in $PM_{10.}$ This indicates that airborne Pb is likely dominated by anthropogenic sources and not wind-blown dust or local soils. The average UCC EF for Pb is 37 for PM_{10} at the Bishkek site and 74 for PM_{10} at the LIDAR site, again indicating an anthropogenic component of Pb in airborne PM_{10}.

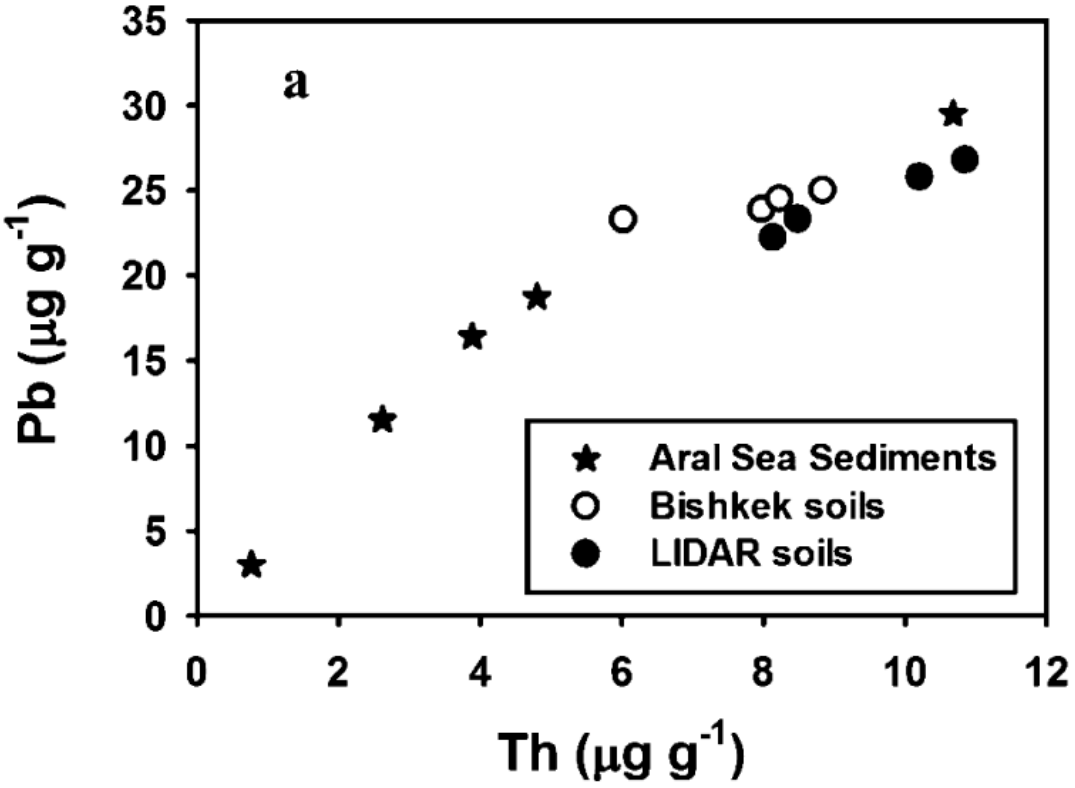

Figure 3.3 (a): Correlation between elemental Pb (μg g^{-1}) and elemental Th (μg g^{-1}) for Aral Sea sediments and Kyrgyzstan soils.

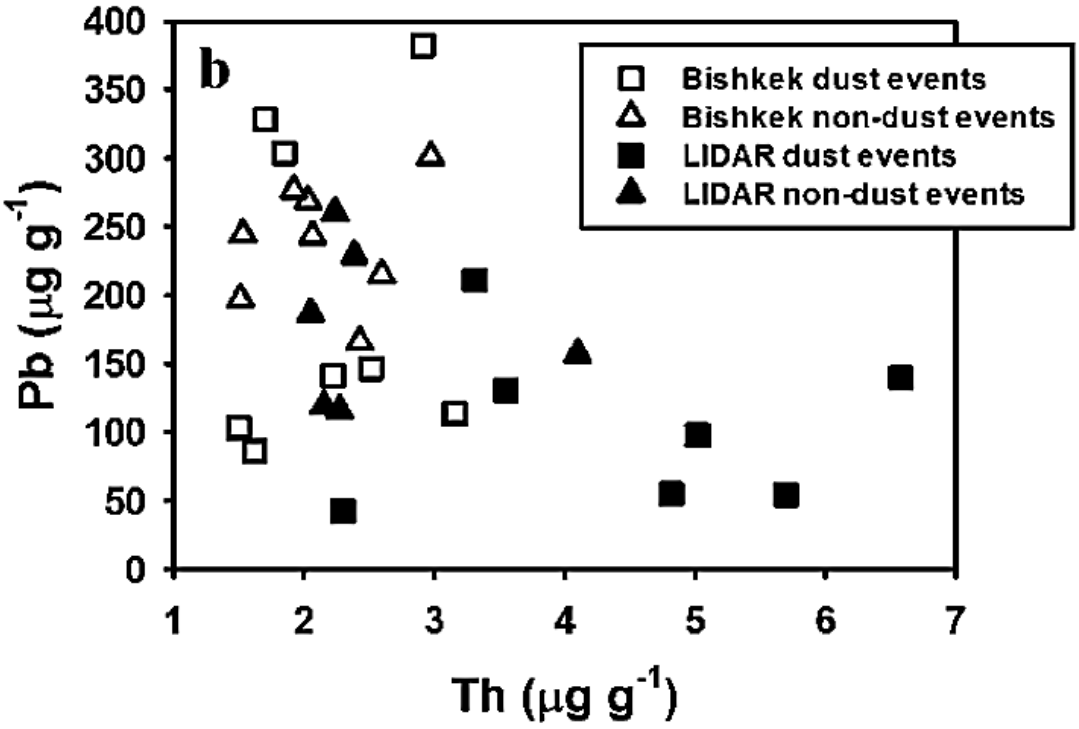

Figure 3.3 (b): Correlation between elemental Pb (μg g^{-1}) and elemental Th (μg g^{-1}) for PM_{10} during dust and non-dust events at the two sampling sites.

Also, elemental ratios are commonly used as tracers for source apportionment studies; for example, potassium to lead ratios are linked to refuse burning [95]. Similar elemental ratios have been studied in the past to determine the source of particulate matter in the atmosphere [96, 97]. The K/Pb ratio for soils and sediments was ~800 whereas the K/Pb ratio for the airborne PM_{10} was in the range 46-112. Since the K/Pb ratio for the PM_{10} is low which suggest that Pb concentration in the atmosphere is more compared to K. Therefore, Pb in PM_{10} is present due to anthropogenic activities.

3.4.3 Sr isotope ratios

Table 3 presents the $^{87}Sr/^{86}Sr$ ratios for the Kyrgyzstan soils, Aral Sea sediments, and PM_{10} collected at the two sites during the dust and the non-dust events. The average $^{87}Sr/^{86}Sr$ ratio for the Aral Sea sediments was 0.70992 (range, 0.70951-0.71064). The average Sr ratio in the surface soils in Kyrgyzstan was 0.71579 (range, 0.71448-0.71739). The airborne PM_{10} collected in Kyrgyzstan has an average $^{87}Sr/^{86}Sr$ ratio of 0.71177 (range, 0.70946-0.71335), which falls between the two potential sources.

Table 3: Average (and range) isotopic ratios of resuspended sediments from the Aral Sea region, and Kyrgyzstan soils, and airborne PM_{10} collected at the Bishkek and LIDAR sites during dust and non-dust events. The uncertainty represents the coefficient of variation (CV) of the multiple measurements.

Samples	$^{87}Sr/^{86}Sr$	$^{206}Pb/^{204}Pb$	$^{208}Pb/^{204}Pb$	$^{208}Pb/^{206}Pb$
Aral Sea sediments (n=5)	0.70992 ± 0.00067 (0.70951-0.71064)	18.634 ± 0.008 (18.493-18.872)	39.049 ± 0.008 (38.813-39.584)	2.0955 ± 0.0016 (2.0903-2.0988)
Bishkek non-dust events PM_{10} (n=21)	0.71104 ± 0.00101 (0.71027-0.71218)	18.053 ± 0.002 (17.985-18.088)	37.994 ± 0.001 (37.893-38.059)	2.1046 ± 0.0006 (2.1028-2.1070)
Bishkek dust events PM_{10} (n=8)	0.71047 ± 0.00120 (0.70946-0.71156)	18.098 ± 0.006 (17.846-18.241)	38.103 ± 0.006 (37.569-38.278)	2.1070 ± 0.0023 (2.1014-2.1169)
Bishkek soils (n=4)	0.71577 ± 0.00023 (0.71561-0.71601)	18.970 ± 0.011 (18.831-19.281)	39.195 ± 0.008 (39.013-39.659)	2.0661 ± 0.0031 (2.0569-2.0717)
LIDAR soils (n=4)	0.71582 ± 0.00171 (0.71448-0.71739)	19.449 ± 0.019 (19.165-20.011)	39.524 ± 0.008 (39.158-39.908)	2.0325 ± 0.0125 (1.9942-2.0480)
LIDAR dust events PM_{10} (n=7)	0.71240 ± 0.00119 (0.71088-0.71335)	18.235 ± 0.006 (18.112-18.392)	38.264 ± 0.004 (38.107-38.487)	2.0991 ± 0.0029 (2.0912-2.1080)
LIDAR non-dust events PM_{10} (n=18)	0.71179 ± 0.00094 (0.71100-0.71285)	18.162 ± 0.005 (18.007-18.242)	38.291 ± 0.006 (37.866-38.483)	2.1082 ± 0.0016 (2.1029-2.1127)

To help infer the source of dust in the PM_{10}, $^{87}Sr/^{86}Sr$ vs. 1/Sr ($\mu g\ g^{-1}$) has been presented in Figure 3.4. In the 1/Sr domain, a mixture consisting of only the two end-members (sources) (e.g. Aral Sea sediments and local soils) will lie on the straight line between the end-members. If not, then additional sources are likely to present. In Figure 3.4, Aral Sea sediments are encircled and Kyrgyzstan soils are inside the rectangle. The dotted horizontal lines represent the average of the Sr ratios for each potential end-member. The average $^{87}Sr/^{86}Sr$ ratio in surface soils ratio at the LIDAR site is 0.71582 (range, 0.71448-0.71739), which is similar to the Bishkek soils with an average of 0.71577 (range, 0.71561-0.71601) (*t*-test, $p < 0.05$).

Aral Sea sediments exhibit lower $^{87}Sr/^{86}Sr$ ratio and higher total Sr concentrations than the Kyrgyzstan soils. The average $^{87}Sr/^{86}Sr$ ratio of Aral Sea sediments (0.70992) is significantly different than the Kyrgyzstan soils (0.71579), (*t*-test, $p < 0.05$). The Aral Sea sediment ratio is similar to the saline lacustrine (lake) deposits and sediment (loess) ratios observed in the north Tien-Shan region in Northern China [98], and therefore, Sr ratios for Aral Sea sediments are likely indicative of aeolian sediments. This similarity is also consistent with the high calcium content measured in the Aral Sea sediments. The Kyrgyzstan soils ratio were similar to the loess-like deposits and river deposit ratios observed in the southwest Tarim Basin in Northwest China; desert sand deposit ratios observed in Northeastern China [98] and loess and paleosol ("fossil" soils) ratios observed in three distant areas (Xining, Jixian, and Xifeng) of the Central Loess Plateau in China [99].

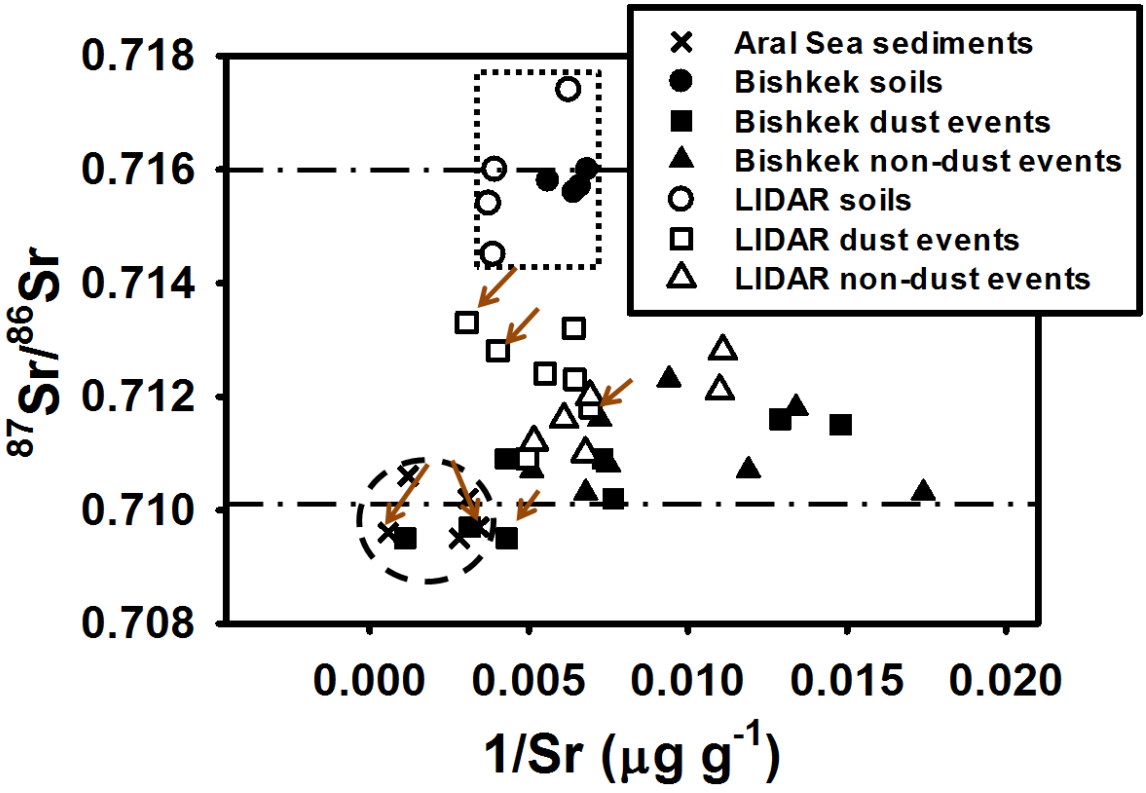

Figure 3.4: $^{87}Sr/^{86}Sr$ *vs.* 1/Sr concentration for Aral Sea sediments (in circle), Kyrgyzstan soils (in rectangle), and ambient PM_{10} observed at both sites during dust events and non-dust events, respectively. The dotted horizontal lines represent the average of the Sr ratio for each potential end-member. The arrows indicate that the Aral Sea had an impact on dust events at Bishkek and LIDAR sites.

Figure 3.4 and Table 3 also present the $^{87}Sr/^{86}Sr$ ratios for PM_{10} at the Bishkek and LIDAR sites during dust and non-dust events. $^{87}Sr/^{86}Sr$ ratios show an average of 0.71047 (range, 0.70946-0.71156) for PM_{10} at Bishkek during dust events compared with an average of 0.71104 (range, 0.71027-0.71218) during non-dust events. Although averages are not significantly different (*t*-test, $p > 0.05$), the Sr isotope ratios at Bishkek tend towards the Aral Sea ratios during dust events. The average $^{87}Sr/^{86}Sr$ ratio for dust events ratio at the LIDAR site (0.71240, range 0.71088-0.71335) also is not statistically different (*t*-test, $p > 0.05$) than that measured during non-dust events (0.71179, range 0.71100-0.71285). Overall, Sr isotopic ratios in airborne PM_{10} are more similar to the Aral Sea sediments or other deserts (soils) in the region than to the local soils [98], suggesting that local soils are not a major source of PM_{10} at the receptor sites. The isotopic composition of the Aral Sea sediments and the soils collected in the vicinity of the sampling sites are indistinguishable from soils of Western and Central China.

The arrows in Figure 3.4 indicate that the Aral Sea had an impact on dust events at Bishkek and LIDAR sites based on backward HYSPLIT (Hybrid Single Particle Lagrangian Integrated Trajectory) model [100, 101]. Also, based on back trajectory analysis; Gobi Desert, Libya, Iran, Algeria, and the Mediterranean Sea had an impact on dust events at the sampling sites. Although the HYSPLIT model indicates that the Aral Sea may have some impact, it is important to note that there is no statistical difference in Sr isotope ratio between dust events which passed over the Aral Sea and those which took a different trajectory. This is further evidence that the Aral Sea sediments have only a minor influence, at best, in Kyrgyzstan. Since the PM_{10} Sr ratios do not fall on a linear

mixing line between the two potential end members, it is likely that one or more other dust sources are present but not measured in this study. Other regional deserts (e.g. Circum-Aral Karakum and others near the Aral Sea, Gobi, Taklamakan) or long-range transport from Africa or the Middle East also may be important sources to Kyrgyzstan [81, 82, 83].

REEs are generally depleted in the dust relative to the sediments because the amount of dust from a local source varies based on environmental factors, wind patterns, and long-range transport [102]. The geochemical differences between the lighter and heavier lanthanides have concentrated the lighter lanthanide like Ce and La in the Earth's crust [103]. La/Sm values demonstrate a clear fractionation of atmospheric PM in comparison with lithospheric compositions [104] and therefore, the end member can not only be characterized by $^{87}Sr/^{86}Sr$ ratio but also by La/Sm ratio [105].

To further trace the source of the dust, La/Sm concentration ratios were plotted against $^{87}Sr/^{86}Sr$ ratios for the Aral Sea sediments and Kyrgyzstan soils (Figure 3.5). The soils collected in Kyrgyzstan exhibit an average La/Sm ratio of 4.42 (range, 3.90- 4.77), whereas the Aral Sea sediments show an average La/Sm ratio of 5.71 (range, 5.31- 6.33), indicating two different sources. PM_{10} had an average La/Sm ratio of 5.88 (range, 4.17- 6.52), which is higher than the Kyrgyzstan soils and more closely aligned with the Aral Sea sediments.

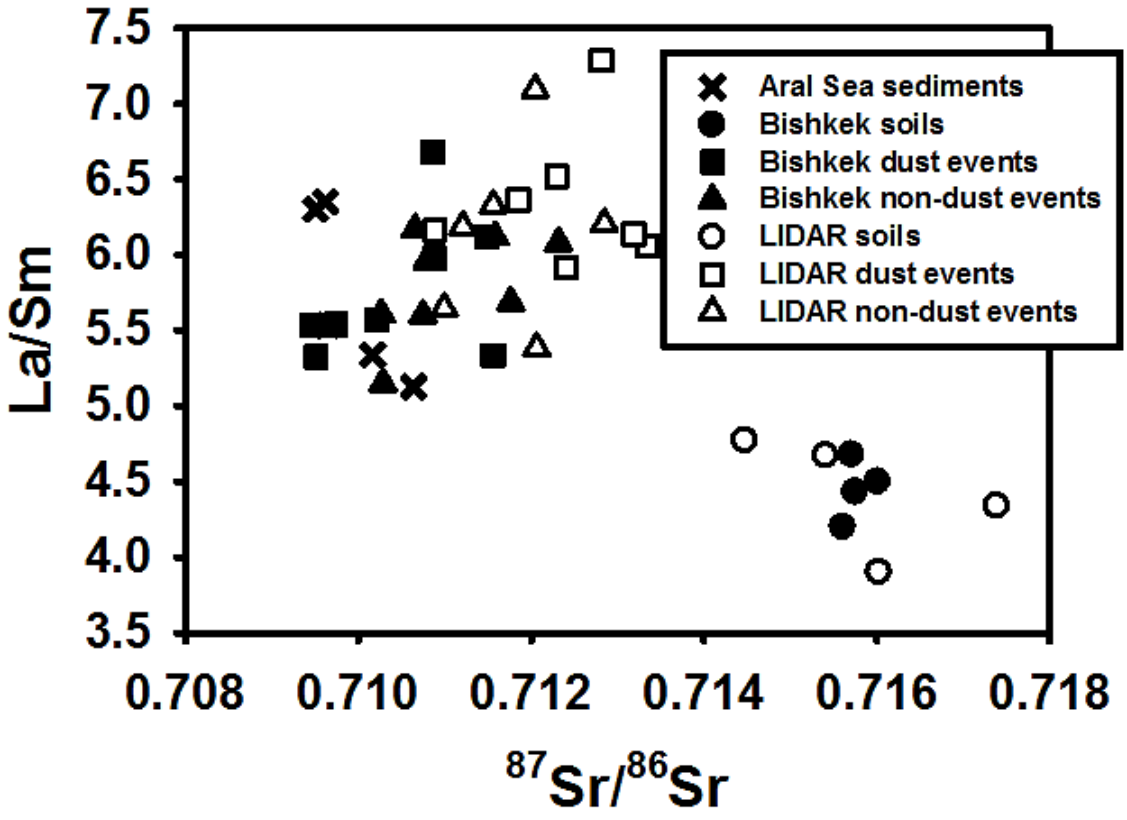

Figure 3.5: La/Sm ratios versus $^{87}Sr/^{86}Sr$ ratios to examine the origin of PM_{10} in the Aral Sea sediments, PM_{10}, and Kyrgyzstan soils.

PM_{10} La/Sm ratios were similar to the loess and paleosol ratios observed in three areas (Xining, Jixian, and Xifeng) of the Central Loess Plateau in China [99]. The La/Sm ratios were higher during dust than non-dust events at both sampling sites, although the difference is not statistically significant (*t*-test, $p > 0.05$).

Aluminum is a marker of crustal emissions and therefore, La/Al ratio further helps in the characterization of the end member [102]. Figure 3.6 shows La/Al ratios plotted against $^{87}Sr/^{86}Sr$ ratios for Aral Sea sediments, PM_{10}, and Kyrgyzstan soils. Kyrgyzstan soils had an average La/Al (x 10,000) ratio of 3.64 (range, 2.54 – 4.79), the Aral Sea sediments 5.90 (range, 3.69 – 7.33), and PM_{10} 5.75 (range, 4.02 – 7.87). Based on the elemental and Sr isotope ratios, the PM_{10} observed at the monitoring sites appears to be chemically more similar to the Aral Sea sediments than the local soils.

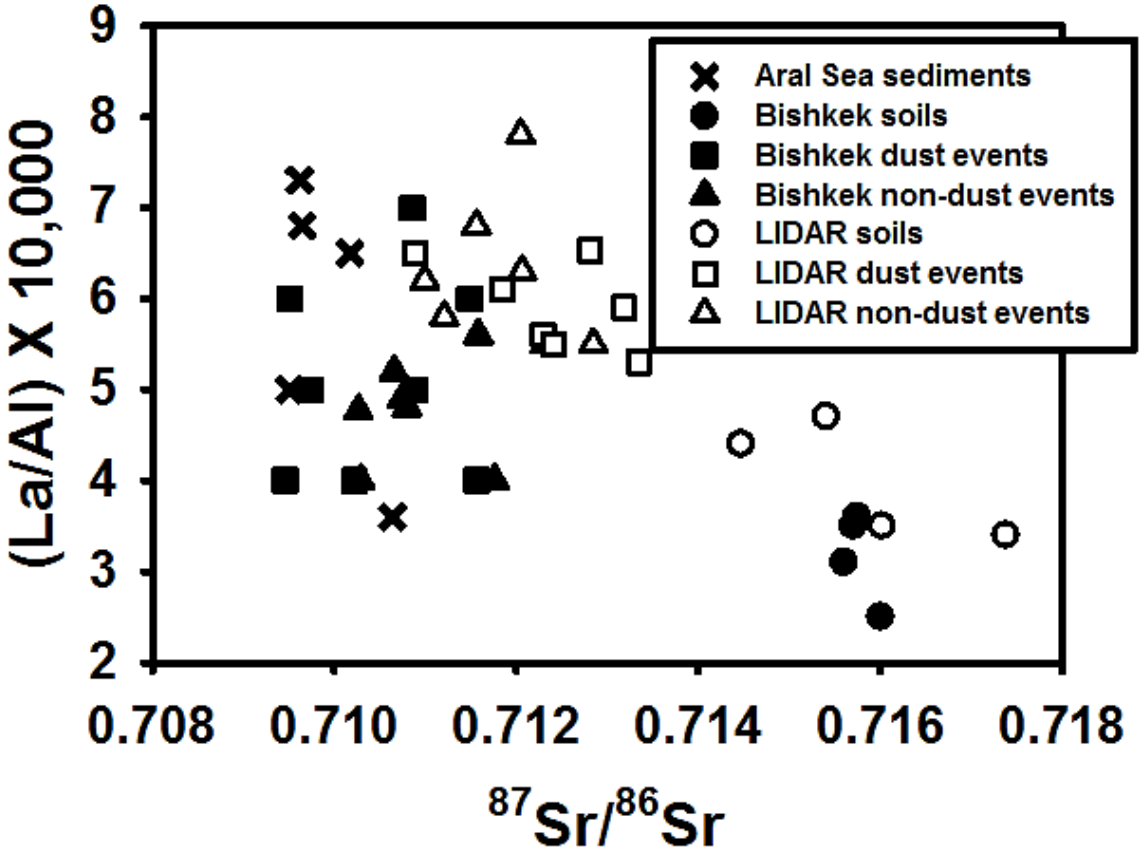

Figure 3.6: La/Al ratios versus $^{87}Sr/^{86}Sr$ ratios to examine the origin of PM_{10} in the Aral Sea sediments, PM_{10}, and Kyrgyzstan soils.

3.4.4 Pb isotope ratios

Stable lead isotope ratios ($^{206}Pb/^{204}Pb$, $^{208}Pb/^{204}Pb$, and $^{208}Pb/^{206}Pb$) for the Aral Sea sediments, Kyrgyzstan soils, and PM_{10} during dust and non-dust events are presented in Table 3. Figure 3.7 shows the $^{208}Pb/^{206}Pb$ ratios plotted against the $^{207}Pb/^{206}Pb$ ratio for Aral sediments (encircled in middle) and Kyrgyzstan soils (encircled, dotted line). Significant differences were observed in both the $^{207}Pb/^{206}Pb$ and $^{208}Pb/^{206}Pb$ ratios. The average $^{208}Pb/^{206}Pb$ ratio, of the Kyrgyzstan soils, is 2.069 (range, 1.994 –2.071), which suggests a natural Pb source [106]. This is consistent with the low UCC EF of 1.54 and high K/Pb ratio of 819. The Aral Sea sediments exhibit a mean $^{208}Pb/^{206}Pb$ ratio of 2.095, which is significantly different than Kyrgyzstan soils. Lead isotope ratios associated with weathering of exposed silicate from continental crust (natural origin) in Central Asia and by conjecture, that of Chinese Loess, are in the range of: $^{206}Pb/^{204}Pb = 18.97 \pm 0.06$, $^{207}Pb/^{204}Pb = 15.67 \pm 0.02$, $^{207}Pb/^{206}Pb = 0.8234 \pm 0.0282$, $^{208}Pb/^{206}Pb = 2.065 \pm 0.035$, and $^{208}Pb/^{204}Pb = 39.19 \pm 0.11$ [107]. These values are similar to those observed in Aral Sea sediments: $^{206}Pb/^{204}Pb = 18.63 \pm 0.04$, $^{207}Pb/^{204}Pb = 15.64 \pm 0.02$, $^{207}Pb/^{206}Pb = 0.8398 \pm 0.0029$, $^{208}Pb/^{206}Pb = 2.095 \pm 0.0031$ and $^{208}Pb/^{204}Pb = 39.04 \pm 0.09$. These data indicate that the Pb in the Aral Sea sediments also is comparable to Chinese Loess and is also of natural origin.

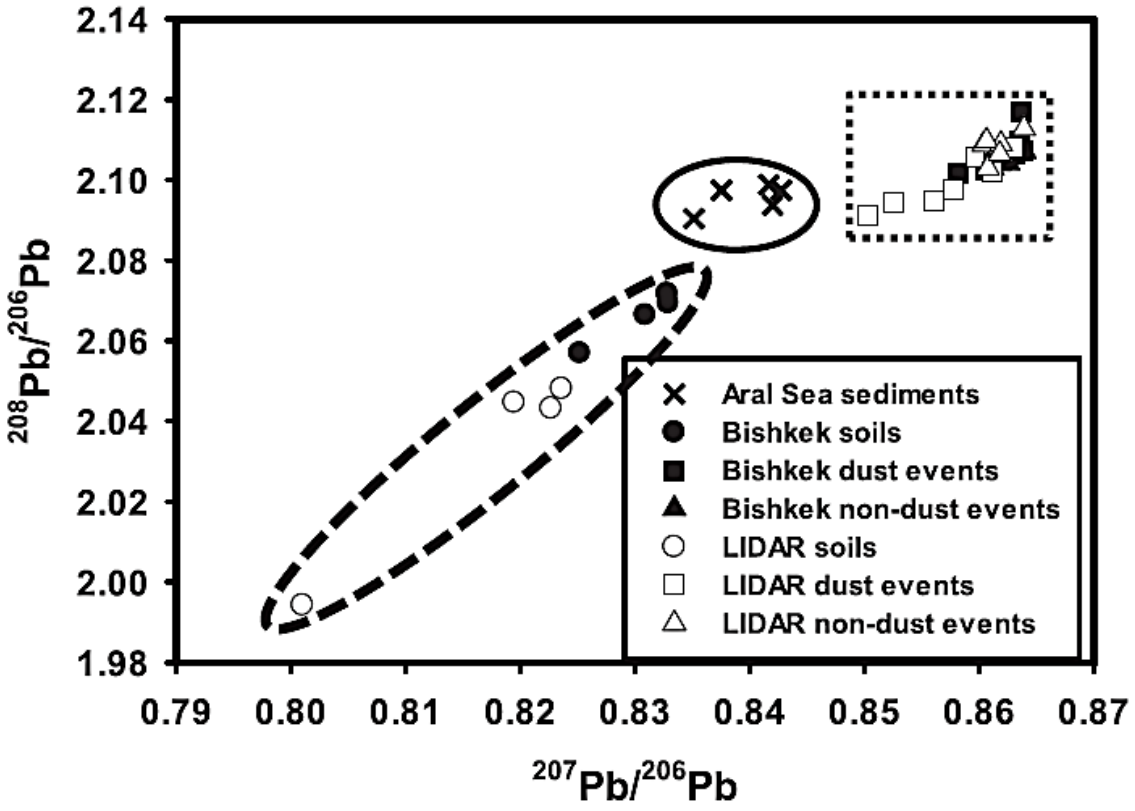

Figure 3.7: $^{208}Pb/^{206}Pb$ *vs.* $^{207}Pb/^{206}Pb$ in Kyrgyzstan soils (encircled), Aral Sea sediments (encircled in middle), and PM_{10} (in rectangle) during dust and non-dust events.

The mean PM_{10} $^{208}Pb/^{206}Pb$ ratio for dust and non-dust events (Figure 3.7, in rectangle) is 2.115, high compared to the Aral Sea sediments and Kyrgyzstan soils. Similarly, the PM_{10} $^{207}Pb/^{206}Pb$ ratio is 0.8607 is higher than the soils and sediments. If the PM_{10} were a mixture of only these two sources, then we would expect the PM_{10} data to fall between the two end-members. However, the stable Pb isotope results indicate that the airborne Pb is a mixture of Aral Sea sediments (or China Loess) or possibly other regional deserts, where the Pb isotope ratios are unknown. Due to the elevated UCC EF (range, 20-80) and low K/Pb ratio (range, 46-112), the unknown source is likely anthropogenic.

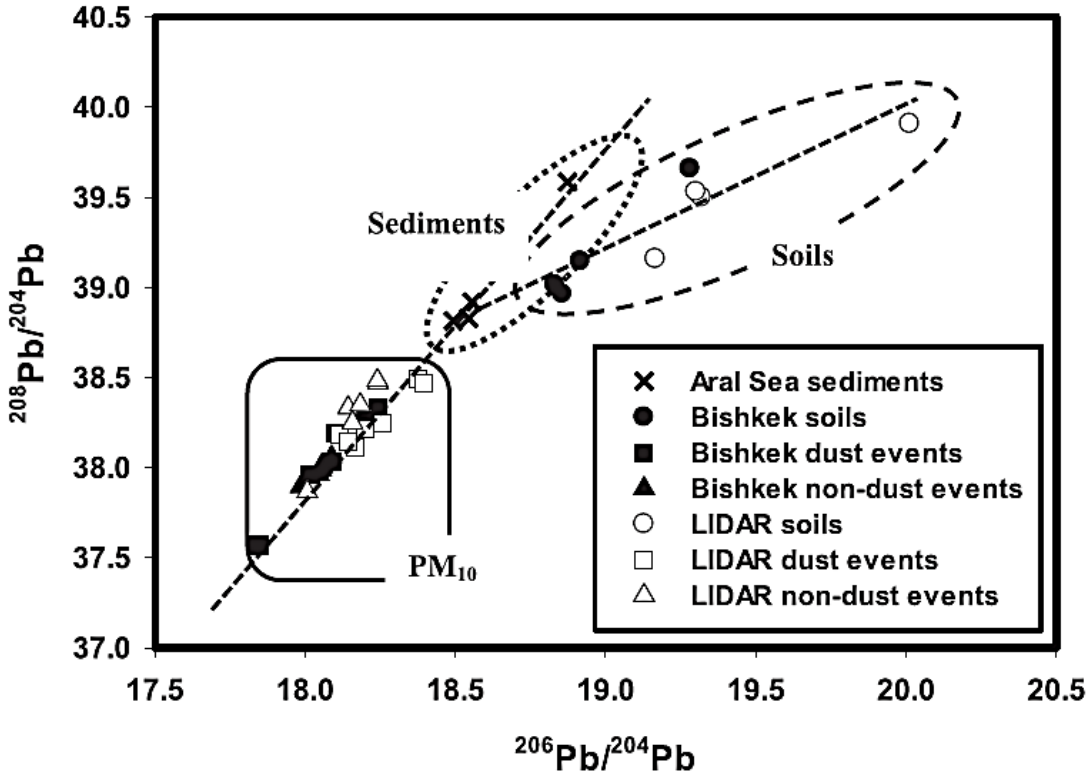

Figure 3.8: $^{208}Pb/^{204}Pb$ and $^{206}Pb/^{204}Pb$ in Kyrgyzstan soils, Aral Sea sediments, and PM_{10} during dust and non-dust events.

Figure 3.8 presents the normalized binary mixing relationship ($^{208}Pb/^{204}Pb$ ratios plotted against $^{206}Pb/^{204}Pb$ ratios) between Kyrgyzstan soils, Aral Sea sediments, and airborne PM_{10}. Kyrgyzstan soils and the Aral Sea sediments have an average $^{206}Pb/^{204}Pb$ ratio of 19.21 and 18.63, respectively. Airborne PM_{10} has an average $^{206}Pb/^{204}Pb$ ratio of 18.14, which does not lie between the soil and sediment results, but does lie on the same line as the Aral Sea sediments. Kyrgyzstan soils fall along a different binary mixing line, implying, as discussed earlier, that they are not an important source of PM_{10} to the sampling sites. Along with results shown in Figure 3.7, these results suggest a possible contribution from the Aral Sea region or other deserts affecting the region, but a significant end-member is unaccounted for and further studies are required to characterize this source.

3.5 Conclusions

Significant differences in elemental composition and in Sr and Pb stable isotope ratios between Aral Sea sediments and Kyrgyzstan soils were reported. Metrics indicate that local soils likely only contribute slightly to the ambient PM_{10} collected in Bishkek and LIDAR. The importance of wind-blown dust from the Aral Sea basin was estimated. While PM_{10}, Sr and Pb stable isotope ratios are more similar to those measured in sediments associated with the Aral Sea basin than the local soils, the elemental and Pb isotope data strongly suggest that the Aral Sea basin is not a major source of PM to the region. In Central Asia, the increase in PM_{10} during the dust events appears to be associated with both western (dust emitted from Central Asia and further west) and

eastern wind trajectories (consistent with our HYSPLIT data) (Taklamakan Desert from Western China) [81, 82, 83]. Therefore, transport from other dust sources, such as Western China, Africa, or Middle Eastern regions [108, 109], may be impacting PM_{10} levels in Kyrgyzstan.

The Pb isotopic composition of Aral Sea sediments and Kyrgyzstan soils suggest a dominating natural Pb component, which is in agreement with high K/Pb ratios and low UCC EFs. Pb isotope ratios for airborne Pb are in agreement with the Sr data where values are closer to those of the Aral Sea basin, relative to local soils. However, results also clearly show that other sources are likely more important than the Aral Sea basin. Combined with the elemental data, the Pb isotope ratios suggest a strong unidentified anthropogenic source of Pb, perhaps resulting from transport from the nearby Ferghana Valley and Tashkent in Uzbekistan, industrial Europe, or from the Middle East [81, 82, 83]. The lack of Pb enrichment in native soils suggests that Pb is transported into the region, rather than a result of local sources.

One of the major objectives of the overall study was to examine the potential impact of transported dust from recently exposed sediments around the Aral Sea on receptor sites in Kyrgyzstan. Results presented here and elsewhere [81, 82, 83] indicate that although the Aral Sea has undergone significant desiccation, introducing a potentially large dust source to the region, the overall impact within Kyrgyzstan relative to other deserts in and outside of Central Asia is small.

3.6 Acknowledgements

The authors thank Dr. Gwyneth Gordon and Dr. Rasmus Andreason for their help and guidance in Sr ratios measurements. The authors gratefully acknowledge the NOAA Air Resources Laboratory (ARL) for the provision of the HYSPLIT transport and dispersion model and/or READY website (http://www.ready.noaa.gov) used in this publication. We acknowledge the Association of Public Health Laboratories (APHL) for funding through their Environmental Health Fellows program. The US Environmental Protection Agency, through its Office of Research and Development, funded and collaborated in the research described here under Contract EP-D-06-001 to the University of Wisconsin-Madison as a component of the International Science & Technology Center (ISTC) project # 3715 (Transcontinental Transport of Air Pollution from Central Asia to the US). It has been subjected to the Agency review and approved for publication. The isotope portion of this study was funded through a PROF Grant at the University of Denver.

Chapter Four: Effect of pollution controls on atmospheric $PM_{2.5}$ composition during Universiade in Shenzhen, China

4.1 Abstract

The 16th Universiade, an international multi-sport event, was hosted in Shenzhen, China from 12th to 23rd August 2011. During this time, officials instituted the Pearl River Delta action plan in order to enhance the air quality of Shenzhen. To determine the effect of these controls, the current study examined the trace elements, water-soluble ions, and stable lead isotopic ratios in atmospheric particulate matter collected during the controlled (when the restrictions were in place) and uncontrolled periods. Fine particles ($PM_{2.5}$) were collected at two sampling sites in Shenzhen: "LG"—a residential building in the Longgang District, with significant point sources around it and "PU"—Peking University Shenzhen School in the Nanshan District, with no significant point sources. Results from this study showed a significant increase in the concentrations of elements during the uncontrolled periods. For instance, samples at the LG site showed (controlled to uncontrolled periods) concentrations (in ng m^{-3}) of: Fe (152 to 290), As (3.65 to 8.38), Pb (9.52 to 70.8), and Zn (98.6 to 286). Similarly, samples at the PU site showed elemental concentrations (in ng m^{-3}) of: Fe (114 to 301), As (0.634 to 8.36), Pb (4.86 to 58.1), and Zn (29.5 to 259). Soluble Fe ranged from 7-15% for the total measured Fe, indicating an urban source of Fe. Ambient $PM_{2.5}$ collected at the PU site has an average

$^{206}Pb/^{204}Pb$ ratio of 18.257 and 18.260 during controlled and uncontrolled periods, respectively. At the LG site has an average $^{206}Pb/^{204}Pb$ ratio of 18.183 and 18.030 during controlled and uncontrolled periods, respectively. The $^{206}Pb/^{204}Pb$ ratios at the PU and the LG sites during the controlled and uncontrolled periods were similar, indicating a common Pb source. To characterize the sources of trace elements, principal component analysis was applied to the elements and ions. Although the relative importance of each component varied, the major sources for both sites were identified as residual oil combustion, secondary inorganic aerosols, sea spray, and combustion. The $PM_{2.5}$ levels were severely decreased during the controlled period, but it is unclear if this was a result of the controls or change in meteorology.

4.2 Introduction

Due to an increase in urbanization and economic growth in China, air pollution has become a severe problem. $PM_{2.5}$ is a key pollutant strongly impacted by the rapid development in China [110, 111, 112]. High $PM_{2.5}$ levels are associated with human mortality [2, 6, 113], climate change [114], visibility [115, 116], and agricultural yield reduction [117]. Increased morbidity and mortality rates and the adverse health effects of particle exposure are predominantly linked to the chemical composition of PM [118, 119]. From a toxicological viewpoint, the trace metals play an important role in increasing the redox activity of ambient PM [9, 120, 121]. Metals are hard to eliminate and they, therefore, accumulate in organisms and plants and can cause severe human health related problems and environmental pollution [122, 123]. The inhalation of metals

is associated with disruption of the nervous system and the functioning of internal organs [124, 125, 126].

Shenzhen (22^{o} 33' N, 114° 06' E), home to a population of 10.62 million residents, is one of the most important industrial centers in China. It is a coastal city in the Guangdong Province located at the mouth of the Pearl River Delta (PRD), bordering Hong Kong. Previous studies measured $PM_{2.5}$ mass concentrations during winter and summer months in Shenzhen and Hong Kong. The $PM_{2.5}$ levels (in μg m^{-3}) were higher at Shenzhen, (47 ± 17) and (61 ± 18), relative to Hong Kong, (31 ± 17) and (55 ± 23), during summer and winter months, respectively [127, 128]. Overall, Shenzhen displayed maximum $PM_{2.5}$ levels in winter months relative to summer months [129], both of which exceed the 24 hours mean ambient air quality standards of the world health organization (WHO) of 25 μg m^{-3} [130] and the annual ambient air quality standards of People's Republic of China (GB 3095-2012) of 35 μg m^{-3} [131].

The 16^{th} Universiade, an international multi-sport and cultural event organized for university athletes by the International University Sports Federation, was hosted in Shenzhen, China from August 12^{th} to 23^{rd} in 2011. During this time, officials instituted several restrictions such as (a) the PRD action plan [132], which includes the prevention and control of industrial pollution, flow source pollution, and dust and point source pollution; (b) an ozone controlling plan which includes control of emissions of volatile organic compounds (VOCs) and promotion of an oil to gas project for thermal power plants; and (c) traffic-control actions such as restricting access within the region in order to enhance the air quality of Shenzhen. In this study, airborne $PM_{2.5}$ (aerodynamic

diameter < 2.5 μm) was collected at two sampling sites in Shenzhen during the controlled period (when the restrictions were implied) and during the uncontrolled period (when the restrictions were released). A previous study had evaluated the impact of emission controls and traffic intervention measures during the 29th Olympic and Paralympics games in Beijing [133], where significant reductions in vehicle emissions and ambient traffic-related air pollutants were observed.

In this study, we employed several chemical and statistical methods to determine the impact of the emission restrictions on $PM_{2.5}$ and trace elements. We report trace elements as well as water-soluble major ions. For the first time in the region, Pb isotopic ratios, as well as soluble iron oxidation state speciation, are reported. In addition to quantification, we employ principal component analysis (PCA) to determine the source of trace elements, allowing a unique interpretation of the quantitative data.

4.3 Experimental

4.3.1 Sample collection

Airborne $PM_{2.5}$ was collected at two sampling sites (LG and PU) in Shenzhen in 2011 both during the controlled period (12th August–23rd August) and uncontrolled period (24th August–4th September) of Universiade. The map of the region showing the two sampling sites is shown in Figure 4.1 [134]. The "LG" site (22.70° N, 114.21° E), about 500 m away from the main venue, is located on top of a 31st floor Lotus residential building in the Longgang District, with significant point sources (e.g., plastic processing plants, glass factories, papermaking and painting industries) nearby. During the controlled periods,

these point sources were supposed to be closed. However, we note that there was no accountability and no way of verification. The "PU" site (22.60° N, 113.97° E) is located at the top of Building E of the Peking University Shenzhen Graduate School in the Nanshan District, with no significant point sources around it and about 33 km away from the main venue. The LG site was located at 161 m and the PU site was located at 50 m above ground level, with no major geological features between the sites. The distance between the two sampling sites is about 45 km. A previous study during the same time period at these sites showed that both PM mass and PM composition (EC/OC) were significantly (and similarly) altered when comparing the controlled and uncontrolled periods [132].

Co-located samples were collected on both 47 mm quartz and Teflon filters (Whatman, U.S.A.) each for 24 hours from 12th August to 4th September with a flow rate of 21 L min^{-1} using dual channel samplers (GUCAS 1.0) [135]. The quartz filters were used for EC/OC analysis following the protocol mentioned in EPA/NIOSH [136] and these results are reported elsewhere [132]. All sample preparation was performed under positive pressure HEPA filtered air. A microbalance (Mettler Toledo AX105DR) was used for determination of mass (estimated total uncertainty of ± 6 μg). Prior to weighing, the filters were equilibrated in a constant humidity (40% ± 3%) and temperature (20 ± 1 °C) environment for 48 hours.

The temperature, pressure, wind directions, and relative humidity were constant during the controlled periods. Based on the 72 hours backward HYSPLIT (Hybrid Single Particle Lagrangian Integrated Trajectory) model [100, 101], the air mass was transported

from the South Sea at both sampling sites during the controlled periods. During the uncontrolled periods, the wind directions were more variable, but northern winds were more prominent and, based on trajectory analysis, air mass was transported from an industrial zone to both sites. Additional details of the meteorology during this time can be found in a previous manuscript [132]. There were two minor rain events during the controlled and three during the uncontrolled periods, all less than 12 mm. There were no reductions observed in the overall PM mass during those days.

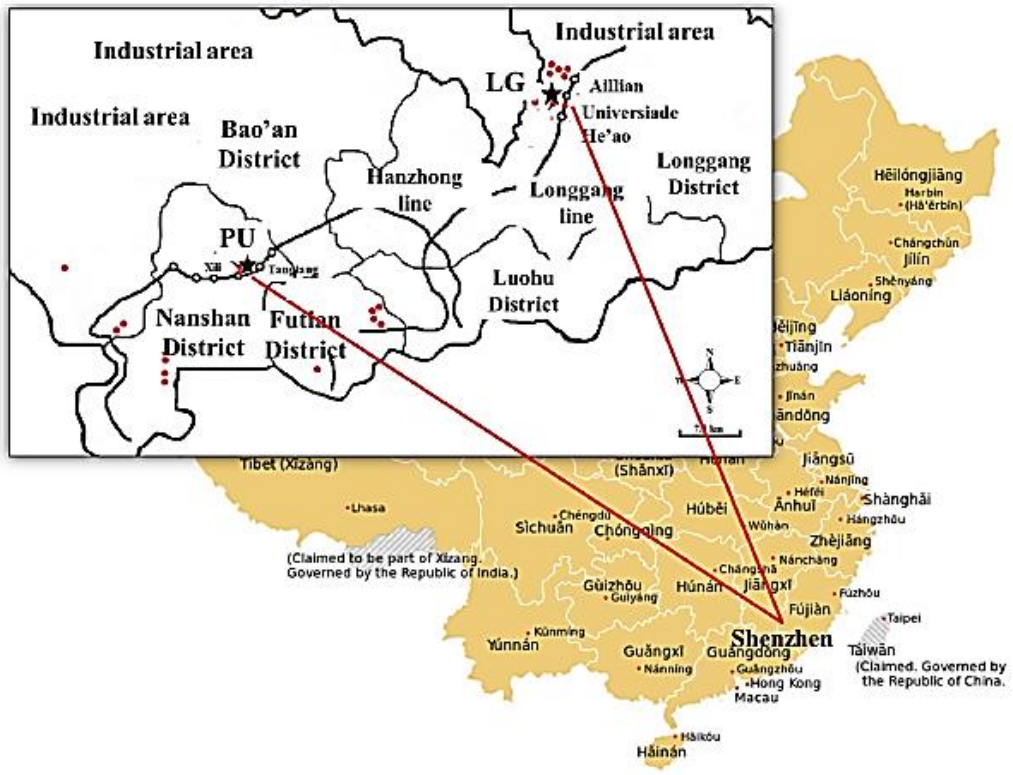

Figure 4.1: Map showing the geographical location of the PU and LG sampling sites (shown as stars) relative to the Universiade center in Shenzhen. The red dots on the map represent the stadiums where the events were held [134].

4.3.2 Total elemental analysis

Prior to digestion, the polypropylene ring was removed from the Teflon filter using a ceramic blade. The Teflon filters were digested in sealed, pre-cleaned Teflon digestion bombs in a 30-position microwave rotor (Milestone Ethos) with trace metal grade acid matrix (Fisher, U.S.A.) consisting of 1.5 mL of nitric acid (16 M), 750 µL of hydrochloric acid (12 M), 200 µL of hydrofluoric acid (28 M), and 200 µL of 30% hydrogen peroxide. Digestates were diluted to 30 mL with high purity water (>18 MΩcm, MQ) and elemental concentrations (Al, As, Ba, Ca, Cd, Cr, Cu, Fe, K, Mg, Mn, Mo, Na, Ni, Pb, Rb, Sb, Se, Sr, Ti, V, and Zn) were quantified by quadrupole inductively coupled plasma-mass spectrometry (ICP-MS, Agilent 7700) with indium (In) as an internal standard. The accuracy of the results from the elemental analysis was verified by National Institute of Standards and Technology (NIST) Standard Reference Materials (SRMs). The SRMs, San Joaquin Soil (NIST 2709) and Urban Dust (NIST 1649a), were digested and analyzed with every batch of 25 samples. The percent recovery of the reported elements from these SRMs was 85%–120%. Also, data were blank-corrected using the average of multiple field filter blanks. Blank concentrations (in µg L^{-1}) ranged from 0.0041 (2.4% of the total) to 14.65 (5.3% of the total) for the elements during the controlled and uncontrolled periods at the two sampling sites. The uncertainty associated with each element in every sample was calculated from an error propagation analysis, which included uncertainty in the field blanks and in the air flow rates.

4.3.3 Soluble ion analysis

For soluble ion analysis, the Teflon filters were leached in 10 mL high purity water for 2 hours. Water-soluble ions were analyzed from the unacidified portion using ion exchange chromatography (Dionex-ICS5000) followed by a self-regeneration suppressor (model CSR 300 for cations and ASR 300 for anions) and coupled with conductivity detector (Thermo). Cations (NH_4^+, K^+, Na^+, and Mg^{+2}) were separated by Dionex IonPac CS12A column and using 20 mM of methanesulfonic acid as a mobile phase at a flow rate of 0.5 mL min^{-1}. For anions (Cl^-, NO_3^-, and SO_4^{2-}), a Dionex IonPac AS22 column was used for separation along with a mixture of 4.5 mM sodium carbonate and 1.4 mM sodium bicarbonate as a mobile phase with a flow rate of 0.5 mL min^{-1}. A calibration curve of authentic standard (Dionex) for target ions was used to identify and quantify cations and anions in the samples. Details about calibration, method, and instrument detection limits, and other measurement parameters have been previously reported [137].

4.3.4 Iron oxidation state analysis

Iron (Fe) speciation analysis was also performed with the water-soluble extracts. 1.8 mL of the soluble extract was mixed with 0.2 mL of 5.88 µM Ferrozine reagent ((3–(2–pyridyl)–5,6–diphenyl–1,2,4–triazine–4',4"–disulfonic acid sodium salt), Sigma). The absorbance of the Fe (II)–Ferrozine complex was measured at 560 nm using a 1 m liquid waveguide capillary cell spectrophotometer [138, 139]. The pH for all water extracts (each site, controlled *vs.* uncontrolled) ranged between 4.28 and 4.41. This suggests that,

despite an unbuffered extract solution, pH effects were not important. The calibration curve generated using known Fe(II)-Ferrozine solutions provided Fe (II) concentration. Soluble Fe (III) was then determined by subtracting total soluble Fe concentration (from ICP-MS) from the soluble Fe (II) concentration.

4.3.5 Stable Pb isotope analysis

Stable Pb isotopic ratios were measured in the digested extracts with no further purification using high-resolution magnetic sector inductively coupled plasma mass spectrometer (MC)-ICP-MS (Thermo-Finnigan Neptune Plus). For the Pb isotope analysis, the digests were evaporated in Teflon vials (Savillex, U.S.A.) and diluted to 2 mL using 2% optima grade HNO_3 acid (Fisher, U.S.A.). The Pb content of the digests ranged from 15 to 30 ng. The uncertainties for Pb isotope ratios depended on the isotope system and were in the range of 0.0025 and 0.0034 for $^{206}Pb/^{204}Pb$ and $^{207}Pb/^{206}Pb$, respectively. Analysis of the common Pb isotopic standard (NIST 981) yielded $^{206}Pb/^{204}Pb = 16.937 \pm 0.018$ ($n = 18$) and $^{207}Pb/^{206}Pb = 0.9145 \pm 0.0001$ ($n = 17$) *versus* the certified values of 16.944 ± 0.015 and 0.9146 ± 0.0003, respectively.

4.3.6 Principal component analysis (PCA)

To identify the potential origin of the elements in $PM_{2.5}$, PCA was conducted using SPSS statistical software (SPSS, version 22). A varimax rotation was employed for interpretation of the principal components and factors with eigenvalues greater than unity were retained in the analysis [140]. Given that the bulk properties, Pb isotope ratios, and

elements trends were similar at each site, it is clear that similar sources affect each site. Therefore, the sites were grouped together for the PCA analysis. Prior to conducting factor analysis, we performed a Pearson correlation matrix of 52 samples collected at two sampling sites during controlled and uncontrolled periods. Based on correlations matrix, we had a total of 26 samples with OC [132], 8 elements, and 6 ions as variables, resulting in a sample/variable ratio consistent with recommended criteria for a robust PCA analysis with KMO test of sampling adequacy > 0.5 [141]. In addition, the significance value (0.000) for Bartlett's test of sphericity indicates that the correlations are appropriate for this data set.

4.4 Results and discussion

4.4.1 Trace element concentrations

One previous study [132] has shown that during the controlled periods, the monitored $PM_{2.5}$ mass concentrations were 12.9 ± 3.7 μg m^{-3} at the PU site and 25.2 ± 5.2 μg m^{-3} at the LG site. During uncontrolled periods, significant increases in the $PM_{2.5}$ mass concentrations were observed (PU = 48.0 ± 8.7 μg m^{-3} and LG = 54.0 ± 6.5 μg m^{-3}). The fact that the wind directions were drastically different during controlled and uncontrolled periods complicate the effects of the controls and this may be another reason why such drastic differences in PM were observed between the two periods. Consistent with the increased PM mass, results from our study showed an increase in the concentrations of most abundant and trace elements in $PM_{2.5}$ collected at the PU and LG sites during uncontrolled periods ((Figure 4.2 (a–d)). For instance, average Ca and Fe

concentrations were ~360 (range, 264–467) and ~290 (range, 216–412) ng m^{-3}, respectively, during uncontrolled periods and ~270 (range, 169–340) and ~152 (range, 90–352) ng m^{-3} during controlled periods at the LG site. Similarly, at the PU site, average Ca and Fe concentrations were ~250 (range, 114–469) and ~300 (range, 201–588) ng m^{-3}, respectively, during uncontrolled periods and ~100 (range, 29–160) and ~115 ng m^{-3} (range, 55–169) during controlled periods. The elemental analysis showed that both Al and K were the dominant elements at both sampling sites. Also, all trace elements, except Ni and V, had higher concentrations during uncontrolled periods at both sites. Both Ni and V are markers for the residual oil combustion, which suggests that oil combustion sources were essentially unaffected by the controls. The significant increase in V during the controlled periods could be attributed to emissions from ships around the Shenzhen city, however, this is speculation as reliable data regarding the ship traffic are not available. There were no large-scale oil power generation plants [142]. Therefore, control of oil combustion sources was likely very challenging, since all of these sources were probably small. Some striking differences include an approximate eleven-fold increase for Pb and an eight-fold difference for Zn for $PM_{2.5}$ during uncontrolled periods at the PU site. Similarly, an approximate eight-fold difference was observed in the concentrations of Pb and a three-fold difference for Zn during uncontrolled periods at the LG site. Overall, the concentrations of most of the elements were higher at the LG site relative to the PU site. This may be because the LG site is close to significant point sources.

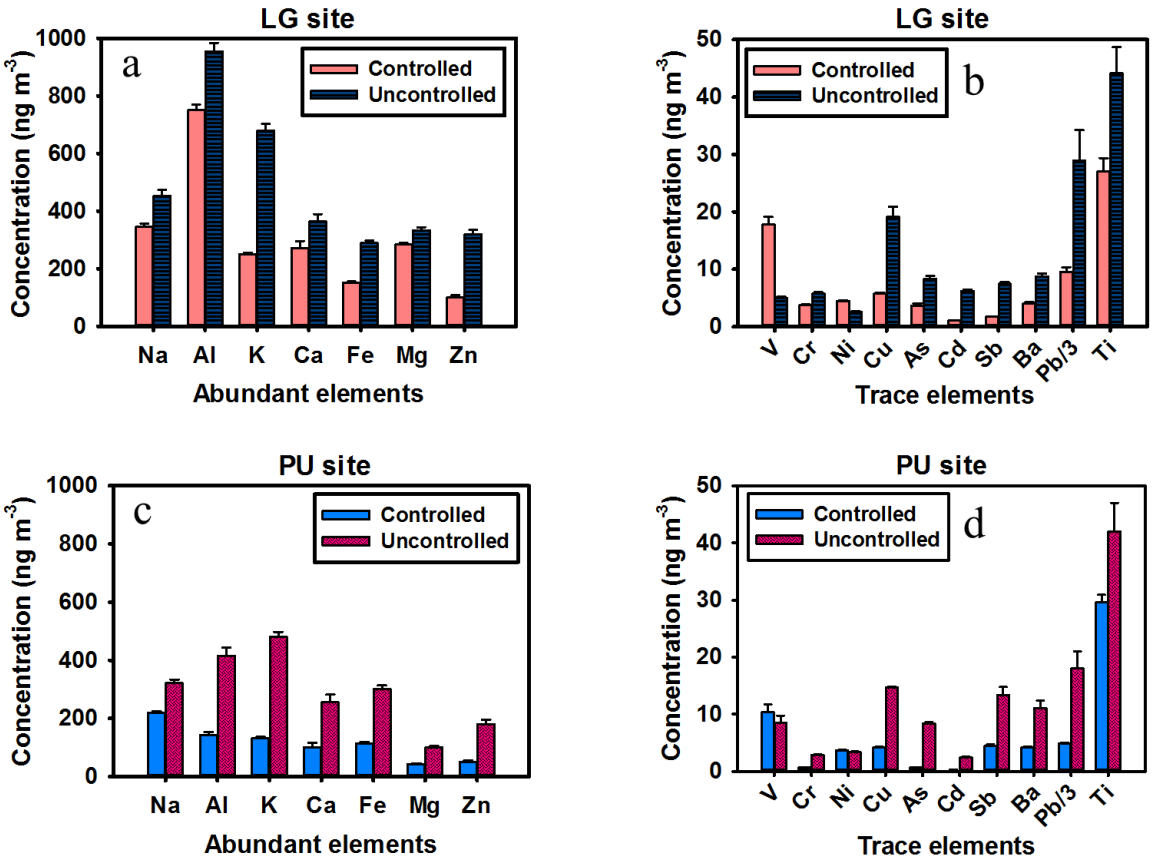

Figure 4.2: Average (ng m^{-3}) abundant and trace elements observed in $PM_{2.5}$ at the LG site (a,b) and PU site (c,d) during controlled and uncontrolled periods

Water-soluble ions were quantified in the $PM_{2.5}$ collected at the two sampling sites during controlled and uncontrolled periods and are presented in Figure 4.3. Elevated levels of SO_4^{2-} were observed in $PM_{2.5}$ during uncontrolled periods at both sites. Sources like coal power plants and industries may be playing an important role in the emissions of sulfur dioxide, which leads to sulfate. NO_3^-/SO_4^{2-} ratio can be used as an indicator of the type of anthropogenic activity [143]. If the ratio is >1, it indicates greater NO_x emissions, indicating vehicular emissions are likely dominant. If the ratio is <1, it indicates greater SO_2 emissions, and that stationary sources are dominant [143, 144]. The average ratio at the PU site was 0.071 ± 0.003 and 0.12 ± 0.02 during controlled and uncontrolled periods respectively, whereas the average ratio at the LG site was 0.15 ± 0.01 and 0.13 ± 0.01 during controlled and uncontrolled periods, respectively. At the two sampling sites, both during controlled and uncontrolled periods, the ratio is lower than 1, indicating that stationary sources like industry emissions and power plants are important contributors to $PM_{2.5}$ emissions in Shenzhen.

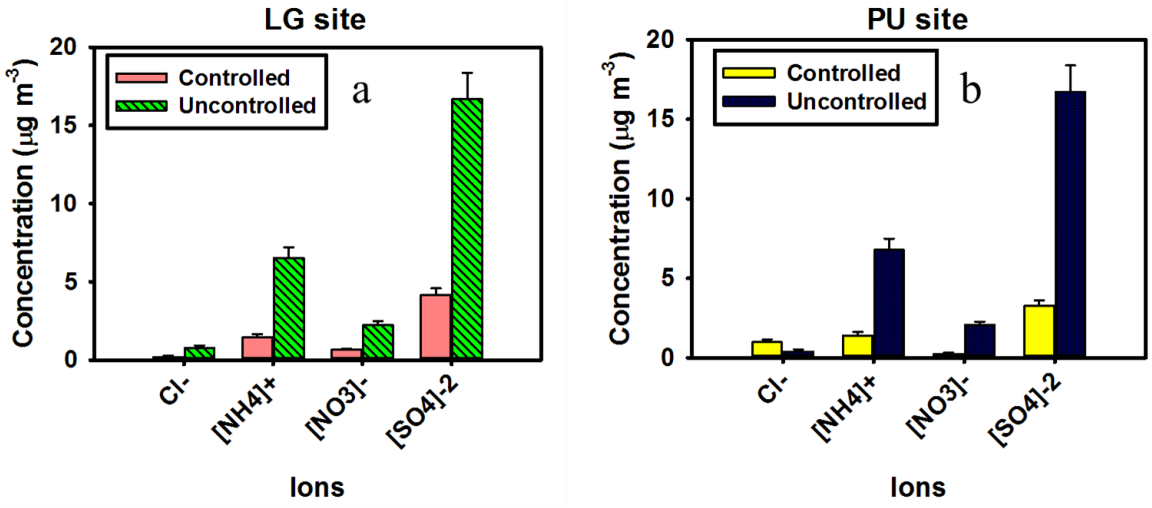

Figure 4.3: Average (µg m^{-3}) water-soluble ions observed in $PM_{2.5}$ at the LG site (a) and PU site (b) during controlled and uncontrolled periods.

4.4.2 Crustal enrichment factors

Enrichment factors (EF) are used to assess whether the elements have a major crustal component [145]. EF of the elements was calculated by first normalizing the measured elemental concentrations in the sample with aluminum (Al), and then dividing by the upper continental crust (UCC) ratio [94, 146]. EF is calculated using the following formula:

$$\mathrm{EF}_{\mathrm{element}} = \frac{(\text{Concentration of element in sample}/\ \text{Concentration of Al in sample})}{(\text{Concentration of element in crust}\ /\ \text{Concentration of Al in crust})}$$

EF is close to unity for the elements related to the reference, Al (a marker for crustal emissions). A high EF (>>10) suggests that particular elements are enriched relative to the crust and thus are anthropogenically derived [147]. The dashed line (EF = 10) on the plots shown in Figure 4.4 (a,b) represents the level above which the element is considered to have a major anthropogenic source. The error bar represents the standard deviation of the 13 samples each during the controlled and uncontrolled periods at the two sites. The dots represent the average EF of the 13 samples for each element.

As observed in Figure 4.4, almost every measured element appears to have some anthropogenic source at the LG site. Conversely, at the PU site, mainly the industrially-sourced elements have high EF. Specifically, As, Cd, Cr, Cu, Ni, Pb, Sb, Se, Pb, V, and Zn, as well as K and Na were highly enriched at the LG site during both the controlled and uncontrolled periods (Figure 4.4a).

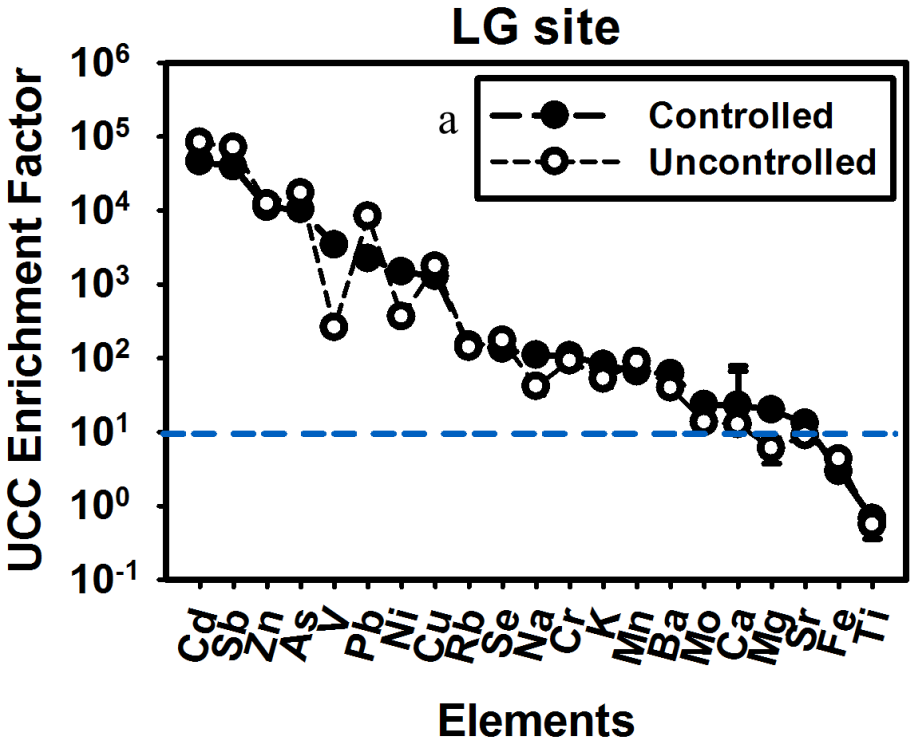

Figure 4.4 (a): Enrichment factor (EF) for $PM_{2.5}$ collected at the LG site during controlled and uncontrolled periods. The error bar represents the standard deviation of the samples.

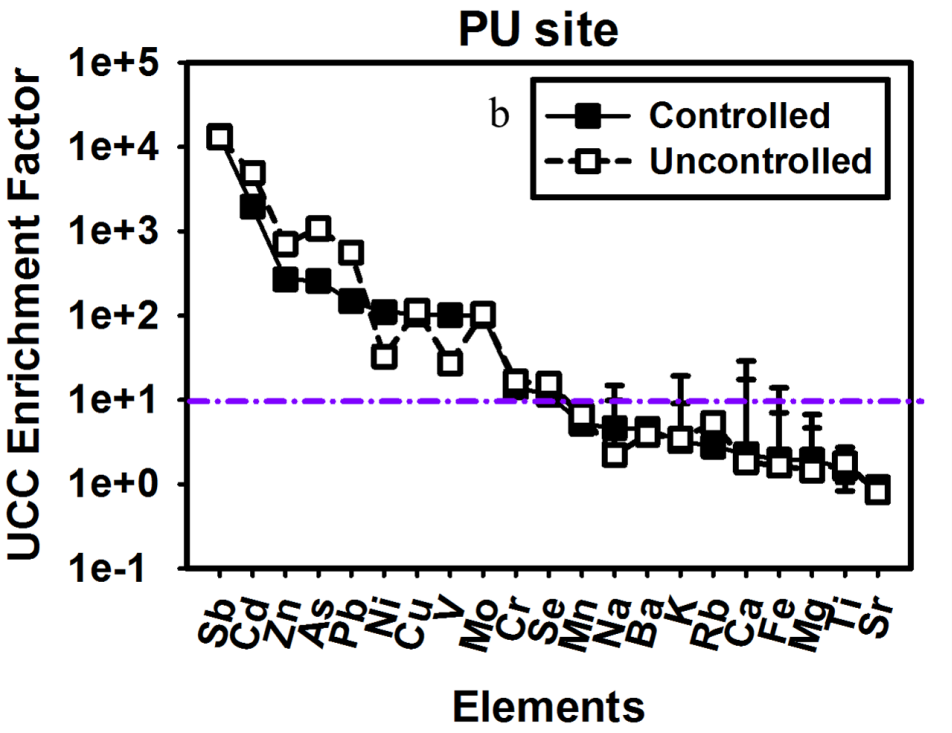

Figure 4.4 (b): Enrichment factor (EF) for $PM_{2.5}$ collected at the PU site during controlled and uncontrolled periods. The error bar represents the standard deviation of the samples.

Similarly, the elements As, Cd, Cr, Cu, Mo, Ni, Pb, Sb, Se, Pb, V, and Zn were associated with an anthropogenic source at the PU site during both the controlled and uncontrolled periods (Figure 4.4b). The fact that these elements are highly enriched is consistent with many other studies in urban areas [148, 149]. It is also important to note that, while the concentrations were increased during uncontrolled periods, the EF essentially did not change. Significant differences in EF, however, were observed between the two sites.

4.4.3 Soluble Fe oxidation state analysis

As most atmospheric Fe is crustally-derived, Fe (III) dominates the major part of total iron in the PM but its relative importance also depends on local sources and the size fraction [150]. For example, crustal Fe is primarily in the Fe (III) oxidation state and shows a solubility of <1% [151], while ambient urban Fe shows solubility ~10% – 20%, with a mixture of Fe (II) and Fe (III) [150], and Fe emitted directly from vehicles has been shown to be up to 70% water-soluble, being mostly Fe (II) sulfate [152]. Consequently, different locations exhibit different Fe solubility, depending on the dominant sources [150]. Our study shows Fe solubility of 7% and 15% during the controlled and uncontrolled periods, consistent with other urban sources. The oxidation state of the soluble Fe is shown in Figure 4.5. The majority of the soluble fraction was comprised of Fe (II) at the two sites both during controlled and uncontrolled periods. As Fe (III) is the dominant form of soluble Fe under oxidizing conditions [153], this implies that the PM contained other compounds which allowed the Fe to be stabilized in the reduced state.

Possibilities include small chain organic acids or even polycyclic aromatic hydrocarbons [154, 155, 156].

At the LG site, the percent soluble Fe (II) of total iron collected on the filter was 5.9% during controlled periods and 12.2% during uncontrolled periods. Similarly, at the PU site, the percent soluble Fe (II) of total iron collected on the filter was 5.4% during controlled periods and 12.6% during uncontrolled periods. Of the soluble Fe, Fe (II) was 82% during controlled periods and 86% during uncontrolled periods at the LG site. Similarly, at the PU site, Fe (II) was 56% of the total soluble, during controlled periods and 61% during uncontrolled periods. Significant differences in relative Fe (II)/Fe (III) solubility between the PU and LG site indicates different sources between sites. However, similarities in Fe (II)/Fe (III) solubility at each site suggest that the sources are similar during the controlled and uncontrolled periods.

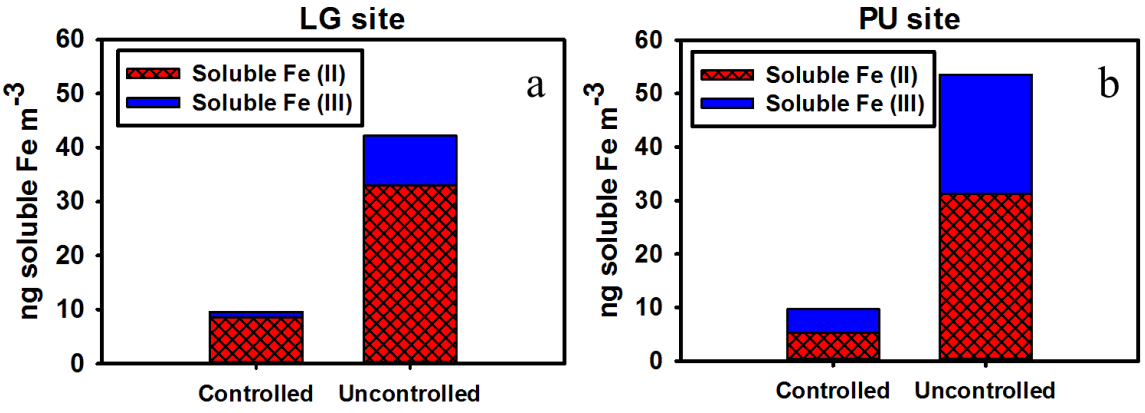

Figure 4.5: Soluble fractions of Fe (II) and Fe (III) at (a) LG site and (b) PU site.

4.4.4 Stable Pb isotope ratios

Anthropogenic activities like mining, industry, and utilization of fossil fuels and tetraethyl lead in gasoline significantly affect the Pb levels in the environment to varying degrees. In this study, the greatest differences in elemental concentrations were Pb (Figure 4.2). Thus, we focus on Pb isotope ratios to help determine if its origin was different during controlled and uncontrolled periods. Pb has four stable isotopes; ^{204}Pb, ^{206}Pb, ^{207}Pb, and ^{208}Pb with the radioactive decay of ^{238}U, ^{235}U, and ^{232}Th eventually producing ^{206}Pb, ^{207}Pb, and ^{208}Pb, respectively. Depending on the geological history, different sources of Pb possess specific Pb isotopic signatures and these ratios do not fractionate during any chemical, physical, or biological process [35]. Therefore, Pb isotopic ratios are useful in distinguishing natural Pb from anthropogenic Pb and its origin in different ecosystems [34, 35]. Stable Pb isotope ratios (^{207}Pb/^{206}Pb) in the range 0.7952–0.8405 can be used as a tracer species to identify natural sources of PM whereas, ^{207}Pb/^{206}Pb ratio in the range of 0.8504–0.9651 can be used to identify anthropogenic sources contributing to airborne PM [26, 106].

Ratios of ^{207}Pb/^{206}Pb *versus* ^{206}Pb/^{204}Pb are presented in Figure 4.6 for the airborne $PM_{2.5}$ collected at the PU and LG sites during controlled and uncontrolled periods, with these ratios depending on local geology, rainfall, wind direction, and traffic [88, 89]. The average ^{207}Pb/^{206}Pb ratios of the $PM_{2.5}$ collected at the LG site during the controlled and uncontrolled periods are 0.8599 (range, 0.8567–0.8590) and 0.8550 (range, 0.8536–0.8563), respectively.

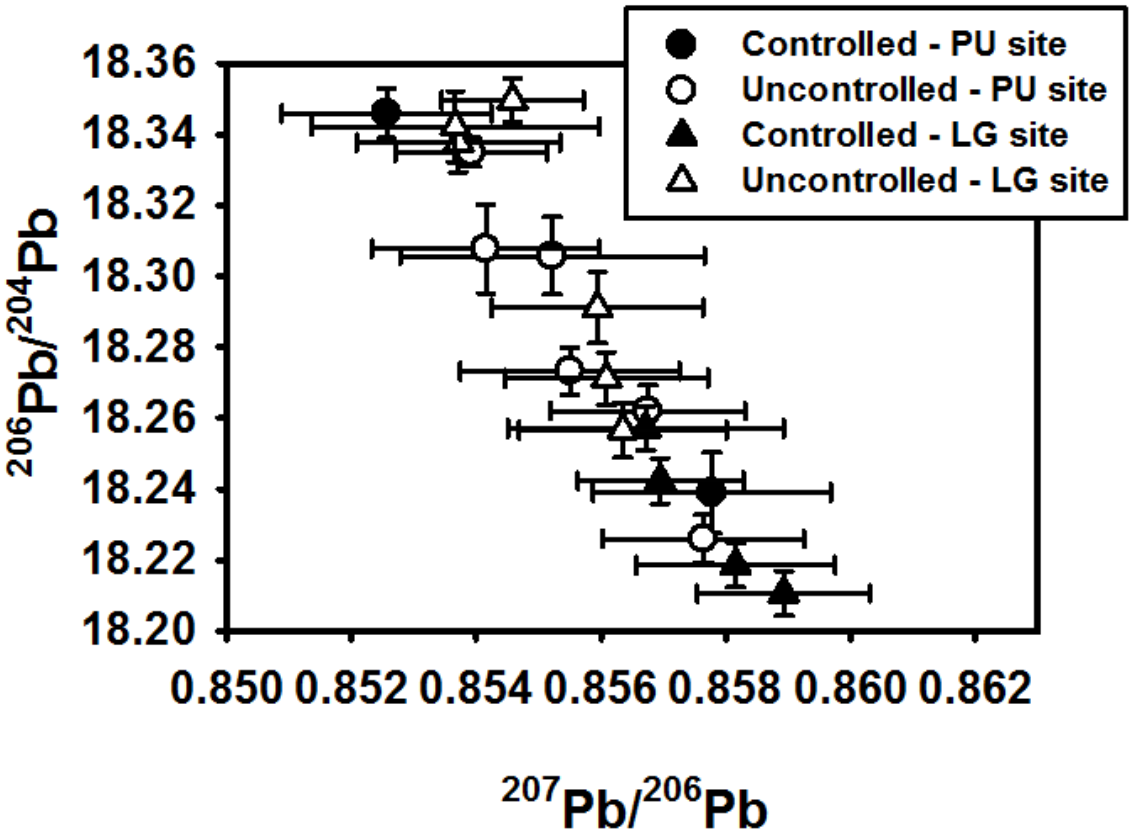

Figure 4.6: Isotopic composition of the $PM_{2.5}$ collected at LG and PU sites during controlled and uncontrolled periods. The error bars represent the standard deviation of the Pb isotopic ratios for all samples.

Similarly, at the PU site, the average $^{207}Pb/^{206}Pb$ ratios during the controlled and uncontrolled periods are 0.8564 (range, 0.8525–0.8591) and 0.8567 (range, 0.8539–0.8576), respectively. These ratios suggest that $PM_{2.5}$ has an anthropogenic Pb source [106], which is also in agreement with the high UCC EF. The $^{206}Pb/^{204}Pb$ ratios at the PU and the LG sites during the controlled and uncontrolled periods were similar (*t*-test, $p < 0.05$), indicating similar Pb sources. The $^{206}Pb/^{204}Pb$ ratios between the two sites during the controlled and uncontrolled periods were also similar (*t*-test, $p < 0.05$).

Industry emissions, coal combustion, and vehicle exhaust are considered to be the three main sources of Pb pollution in China [157, 158]. Previous studies have determined the $^{207}Pb/^{206}Pb$ ratios ranging from 0.850 to 0.872 for wide varieties of Chinese coal [90]. Leaded gasoline, which was phased out in the early 1990s [92], showed an average $^{207}Pb/^{206}Pb$ ratio of 0.901 whereas unleaded exhaust showed the ratio of 0.872 in the PRD region [159]. The average ratio of $^{206}Pb/^{204}Pb$ observed for coal combustion and cement factories in Beijing were 18.09 (range, 17.873–18.326) and 18.05 (range, 17.729–18.365), respectively [92]. There are about 26 coal power plants located in Guangdong Province, China [142]. Shenzhen is a major city in the Guangdong Province. These power plants are within 97 km of the sampling sites. A map of these power plants relative to the sampling sites is shown in Figure B1 (Appendix B). Overall, the $PM_{2.5}$ Pb ratios are similar to the Pb ratios observed for coal varieties, which implies that coal combustion may be the primary Pb source(s) between the sampling sites in this study and the previous study [90]. In addition, the Pb isotope ratios were significantly similar at

each site during both controlled and uncontrolled periods. This suggests that local and regional sources affect these two sites in a similar manner.

4.4.5 Source identification using principal component analysis

PCA was used to identify major sources of $PM_{2.5}$. The results of the PCA for the combination of the two sites during controlled periods and uncontrolled periods are presented in the Appendix B (Tables B1 and B2). There were three factors contributing to the $PM_{2.5}$ in Shenzhen during controlled periods whereas five factors were present during uncontrolled periods at the two sites. The difference in reported factors between two periods is determined on the basis of an inflection point in the scree plots and, we have selected the interpretable factors.

At the two sampling sites, during controlled periods, the first principal component has elevated loadings of Pb, Zn, K^+, Al, Na^+, Se, and OC as shown in Table B1 (Appendix B). The major sources of $PM_{2.5}$ are categorized in several groups and these are: coal combustion (Se and Pb), biomass burning (K^+ and OC), and vehicular abrasion (Zn and Sb) [112, 129, 160]. Therefore, we associate this factor with a mixture of combustion sources. We also note a potentially confounding correlation between Al and Se (r^2 = 0.858), which is present at both sites and during both the controlled and uncontrolled periods. For the second factor, characteristic values for V and Ni are the highest, which are tracers of heavy oil combustion [161]. Apart from oil-fired power plants and industries, ship emissions may be a prominent source of such combustion in Shenzhen [162]. Also, the second factor has prominent values for NH_4^+ and SO_4^{2-},

indicating the presence of secondary inorganic aerosols [163]. Sulfur dioxide would be emitted along with Ni and V during oil combustion. The third factor has high loadings of Mg^{+2}, Na^{+}, NH_4^{+} SO_4^{2-}, and Cl^{-}, signifying this source was chiefly associated with partially aged sea salt [129], which is consistent with the fact that Shenzhen is a coastal city.

Table B2 (Appendix B) represents the sources during the uncontrolled periods at the PU and LG sites. The first principal component shows high loadings of NH_4^{+}, SO_4^{2-}, and Sb, which are associated with secondary inorganic aerosols and potentially brake wear [164]. The second factor has elevated Al, Se, and K^{+}. Al is a marker of crustal emissions and Se and K^{+} are associated with coal combustion and biomass burning, respectively. Therefore, the second factor is undetermined. High values of Na^{+}, Mg^{+2}, and Cl^{-} are associated with sea salt spray for the third factor indicating that sea spray is a contributing factor to $PM_{2.5}$ in Shenzhen regardless of wind direction. The fourth factor shows high values of V and Ni, which are tracers of heavy oil combustion emissions. The fifth factor has high values of Pb and OC, which is associated with combustion emission sources containing Pb. This is consistent with the Pb isotope data that the source of Pb is similar at the two sites during controlled and uncontrolled periods.

4.5 Conclusions

The results of this study provide insights into the effects of pollution restrictions in Shenzhen, China. The average $PM_{2.5}$ concentrations at the PU and LG sites during controlled periods were lower than 24 hours mean ambient air quality standard of the

People's Republic of China of 75 μg m^{-3} [131]. Surprisingly, both Ni and V, markers for the residual oil combustion, had lower concentrations relative to other trace elements during uncontrolled periods at the two sampling sites, suggesting that oil combustion emissions were not controlled at all by the restrictions imposed during the Universiade event.

While it is possible that the soluble Fe (II)/Fe (III) ratio depends, to some extent, on the original Fe phases present in the PM, the equilibrium speciation in solution is primarily dependent on the immediate redox environment in the extract solution [153]. Thus, the presence of source-specific organic compounds [154] and ions [165] are the major determinants of Fe speciation and solubility. While this is the first study to measure Fe speciation and solubility in airborne $PM_{2.5}$ in Shenzhen, China, it possesses similarities to previous Fe speciation studies. For instance, at the PU site, soluble Fe (II) and soluble Fe (III) were approximately equal, which was similar to the percentage of soluble Fe (II) at Waukesha, WI, USA [150]. Similarly, at the LG site, soluble Fe (II) was far greater than soluble Fe (III), which was similar to the results reported for Los Angeles, CA, USA [150] and Denver, CO, USA [20].

The $^{206}Pb/^{204}Pb$ ratios measured at the two sites during the controlled and uncontrolled periods, and between the two sites during the controlled and uncontrolled periods, were similar (*t*-test, $p < 0.05$), representing a common anthropogenic Pb source. This suggests that airborne $PM_{2.5}$ is dominated by local or regional combustion sources (as evidenced by the high EF), which was in agreement with the principal component analysis.

Previous studies have presented elemental and water-soluble ion concentrations for airborne $PM_{2.5}$ in southwest China [110, 112]. The source apportionment based on positive matrix factorization (PMF) and chemical mass balances (CMB) revealed that coal combustion, secondary inorganic aerosols, biomass burning, metal industries, crustal dust, and sea spray were common sources in southwest China. The impact of control measures implemented before and during 2008 Olympics in Beijing showed 33% reduction in BC emissions [133] and controls implemented during the Universiade showed 30% reduction in traffic [132]. Although the relative importance of each component varied, the major sources at the two sites during controlled and uncontrolled periods were identified as residual oil combustion, secondary inorganic aerosols, combustion, and sea spray which is also in agreement with the previous studies.

In our study, however, every metric was consistent (e.g., Pb isotopes, PM mass trends, EC/OC trends, and individual element trends) between sites. The $PM_{2.5}$ levels in Shenzhen were mainly dominated by anthropogenic emissions. Reductions in emissions from point sources were observed, but it is unclear if this was due to the restrictions or from changes in meteorological conditions.

4.6 Acknowledgements

The authors thank Dr. Elizabeth A. Stone and Ibrahim Al-Naghemah for their help and guidance in water-soluble ion measurements. We also thank Kate Smith at the Wisconsin State Lab of Hygiene for her assistance with the Pb isotopic ratios measurement. This study was supported by the National Natural Science Foundation of

China (Grant No. 41375131 and 21307129) and the Key Research Program of Chinese Academy of Sciences (Grant No. KJZD-EW-TZ-G06-01-0). We thank the anonymous reviewers for their helpful input to improve the paper.

Chapter Five: Measurement of fine particulate matter in Northern India using trace metals and construction of a soil suspension chamber

5.1 Abstract

Fine particles ($PM_{2.5}$) were collected at two sampling sites in Northern India: Delhi and Jaipur during 2015-2016. The collected $PM_{2.5}$ was characterized using 35 trace metals. Resuspended soil dust is one of the important sources of $PM_{2.5}$ in the atmosphere. We have designed a method to measure the potential of soil to emit fugitive dust in the $PM_{2.5}$ size range.

5.2 Introduction

Air pollution is responsible for many health problems [6, 11, 166, 167]. Recently, the air pollution levels of New Delhi and other cities in India have surpassed the levels of Beijing [168]. Delhi (28^{o} 35' N; 77^{o} 12' E) is the capital of India and the third largest city with a population of 18.6 million. Delhi has a tropical, semi-arid climate with extremely hot summers (average temperature 46°C), rainfall in monsoon months (~73 cms), and cold in winter months (average temperature 5°C) [169]. The major sources of $PM_{2.5}$ pollution in Delhi are industries, power plants, vehicular emissions and dust storms from Rajasthan [169]. Jaipur (26^{o} 55' N, 75^{o} 49' E), is the capital and the largest city of

Rajasthan with a population of 3 million. Jaipur city experiences hot and arid climate with high temperatures (average temperature 42 ^{o}C), rainfall in monsoon months (~66 cms), and cold in winter months (average temperature 10 $^{\circ}$C) [170]. Previous studies have shown that high PM in Jaipur city is due to vehicular and industrial emissions, road dust, garbage burning, use of conventional fuels like wood and cow dung for cooking, and other domestic purposes [170].

$PM_{2.5}$ is used as a standard to measure air quality (AQ). According to air quality guidelines by the U.S. Environmental Protection Agency (EPA), 24 hours mean recommended concentration for $PM_{2.5}$ was 35 μg m^{-3} [171]. The air quality index (AQI) for $PM_{2.5}$ was 234 μg m^{-3} in Delhi and 200 μg m^{-3} in Jaipur, which is much higher than the recommended level [172, 173]. As a result, India has recorded the world's highest death rate because of chronic respiratory diseases and asthma than any other country [174]. Vehicular pollution is the main contributor to air pollution in Delhi and Jaipur. There are around 7.5 million cars in New Delhi alone, with 1,400 more added each day, causing major traffic congestion problems and significantly contributing to the country's pollution problems [174, 175].

Delhi and other cities have taken several steps to reduce the level of air pollution in the city during the last 10 years. Control measures so far instituted are: (i) use of unleaded petrol since 1998, (ii) reduction of sulfur content in diesel since 2000, (iii) construction of flyovers and subways for smooth traffic flow and introduction of Metro rail and compressed natural gas (CNG) for commercial transport vehicles since 2000, (iv)

odd and even vehicles on alternate days since 2015, and (v) development of clean and non-polluting industries since 2015.

Since smaller particles can be transported over hundreds and even thousands of kilometers before they reach the ground, resuspended soil dust is one of the important sources of $PM_{2.5}$ in the atmosphere. We have studied the long-range transport of dust in Chapter 3. To this end, we have constructed a soil resuspension chamber to measure the potential of soil to emit fugitive dust in the $PM_{2.5}$ size range. The present study shows the construction of the soil suspension chamber and preliminary results of the airborne $PM_{2.5}$ collected in Delhi and Jaipur.

5.3 Experimental

5.3.1 Sample collection

Airborne $PM_{2.5}$ was collected at the two sampling sites in Northern India during 2015-2016. The Delhi sampling site is located at the Indian Institute of Technology (IIT) (28.546168, 77.191111). The Jaipur sampling site is located at Malaviya National Institute of Technology (MNIT) (26.860908, 75.809175), which is about 261 km from the Delhi site.

The samples from the Delhi site were collected on 47 mm Teflon filters (Whatman Corporation, U.S.A.) for 24 hours with a flow rate of 4000 L using PEM personal environment monitor samplers (Model 200, MSP Corporation, India). The samples from Jaipur site were collected on 47 mm Teflon filters for 24 hours with a flow rate of 21 m^3 using APM550EL samplers (Envirotech Instruments Private Limited,

India). All sample preparation was performed under positive pressure HEPA filtered air. A Sartorius microbalance (CPA26P, Goettingen, Germany) was used for determination of mass (estimated total uncertainty of ± 1 μg). Prior to weighing, the filters were equilibrated in a constant humidity (50%) and temperature (25 ^{o}C) environment for 48 hours.

5.3.2 Total elemental analysis

The Teflon filters were digested in sealed, pre-cleaned Teflon digestion bombs in a 30-position microwave rotor (Milestone Ethos, U.S.A.) with a trace metal grade acid matrix (Fisher, U.S.A.) consisting of 1.5 mL of nitric acid (16 M), 750 μL of hydrochloric acid (12 M), 200 μL of hydrofluoric acid (28 M), and 200 μL of 30% hydrogen peroxide. Digestates were diluted to 15 mL with high purity water (>18 MΩcm, MQ) and elemental concentrations (Al, Ag, As, Ba, Ca, Cd, Ce, Co, Cr, Cs, Cu, Fe, K, La, Mg, Mn, Mo, Na, Nd, Ni, Pb, Pd, Rb, Sb, Sc, Se, Sm, Sn, Sr, Th, Ti, Tl, U, V, and Zn) were quantified by quadrupole inductively coupled plasma mass spectrometry (ICP-MS, Agilent 7700) with indium (In) as an internal standard. The accuracy of the results from the elemental analysis was verified by standard reference materials (SRMs). The SRMs (NIST 2709a and NIST 1649a) were digested and analyzed with every sampling site batch. The percent recovery of the reported elements from these SRMs was 80-100%. Data were also blank-corrected using a field blank collected at each sampling site.

5.3.3 Construction of soil suspension chamber

The soil was oven dried at 100 ^{o}C for 24 hours to ensure the maximum potential for the soil to emit particles. The dried soil was placed in the dust resuspension chamber (Buchner flask), which was then sealed as shown in Figure 5.1. The air was pulled through a HEPA filter with a pump resuspending soil at the bottom of a Buchner flask. The Buchner flask was fitted with tubing that connected it to a cyclone (URG Corporation, U.S.A.). A measured volume of air (42 L min^{-1}) maintained at pressure of 4.5 inches of water for 10-15 minutes was forced through the soil sample and the upward velocity of the air stream was enough to suspend dust particles of 2.5 μm aerodynamic diameter which was tested using a flow meter (Bios DryCal, Definer 220) and pressure gauge. The inches of water is a non-SI unit for pressure and is used for measuring small pressure differences across an orifice. The suspended particles were collected in a cyclone onto a single pre-cleaned 47 mm Teflon filter (Teflo, Pall-Gelman). The correlation between pressure and the flow rate is presented in Figure 5.2 (slope = 10.229, r^2 = 0.9996).

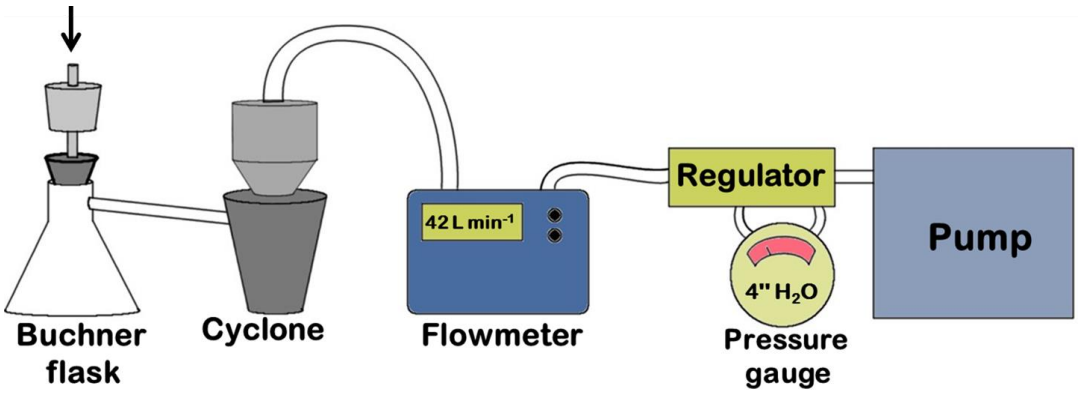

Figure 5.1: Schematic of the soil suspension and collection chamber.

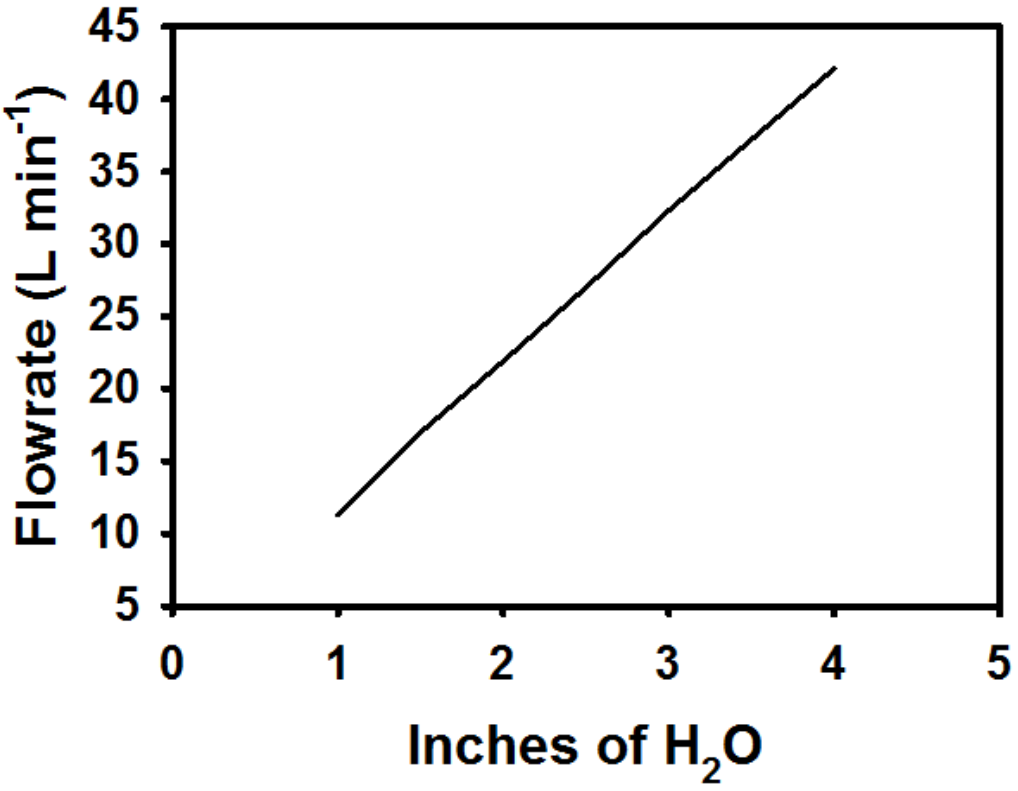

Figure 5.2: Relationship between the pressure and flow rate. An inch of water column is defined as the pressure exerted by a column of water of one inch in height at defined conditions, and is synonymous with an inch of water gauge.

5.4 Results and discussion

Previous studies measured annual average $PM_{2.5}$ mass concentrations in Delhi during 2007-2009 at IIT. The $PM_{2.5}$ concentrations ($\mu g\ m^{-3}$) were 168 ± 78 during winter, 88 ± 56 during summer, 42 ± 20 during the monsoon season, and 128 ± 86 post monsoons [169]. The $PM_{2.5}$ levels ($\mu g\ m^{-3}$) were maximum during winters (271.9) and minimum during summers (85.8) in 2014 [170]. Our study has shown significant increases in the $PM_{2.5}$ levels ($\mu g\ m^{-3}$) were observed (Delhi = 76.40 ± 25.00 and Jaipur = 44.70 ± 18.00), as shown in Table 4.

Results from our study showed an increase in concentrations of most abundant and trace elements in airborne $PM_{2.5}$ with differences observed at the two sampling sites. The elemental analysis showed that K was a dominant abundant element in Delhi whereas Ca was dominant in Jaipur air. The enormous increase in the concentration of tin (Sn) in Delhi samples relative to Jaipur samples indicates that the industrial and vehicular emissions are the main contributor of air pollution in Delhi. Overall, the $PM_{2.5}$ levels were higher in Delhi air compared to Jaipur air as shown in Table 5.1. This may be because Delhi is more populated and industrialized than Jaipur.

Table 4: Average elemental concentrations (ng m^{-3}) of airborne $PM_{2.5}$ collected in Delhi and Jaipur, cities of Northern India.

Element	Delhi samples	Jaipur samples
Na	220 ± 3	560 ± 10
Mg	245 ± 2	290 ± 10
Al	1495 ± 10	1010 ± 28
K	1802 ± 10	512 ± 10
Ca	1163 ± 16	1240 ± 35
Sc	0.56 ± 0.03	0.187 ± 0.064
Ti	1024 ± 6	500 ± 10
V	10.6 ± 0.1	3.5 ± 0.2
Cr	9.70 ± 0.08	3.0 ± 0.1
Mn	28.0 ± 0.1	15 ± 0.5
Fe	1016 ± 2	457 ± 4
Co	0.61 ± 0.01	0.289 ± 0.034
Ni	12.0 ± 0.1	4.1 ± 0.1
Cu	22.1 ± 0.1	7.0 ± 0.1
Zn	227 ± 1	320 ± 4
As	2.92 ± 0.07	1.0 ± 0.1
Se	9.8 ± 0.6	1.6 ± 0.8
Rb	3.50 ± 0.06	1.5 ± 0.1
Sr	7.3 ± 0.1	6.5 ± 0.3
Mo	1.55 ± 0.03	0.16 ± 0.02
Pd	0.51 ± 0.02	0.04 ± 0.01
Ag	0.163 ± 0.008	0.11 ± 0.03
Cd	12.0 ± 0.1	1.23 ± 0.08
Sn	391 ± 1	2.4 ± 0.2
Sb	7.60 ± 0.08	1.3 ± 0.1
Cs	0.222 ± 0.007	0.11 ± 0.01
Ba	20.0 ± 0.2	8.0 ± 0.3
La	0.84 ± 0.01	0.49 ± 0.02
Ce	1.57 ± 0.01	0.99 ± 0.03
Nd	0.72 ± 0.02	0.37 ± 0.04
Sm	0.152 ± 0.006	0.07 ± 0.01
Tl	0.469 ± 0.007	0.18 ± 0.01
Pb	91.8 ± 0.1	68 ± 1
Th	0.323 ± 0.007	0.172 ± 0.008
U	0.086 ± 0.003	0.039 ± 0.007
$PM_{2.5}$	76400 ± 25000	44700 ± 18000

5.5 Conclusions

The results presented here are preliminary. Based on preliminary results, increased levels of $PM_{2.5}$ in Delhi are because of vehicular traffic. Further studies will be done by other graduate students of the lab. Restricting heavy vehicles, periodic vehicle maintenance, and encouraging public transport instead of private vehicles are few considerations to control air pollution due to transportation. Regular monitoring for adequacy of pollution control equipments installed at various industries should be undertaken to check emissions from industrial processes. In addition to above, public awareness for environment protection should be adopted and green plantation should be encouraged. It may, thus be concluded that strict implementation of environmental regulations and adoption of adequate pollution control measures may help to decrease the pollution in the cities.

Chapter Six: Summary and future work

The determination of isotope ratios can provide valuable information in various research areas spanning from geochemistry to physiology. In environmental studies, stable Sr and Pb isotope ratios help to identify the different sources of emission and their possible geographic origins. The major driving force behind this work was to gain an understanding of source apportionment of ambient particulate matter in developing countries using Sr and Pb isotope ratios and quantitative determination of other metals as these other metals are potentially toxic and can pose health and ecological risks while providing important information about their source.

A Pb-Sr-Nd isotope tracer study of atmospheric metal pollution can be easily jeopardized due to insufficient instrument precision and the presence of significant biases, leading to incorrect conclusions. For instance, obtaining precise isotope ratios for samples with a low amount of the target element or limited sample volume is often an issue. In the study presented in Chapter 2, a novel method was developed in order to eliminate the biases and consumption of acids to obtain pure fractions of Sr and Nd for accurate isotopic ratio measurements. The developed method was successfully applied to the airborne PM_{10} collected in Kyrgyzstan (Chapter 3). Simultaneous measurements of different isotopic signals by MC-ICP-MS resulted in very precise isotope ratio values when compared to SRMs. Isobaric interferences by $^{87}Rb^{+}$ were avoided by isolation of Sr using column chemistry, whereas interference from $^{86}Kr^{+}$ was mathematically corrected

by measuring the signal intensity for $^{83}Kr^{+}$. Similarly, on Nd isotopes, isobaric interferences are caused by Sm, Ce, BaO, and BaN. Nd isotope measurements are normalized internally for instrumental mass fractionation to the $^{146}Nd/^{144}Nd$ ratio of 0.7219 using an exponential correction. An obvious extension of the use of Sr. Spec resin is to test its resistance to radiation damage for isolation of radiostrontium. The resin can also function as either a Pb-selective or tetravalent actinide (i.e., Pu (IV), Np (IV))-selective, under appropriate conditions. This versatility suggests that the Sr. Spec resins are likely to find numerous applications beyond those described in the Chapter 2.

Chapter 3 focused on tracing dust sources using stable Sr and Pb isotopes in Central Asia. The study was important because the Aral Sea is the now third largest source of mineral dust in Central Asia and the Aral Sea sediments emitted into the air may be a previously unidentified source of PM in Central Asia. Previous studies have conducted research related to the dust transport from North Africa and the Middle East to East Asia; none has studied if the Aral Sea sediments may be a previously unidentified source of PM in Central Asia. The study showed that the Sr isotopic ratios suggest dust from another region, such as from Western China, Africa, or Middle East regions, may be involved in the origin of PM_{10} in Kyrgyzstan. Also, Kyrgyzstan soils and the Aral Sea sediments have natural Pb whereas airborne PM_{10} is dominated by local anthropogenic sources and not by wind-blown dust from the Aral Sea and local soils. The potential for further work with this project lies with expanding the sample collection of airborne PM, soils, and sediments from the lakes, located in Kyrgyzstan and surrounding deserts, to determine the origin of PM in Kyrgyzstan and extent of dust transport from Central Asia.

Also, further studies are required to characterize the source of Pb in airborne PM_{10} in Kyrgyzstan.

Chapter 4 focused on airborne metal concentrations and their sources during and after pollution restrictions imposed during the 16^{th} Universiade event in Shenzhen. For the first time, we have reported Pb isotope ratios and Fe speciation studies in the region. Fe is the most abundant transition metal in the Earth's crust and in atmospheric PM. Due to its potential for oxidation and reduction, the changes in solubility of Fe affect both environment and human health. Chapter 4 focused on Fe solubilization through atmospheric transport. Previous studies have used models and measurements to understand the transport, deposition, and solubilization of Fe. Our study showed that the soluble Fe ranged from 7-15% for the total measured Fe, indicating an urban source of Fe. With this study, the understanding of this process can be updated. The study showed an overall increase in metal concentrations, except Ni and V, were observed during a post-Universiade event at both the sampling sites. The major sources for both sites were identified as residual oil combustion, secondary inorganic aerosols, sea spray, and combustion. Also, The $PM_{2.5}$ levels were severely decreased during the controlled period, but it is unclear if this was a result of the controls or a change in meteorology. Since some of the restrictions were temporary, it is important to examine changes in emissions after the Universiade event and whether these impact long-term air quality. The potential for further work with this project lies with the measurement of SO_2 with respect to the wind direction to better understand the effect of meteorology on PM in Shenzhen.

Chapter 5 is an ongoing study which focuses on the source apportionment of $PM_{2.5}$ in two urban cities (Delhi and Jaipur) of Northern India. Since Delhi pollution levels (234 μg m^{-3}) have surpassed Beijing levels (197 μg m^{-3}), it is important to elucidate the sources of emissions and dust transport from Rajasthan using stable Sr and Pb isotopes and Fe speciation. This will be the very first study to report the isotopic ratios and Fe speciation in these regions.

These studies have been able to contribute to a growing dataset about air quality in developing countries and fill knowledge gaps. Future researchers can expand on these topics and contribute to the field of environmental and ecological studies.

References

1. Sarkar, B. *Heavy metals in the environment*. Marcel Dekker: New York, 2002; p xvi, 725 p.

2. Davidson, C. I.; Phalen, R. F.; Solomon, P. A. Airborne particulate matter and human health: a review. *Aerosol Sci Tech* 2005, *39*, 737-749.

3. Connell, D. W. *Basic concepts of environmental chemistry*. 2nd ed.; CRC/Taylor & Francis: Boca Raton, FL, 2005; p 462 p.

4. Nriagu, J. O. A global assessment of natural sources of atmospheric trace metals. *Nat* 1989, *338*, 47-49.

5. Fergusson, J. E. editor, *The heavy elements: chemistry, environmental impact and health effects*. Oxford: Pergamon Press;: 1990.

6. Dockery, D. W.; Pope, C. A.; Xu, X. P.; Spengler, J. D.; Ware, J. H.; Fay, M. E.; Ferris, B. G.; Speizer, F. E. An association between air-pollution and mortality in 6 United-States cities. *New Engl J Med* 1993, *329*, 1753-1759.

7. Mortimer, K. M.; Neas, L. M.; Dockery, D. W.; Redline, S.; Tager, I. B. The effect of air pollution on inner-city children with asthma. *Eur Respir J* 2002, *19*, 699-705.

8. Pope, C. A.; Dockery, D. W. Health effects of fine particulate air pollution: lines that connect. *J Air Waste Manage* 2006, *56*, 709-742.

9. Valavanidis, A.; Fiotakis, K.; Bakeas, E.; Vlahogianni, T. Electron paramagnetic resonance study of the generation of reactive oxygen species catalysed by transition metals and quinoid redox cycling by inhalable ambient particulate matter. *Redox Rep* 2005, *10*, 37-51.

10. Hu, S.; Polidori, A.; Arhami, M.; Shafer, M. M.; Schauer, J. J.; Cho, A.; Sioutas, C. Redox activity and chemical speciation of size fractioned PM in the communities of the Los Angeles-Long Beach harbor. *Atmos Chem Phys* 2008, *8*, 6439-6451.

11. Gilmour, P. S.; Brown, D. M.; Lindsay, T. G.; Beswick, P. H.; MacNee, W.; Donaldson, K. Adverse health effects of PM(10) particles: involvement of iron in generation of hydroxyl radical. *Occup Environ Med* 1996, *53*, 817-822.

12. Chillrud, S. N.; Epstein, D.; Ross, J. M.; Sax, S. N.; Pederson, D.; Spengler, J. D.; Kinney, P. L. Elevated airborne exposures of teenagers to manganese, chromium, and iron from steel dust and New York City's subway system. *Environ Sci Technol* 2004, *38*, 732-737.

13. Chillrud, S. N.; Grass, D.; Ross, J. M.; Coulibaly, D.; Slavkovich, V.; Epstein, D.; Sax, S. N.; Pederson, D.; Johnson, D.; Spengler, J. D.; Kinney, P. L.; Simpson, H. J.; Brandt-Rauf, P. Steel dust in the New York City subway system as a source of manganese, chromium, and iron exposures for transit workers. *J Urban Health* 2005, *82*, 33-42.

14. Kam, W.; Delfino, R. J.; Schauer, J. J.; Sioutas, C. A comparative assessment of PM2.5 exposures in light-rail, subway, freeway, and surface street environments in Los Angeles and estimated lung cancer risk. *Environ Sci-Proc Imp* 2013, *15*, 234-243.

15. Ghio, A. J.; Stonehuerner, J.; Dailey, L. A.; Carter, J. D. Metals associated with both the water-soluble and insoluble fractions of an ambient air pollution particle catalyze an oxidative stress. *Inhal Toxicol* 1999, *11*, 37-49.

16. Verma, V.; Shafer, M. M.; Schauer, J. J.; Sioutas, C. Contribution of transition metals in the reactive oxygen species activity of PM emissions from retrofitted heavy-duty vehicles. *Atmos Environ* 2010, *44*, 5165-5173.

17. Johansen, A. M.; Siefert, R. L.; Hoffmann, M. R. Chemical composition of aerosols collected over the tropical North Atlantic Ocean. *J Geophys Res-Atmos* 2000, *105*, 15277-15312.

18. Halliwell, B.; Gutteridge, J. M. C. Oxygen free-radicals and iron in relation to biology and medicine - some problems and concepts. *Arch Biochem Biophys* 1986, *246*, 501-514.

19. Faiola, C.; Johansen, A. M.; Rybka, S.; Nieber, A.; Thomas, C.; Bryner, S.; Johnston, J.; Engelhard, M.; Nachimuthu, P.; Owens, K. S. Ultrafine particulate ferrous iron and anthracene associations with mitochondrial dysfunction. *Aerosol Sci Tech* 2011, *45*, 1109-1122.

20. Cartledge, B. T.; Majestic, B. J. Metal concentrations and soluble iron speciation in fine particulate matter from light rail activity in the Denver-Metropolitan area. *Atmos Pollut Res* 2015, *6*, 495-502.

21. Querol, X.; Minguillon, M. C.; Alastuey, A.; Monfort, E.; Mantilla, E.; Sanz, M. J.; Sanz, F.; Roig, A.; Renau, A.; Felis, C.; Miro, J. V.; Artinano, B. Impact of the implementation of PM abatement technology on the ambient air levels of metals in a highly industrialised area. *Atmos Environ* 2007, *41*, 1026-1040.

22. Lee, P. K. H.; Brook, J. R.; Dabek-Zlotorzynska, E.; Mabury, S. A. Identification of the major sources contributing to PM2.5 observed in Toronto. *Environ Sci Technol* 2003, *37*, 4831-4840.

23. Gotschi, T.; Hazenkamp-von Arx, M.; Heinrich, J.; Bono, R.; Burney, P.; Forsberg, B.; Jarvis, D.; Maldonado, J.; Norback, D.; Stern, W.; Sunyer, J.; Toren, K.; Verlato, G.; Villani, S.; Kunzli, N. Elemental composition and reflectance of ambient fine particles at 21 European locations. *Atmos Environ* 2005, *39*, 5947-5958.

24. Sigel, H.; Sigel, A.; Sigel, R. K. O. Metal ions in biological systems. Taylor & Francis: New York,, 1973; p volumes.

25. Uno, I.; Eguchi, K.; Yumimoto, K.; Takemura, T.; Shimizu, A.; Uematsu, M.; Liu, Z.; Wang, Z.; Hara, Y.; Sugimoto, N. Asian dust transported one full circuit around the globe. *Nat Geosci* 2009, *2*, 557-560.

26. Dewan, N.; Majestic, B. J.; Ketterer, M. E.; Miller-Schulze, J. P.; Shafer, M. M.; Schauer, J. J.; Solomon, P. A.; Artamonova, M.; Chen, B. B.; Imashev, S. A.; Carmichael, G. R. Stable isotopes of lead and strontium as tracers of sources of airborne particulate matter in Kyrgyzstan. *Atmos Environ* 2015, *120*, 438-446.

27. Schauer, J. J.; Rogge, W. F.; Hildemann, L. M.; Mazurek, M. A.; Cass, G. R.; Simoneit, B. R. T. Source apportionment of airborne particulate matter using organic compounds as tracers. *Atmos Environ* 1996, *30*, 3837–3855.

28. Wang, Y.; Hopke, P. K.; X., X.; V., R. O.; C., C. D.; Utell, M. J. Source apportionment of airborne particulate matter using inorganic and organic species as tracers. *Atmos Environ* 2012, *55*, 525-532.

29. Geagea, M. L.; Stille, P.; Gauthier-Lafaye, F.; Millet, M. Tracing of industrial aerosol sources in an urban environment using Pb, Sr, and Nd isotopes. *Environ Sci Technol* 2008, *42*, 692-698.

30. Schauer, J. J.; Majestic, B. J.; Sheesley, R. J.; Shafer, M. M.; Deminter, J. T.; Mieritz, M.; Committee, H. H. R. Improved source apportionment and speciation of low-volume particulate matter samples. *Res Rep* 2010, *153*, 3-75.

31. Belis, C. A.; Karagulian, F.; Larsen, B. R.; Hopke, P. K. Critical review and meta-analysis of ambient particulate matter source apportionment using receptor models in Europe. *Atmos Environ* 2013, *69*, 94-108.

32. Hopke, P. K.; Cohen, D. D. Application of receptor modeling methods. *Atmos Pollut Res* 2011, *2*, 122-125.

33. Fragkou, E.; Douros, I.; Moussiopoulos, N.; Belis, C. A. Current trends in the use of models for source apportionment of air pollutants in Europe. *Int J Environ Pollut* 2012, *50*, 363-375.

34. Kendall, C.; McDonnell, J. J. *Isotope tracers in catchment hydrology*. Elsevier: Amsterdam ; New York, 1998; p xxix, 839 p.

35. Dickin, A. P. *Radiogenic isotope geology*. 2nd ed.; Cambridge University Press: Cambridge, UK ; New York, 2005; p xvi, 492 p.

36. Faure, G.; Mensing, T. M. *Isotopes : principles and applications*. 3rd ed.; Wiley: Hoboken, N.J., 2005; p xxvii, 897 p.

37. Patterson, C. Age of meteorites and the earth. *Geochim Cosmochim Ac* 1956, *10*, 230-237.

38. Farmer, J. G.; Eades, L. J.; Graham, M. C.; Bacon, J. R. The changing nature of the Pb-206/Pb-207 isotopic ratio of lead in rainwater, atmospheric particulates, pine needles and leaded petrol in Scotland, 1982-1998. *J Environ Monitor* 2000, *2*, 49-57.

39. Doe, B. R. Lead isotopes. Springer-Verlag: New York, 1970.

40. Simonetti, A.; Gariepy, C.; Banic, C. M.; Tanabe, R.; Wong, H. K. Pb isotopic investigation of aircraft-sampled emissions from the Horne smelter (Rouyn, Quebec): implications for atmospheric pollution in northeastern North America. *Geochim Cosmochim Ac* 2004, *68*, 3285-3294.

41. Kylander, M. E.; Klaminder, J.; Bindler, R.; Weiss, D. J. Natural lead isotope variations in the atmosphere. *Earth Planet Sc Lett* 2010, *290*, 44-53.

42. Sturges, W. T.; Barrie, L. A. Lead-206/207 isotope ratios in the atmosphere of North-America as tracers of United-States and Canadian emissions. *Nat* 1987, *329*, 144-146.

43. Shirahata, H.; Elias, R. W.; Patterson, C. C.; Koide, M. Chronological variations in concentrations and isotopic compositions of anthropogenic atmospheric lead in sediments of a remote Subalpine Pond. *Geochim Cosmochim Ac* 1980, *44*, 149-162.

44. Townsend, A. T.; Snape, I. Multiple Pb sources in marine sediments near the Australian Antarctic station, Casey. *Sci Total Environ* 2008, *389*, 466-474.

45. Erel, Y.; Dubowski, Y.; Halicz, L.; Erez, J.; Kaufman, A. Lead concentrations and isotopic ratios in the sediments of the Sea of Galilee. *Environ Sci Technol* 2001, *35*, 292-299.

46. Wedepohl, K. H. The composition of the continental-crust. *Geochim Cosmochim Ac* 1995, *59*, 1217-1232.

47. Aberg, G. The use of natural strontium isotopes as tracers in environmental-studies. *Water Air Soil Poll* 1995, *79*, 309-322.

48. Basile, I.; Grousset, F. E.; Revel, M.; Petit, J. R.; Biscaye, P. E.; Barkov, N. I. Patagonian origin of glacial dust deposited in East Antarctica (Vostok and Dome C) during glacial stages 2, 4 and 6. *Earth Planet Sc Lett* 1997, *146*, 573-589.

49. Grousset, F. E.; Biscaye, P. E. Tracing dust sources and transport patterns using Sr, Nd and Pb isotopes. *Chem Geol* 2005, *222*, 149-167.

50. Gaiero, D. M. Dust provenance in Antarctic ice during glacial periods: from where in southern South America? *Geophys Res Lett* 2007, *34*.

51. Yang, L. Accurate and precise determination of isotopic ratios by MC-ICP-MS: a review. *Mass Spectrom Rev* 2009, *28*, 990-1011.

52. White, W. M.; Albarede, F.; Telouk, P. High-precision analysis of Pb isotope ratios by multi-collector ICP-MS. *Chem Geol* 2000, *167*, 257-270.

53. Hinners, T. A.; Hughes, R.; Outridge, P. M.; Davis, W. J.; Simon, K.; Woolard, D. R. Interlaboratory comparison of mass spectrometric methods for lead isotopes and trace elements in NIST SRM 1400 Bone Ash. *J Anal Atom Spectrom* 1998, *13*, 963-970.

54. Reuer, M. K.; Boyle, E. A.; Grant, B. C. Lead isotope analysis of marine carbonates and seawater by multiple collector ICP-MS. *Chem Geol* 2003, *200*, 137-153.

55. Urey, H. C. The thermodynamic properties of isotopic substances. *J Chem Soc* 1947, 562-581.

56. Hamelin, B.; Manhes, G.; Albarede, F.; Allegre, C. J. Precise lead isotope measurements by the double spike technique: a reconsideration. *Geochim Cosmochim Ac* 1985, *49*, 173-182.

57. Oversby, V. M.; Gast, P. W. Lead isotope compositions and uranium decay series disequilibrium in recent volcanic rocks. *Earth Planet Sc Lett* 1968, *5*, 199-206.

58. Taylor, R. N.; Ishizuka, O.; Michalik, A.; Milton, A.; Croudace, I. W. Evaluating the precision of Pb isotope measurement by mass spectrometry. *J Anal Atom Spectrom* 2015, *30*, 198-213.

59. Wasserburg, G. J.; Depaolo, D. J. Models of earth structure inferred from neodymium and strontium isotopic abundances. *P Natl Acad Sci USA* 1979, *76*, 3594-3598.

60. Bentley, R. A. Strontium isotopes from the earth to the archaeological skeleton: a review. *J Archaeol Method Th* 2006, *13*, 135-187.

61. Hamelin, B.; Grousset, F. E.; Biscaye, P. E.; Zindler, A.; Prospero, J. M. Lead isotopes in trade-wind aerosols at Barbados - the influence of European emissions over the North-Atlantic. *J Geophys Res-Oceans* 1989, *94*, 16243-16250.

62. Capo, R. C.; Stewart, B. W.; Chadwick, O. A. Strontium isotopes as tracers of ecosystem processes: theory and methods. *Geoderma* 1998, *82*, 197-225.

63. Mikova, J.; Denkova, P. Modified chromatographic separation scheme for Sr and Nd isotope analysis in geological silicate samples. *J Geosci* 2007, *52*, 221-226.

64. Aldrich, L. T.; Doak, J. B.; Davis, G. L. The use of ion exchange columns in mineral analysis for age determination. *Am J Sci* 1953, *251*, 377-387.

65. Pin, C.; Briot, D.; Bassin, C.; Poitrasson, F. Concomitant separation of strontium and samarium-neodymium for isotopic analysis in silicate samples, based on specific extraction chromatography. *Anal Chim Acta* 1994, *298*, 209-217.

66. Horwitz, E. P.; Dietz, M. L.; Fisher, D. E. Separation and preconcentration of strontium from biological, environmental, and nuclear waste samples by extraction chromatography using a crown-ether. *Anal Chem* 1991, *63*, 522-525.

67. Horwitz, E. P.; Dietz, M. L.; Chiarizia, R. The application of novel extraction chromatographic materials to the characterization of radioactive-waste solutions. *J Radioan Nucl Ch Ar* 1992, *161*, 575-583.

68. Pin, C.; Zalduegui, J. F. S. Sequential separation of light rare-earth elements, thorium and uranium by miniaturized extraction chromatography: application to isotopic analyses of silicate rocks. *Anal Chim Acta* 1997, *339*, 79-89.

69. Takahashu, T.; Hirahara, Y.; Miyazaki, T.; Vaglarov, B. S.; Chang, Q.; Kimura, J.; Tatsumi, Y. Precise determination of Sr isotope ratios in igneous rock samples and application to micro-analysis of plagioclase phenocrysts. *Earth Sc Technol* 2009, 59-64.

70. Huang, K.; Blusztajn, J.; Oppo, D. W.; Curry, W. B.; Ehrenbrink, B. P. High-precision and accurate determinations of neodymium isotopic compositions at nanogram levels in natural materials by MC-ICP-MS. *J Anal At Spectrom* 2012, *27*, 1560-1567.

71. Raczek, I.; Jochum, K. P.; Hofmann, A. W. Neodymium and strontium isotope data for USGS reference materials BCR-1, BCR-2, BHVO-1, BHVO-2, AGV-1, AGV-2F GSP-1, GSP-2 and eight MPI-DING reference glasses. *Geostandard Newslett* 2003, *27*, 173-179.

72. Potter, T. D.; Colman, B. R. *Handbook of weather, climate, and water : atmospheric chemistry, hydrology, and societal impacts*. Wiley-Interscience: Hoboken, N.J., 2003; p xxix, 966 p.

73. Solomon, P. A.; Costantini, M.; Grahame, T. J.; Gerlofs-Nijland, M. E.; Cassee, F. R.; Russell, A. G.; Brook, J. R.; Hopke, P. K.; Hidy, G.; Phalen, R. F.; Saldiva, P.; Sarnat, S. E.; Balmes, J. R.; Tager, I. B.; Ozkaynak, H.; Vedal, S.; Wierman, S. S. G.; Costa, D. L. Air pollution and health: bridging the gap from sources to health outcomes: conference summary. *Air Qual Atmos Hlth* 2012, *5*, 9-62.

74. Fischer, E. V.; Hsu, N. C.; Jaffe, D. A.; Jeong, M. J.; Gong, S. L. A decade of dust: Asian dust and springtime aerosol load in the US Pacific Northwest. *Geophys Res Lett* 2009, *36*.

75. Park, C. B.; Sugimoto, N.; Matsui, I.; Shimizu, A.; Tatarov, B.; Kamei, A.; Lee, C. H.; Uno, I.; Takemura, T.; Westphal, D. L. Long-range transport of Saharan dust to East Asia observed with Lidars. *Sola* 2005, *1*, 121-124.

76. McKendry, I. G.; Strawbridge, K. B.; O'Neill, N. T.; Macdonald, A. M.; Liu, P. S. K.; Leaitch, W. R.; Anlauf, K. G.; Jaegle, L.; Fairlie, T. D.; Westphal, D. L. Trans-Pacific transport of Saharan dust to western North America: a case study. *J Geophys Res-Atmos* 2007, *112*.

77. Lee, H. N.; Igarashi, Y.; Chiba, M.; Aoyama, M.; Hirose, K.; Tanaka, T. Global model simulations of the transport of Asian and Sahara dust: total deposition of dust mass in Japan. *Water Air Soil Poll* 2006, *169*, 137-166.

78. Mead, C.; Herckes, P.; Majestic, B. J.; Anbar, A. D. Source apportionment of aerosol iron in the marine environment using iron isotope analysis. *Geophys Res Lett* 2013, *40*, 5722-5727.

79. Swap, R.; Garstang, M.; Greco, S.; Talbot, R.; Kallberg, P. Saharan dust in the Amazon Basin. *Tellus B* 1992, *44*, 133-149.

80. Prospero, J. M. Long-range transport of mineral dust in the global atmosphere: impact of African dust on the environment of the southeastern United States. *P Natl Acad Sci USA* 1999, *96*, 3396-3403.

81. Kulkarni, S.; Sobhani, N.; Miller-Schulze, J. P.; Shafer, M. M.; Schauer, J. J.; Solomon, P. A.; Saide, P. E.; Spak, S. N.; Cheng, Y. F.; van der Gon, H. A. C. D.; Lu, Z.; Streets, D. G.; Janssens-Maenhout, G.; Wiedinmyer, C.; Lantz, J.; Artamonova, M.; Chen, B.; Imashev, S.; Sverdlik, L.; Deminter, J. T.; Adhikary, B.; D'Allura, A.; Wei, C.; Carmichael, G. R. Source sector and region contributions to BC and PM2.5 in Central Asia. *Atmos Chem Phys* 2015, *15*, 1683-1705.

82. Chen, B. B.; Sverdlik, L. G.; Imashev, S. A.; Solomon, P. A.; Lantz, J.; Schauer, J. J.; Shafer, M. M.; Artamonova, M. S.; Carmichael, G. R. Empirical relationship between particulate matter and aerosol optical depth over Northern Tien-Shan, Central Asia. *Air Qual Atmos Hlth* 2012, *6*, 385-396.

83. Chen, B. B.; Sverdlik, L.; Imashev, S. A.; Solomon, P. A.; Lantz, J.; Schauer, J. J.; Shafer, M. M.; Artamonova, A.; Carmichael, G. R. Lidar measurements of the vertical distribution of aerosol optical and physical properties over Central Asia. *Int J Atmos Sci* 2013, *2013*, 1-17.

84. Singer, A.; Zobeck, T.; Poberezsky, L.; Argaman, E. The PM10 and PM2.5 dust generation potential of soils/sediments in the Southern Aral Sea Basin, Uzbekistan. *J Arid Environ* 2003, *54*, 705-728.

85. Huang, X. T.; Oberhansli, H.; von Suchodoletz, H.; Sorrel, P. Dust deposition in the Aral Sea: implications for changes in atmospheric circulation in central Asia during the past 2000 years. *Quaternary Sci Rev* 2011, *30*, 3661-3674.

86. Friedrich, J. Uranium contamination of the Aral Sea. *J Marine Syst* 2009, *76*, 322-335.

87. Chen, J.; Li, G. J.; Yang, J. D.; Rao, W. B.; Lu, H. Y.; Balsam, W.; Sun, Y. B.; Ji, J. F. Nd and Sr isotopic characteristics of Chinese deserts: implications for the provenances of Asian dust. *Geochim Cosmochim Ac* 2007, *71*, 3904-3914.

88. Monna, F.; Lancelot, J.; Croudace, I. W.; Cundy, A. B.; Lewis, J. T. Pb isotopic composition of airborne particulate material from France and the southern United Kingdom: implications for Pb pollution sources in urban areas. *Environ Sci Technol* 1997, *31*, 2277-2286.

89. Simonetti, A.; Gariepy, C.; Carignan, J. Pb and Sr isotopic compositions of snowpack from Quebec, Canada: inferences on the sources and deposition budgets of atmospheric heavy metals. *Geochim Cosmochim Ac* 2000, *64*, 5-20.

90. Bollhofer, A.; Rosman, K. J. R. Isotopic source signatures for atmospheric lead: The Northern Hemisphere. *Geochim Cosmochim Ac* 2001, *65*, 1727-1740.

91. Veysseyre, A. M.; Bollhofer, A. F.; Rosman, K. J. R.; Ferrari, C. P.; Boutron, C. F. Tracing the origin of pollution in French Alpine snow and aerosols using lead isotopic ratios. *Environ Sci Technol* 2001, *35*, 4463-4469.

92. Widory, D.; Liu, X. D.; Dong, S. P. Isotopes as tracers of sources of lead and strontium in aerosols (TSP & PM2.5) in Beijing. *Atmos Environ* 2010, *44*, 3679-3687.

93. Miller-Schulze, J. P.; Shafer, M. M.; Schauer, J. J.; Solomon, P. A.; Lantz, J.; Artamonova, M.; Chen, B.; Imashev, S.; Sverdlik, L.; Carmichael, G. R.; Deminter, J. T. Characteristics of fine particle carbonaceous aerosol at two remote sites in Central Asia. *Atmos Environ* 2011, *45*, 6955-6964.

94. Taylor, S. R.; Mclennan, S. M. The geochemical evolution of the continental-crust. *Rev Geophys* 1995, *33*, 241-265.

95. Meyers, R. A. *Encyclopedia of environmental analysis and remediation*. Wiley: New York, 1998.

96. Zhang, X. Y.; An, Z. S.; Liu, D. S.; Chen, T.; Zhang, G. Y.; Arimoto, R.; Zhu, G. H.; Wang, X. F. Study on 3 dust storms in China - source characterization of atmospheric trace-element and transport process of mineral aerosol-particles. *Chinese Sci Bull* 1992, *37*, 940-945.

97. Lin, Y. C.; Tsai, C. J.; Wu, Y. C.; Zhang, R.; Chi, K. H.; Huang, Y. T.; Lin, S. H.; Hsu, S. C. Characteristics of trace metals in traffic-derived particles in Hsuehshan Tunnel, Taiwan: size distribution, potential source, and fingerprinting metal ratio. *Atmos Chem Phys* 2015, *15*, 4117-4130.

98. Liu, C. Q.; Masuda, A.; Okada, A.; Yabuki, S.; Fan, Z. L. Isotope geochemistry of quaternary deposits from the arid lands in Northern China. *Earth Planet Sc Lett* 1994, *127*, 25-38.

99. Jahn, B. M.; Gallet, S.; Han, J. M. Geochemistry of the Xining, Xifeng and Jixian sections, Loess Plateau of China: eolian dust provenance and paleosol evolution during the last 140 ka. *Chem Geol* 2001, *178*, 71-94.

100. Draxler, R. R.; Rolph, G. D. 2014. HYSPLIT (Hybrid Single-Particle Lagrangian Integrated Trajectory) Model via NOAA ARL READY. http://www.arl.noaa.gov/HYSPLIT.php.

101. Rolph, G. D. 2014. Real-time Environmental Applications and Display SYstem (READY). http://www.ready.noaa.gov.

102. Reheis, M. C.; Budahn, J. R.; Lamothe, P. J. Geochemical evidence for diversity of dust sources in the southwestern United States. *Geochim Cosmochim Ac* 2002, *66*, 1569-1587.

103. Hendrick, J. C. The global rare-earth cycle. *J Alloy Compd* 1995, *225*, 609-618.

104. Moreno, T.; Querol, X.; Alastuey, A.; Pey, J.; Minguillon, M. C.; Perez, N.; Bernabe, R. M.; Blanco, S.; Cardenas, B.; Gibbons, W. Lanthanoid geochemistry of urban atmospheric particulate matter. *Environ Sci Technol* 2008, *42*, 6502-6507.

105. Gueguen, F.; Stille, P.; Dietze, V.; Giere, R. Chemical and isotopic properties and origin of coarse airborne particles collected by passive samplers in industrial, urban, and rural environments. *Atmos Environ* 2012, *62*, 631-645.

106. Komerek, M.; Ettler, V.; Chrastny, V.; Mihailovic, M. Lead isotopes in environmental sciences: a review. *Environ Int* 2008, *34*, 562-577.

107. Pettke, T.; Halliday, A. N.; Hall, C. M.; Rea, D. K. Dust production and deposition in Asia and the north Pacific Ocean over the past 12 Myr. *Earth Planet Sc Lett* 2000, *178*, 397-413.

108. Ginoux, P.; Chin, M.; Tegen, I.; Prospero, J. M.; Holben, B.; Dubovik, O.; Lin, S. J. Sources and distributions of dust aerosols simulated with the GOCART model. *J Geophys Res-Atmos* 2001, *106*, 20255-20273.

109. Tanaka, T. Y.; Kurosaki, Y.; Chiba, M.; Matsumura, T.; Nagai, T.; Yamazaki, A.; Uchiyama, A.; Tsunematsu, N.; Kai, K. Possible transcontinental dust transport from North Africa and the Middle East to East Asia. *Atmos Environ* 2005, *39*, 3901-3909.

110. Hagler, G. S.; Bergin, M. H.; Salmon, L. G.; Yu, J. Z.; Wan, E. C. H.; Zheng, M.; Zeng, L. M.; Kiang, C. S.; Zhang, Y. H.; Lau, A. K. H.; Schauer, J. J. Source areas and chemical composition of fine particulate matter in the Pearl River Delta region of China. *Atmos Environ* 2006, *40*, 3802-3815.

111. Yang, F.; Tan, J.; Zhao, Q.; Du, Z.; He, K.; Ma, Y.; Duan, F.; Chen, G.; Zhao, Q. Characteristics of PM2.5 speciation in representative megacities and across China. *Atmos Chem Phys* 2011, *11*, 5207-5219.

112. Tao, J.; Gao, J.; Zhang, L.; Zhang, R.; Che, H.; Zhang, Z.; Lin, Z.; Jing, J.; Cao, J.; Hsu, S. C. PM2.5 pollution in a megacity of southwest China: source apportionment and implication. *Atmos Chem Phys* 2014, *14*, 8679-8699.

113. Englert, N. Fine particles and human health - a review of epidemiological studies. *Toxicol Lett* 2004, *149*, 235-242.

114. Charlson, R. J.; Schwartz, S. E.; Hales, J. M.; Cess, R. D.; Coakley, J. A.; Hansen, J. E.; Hofmann, D. J. Climate forcing by anthropogenic aerosols. *Sci* 1992, *255*, 423-430.

115. Lee, Y. L.; Sequeira, R. Water-soluble aerosol and visibility degradation in Hong Kong during autumn and early winter, 1998. *Environ Pollut* 2002, *116*, 225-233.

116. Deng, X. J.; Tie, X. X.; Wu, D.; Zhou, X. J.; Bi, X. Y.; Tan, H. B.; Li, F.; Hang, C. L. Long-term trend of visibility and its characterizations in the Pearl River Delta (PRD) region, China. *Atmos Environ* 2008, *42*, 1424-1435.

117. Chameides, W. L.; Yu, H.; Liu, S. C.; Bergin, M.; Zhou, X.; Mearns, L.; Wang, G.; Kiang, C. S.; Saylor, R. D.; Luo, C.; Huang, Y.; Steiner, A.; Giorgi, F. Case study of the effects of atmospheric aerosols and regional haze on agriculture: an opportunity to enhance crop yields in China through emission controls? *P Natl Acad Sci USA* 1999, *96*, 13626-13633.

118. Tsai, F. C.; Apte, M. G.; Daisey, J. M. An exploratory analysis of the relationship between mortality and the chemical composition of airborne particulate matter. *Inhal Toxicol* 2000, *12*, 121-135.

119. Verma, V.; Polidori, A.; Schauer, J. J.; Shafer, M. M.; Cassee, F. R.; Sioutas, C. Physicochemical and toxicological profiles of particulate matter in Los Angeles during the october 2007 Southern California wildfires. *Environ Sci Technol* 2009, *43*, 954-960.

120. Shi, T. M.; Schins, R. P. F.; Knaapen, A. M.; Kuhlbusch, T.; Pitz, M.; Heinrich, J.; Borm, P. J. A. Hydroxyl radical generation by electron paramagnetic resonance as a new method to monitor ambient particulate matter composition. *J Environ Monitor* 2003, *5*, 550-556.

121. Prahalad, A. K.; Soukup, J. M.; Inmon, J.; Willis, R.; Ghio, A. J.; Becker, S.; Gallagher, J. E. Ambient air particles: effects on cellular oxidant radical generation in relation to particulate elemental chemistry. *Toxicol Appl Pharm* 1999, *158*, 81-91.

122. Alloway, B. J. *Heavy metals in soils*. Blackie ; Halsted Press: Glasgow, New York, 1990; p xiii, 339 p.

123. Lee; Li, X. D.; Shi, W. Z.; Cheung, S. C.; Thornton, I. Metal contamination in urban, suburban, and country park soils of Hong Kong: a study based on GIS and multivariate statistics. *Sci Total Environ* 2006, *356*, 45-61.

124. Nriagu, J. O. A silent epidemic of environmental metal poisoning. *Environ Pollut* 1988, *50*, 139-161.

125. Bocca, B.; Alimonti, A.; Petrucci, F.; Violante, N.; Sancesario, G.; Forte, G.; Senofonte, O. Quantification of trace elements by sector field inductively coupled plasma mass spectrometry in urine, serum, blood and cerebrospinal fluid of patients with Parkinson's disease. *Spectrochim Acta B* 2004, *59*, 559-566.

126. Thompson, C. M.; Markesbery, W. R.; Ehmann, W. D.; Mao, Y. X.; Vance, D. E. Regional brain trace-element studies in Alzheimers-disease. *Neurotoxicology* 1988, *9*, 1-8.

127. Cao, J. J.; Lee, S. C.; Ho, K. F.; Zhang, X. Y.; Zou, S. C.; Fung, K.; Chow, J. C.; Watson, J. G. Characteristics of carbonaceous aerosol in Pearl River Delta Region, China during 2001 winter period. *Atmos Environ* 2003, *37*, 1451-1460.

128. Cao, J. J.; Lee, S. C.; Ho, K. F.; Zou, S. C.; Fung, K.; Li, Y.; Watson, J. G.; Chow, J. C. Spatial and seasonal variations of atmospheric organic carbon and elemental carbon in Pearl River Delta Region, China. *Atmos Environ* 2004, *38*, 4447-4456.

129. Dai, W.; Gao, J. Q.; Cao, G.; Ouyang, F. Chemical composition and source identification of PM2.5 in the suburb of Shenzhen, China. *Atmos Res* 2013, *122*, 391-400.

130. WHO air quality guidelines for particulate matter, ozone, nitrogen dioxide and sulfur dioxide http://apps.who.int/iris/bitstream/10665/69477/1/WHO_SDE_PHE_OEH_06.02_eng.pdf (accessed 10 February 2016).

131. HORIBA technical reports -the trends in environmental regulations in China. http://www.horiba.com/uploads/media/R41E_05_010_01.pdf (accessed 10 February 2016).

132. Wang, Y. Q.; Zhang, Y. X.; Zhang, Y.; Li, Z. Q.; He, L. Y.; Huang, X. F. Characterization of carbonaceous aerosols during and post-Shenzhen Universiade period. *China Environ Sci* 2014, *34*, 1622-1632.

133. Wang, X.; Westerdahl, D.; Chen, L. C.; Wu, Y.; Hao, J. M.; Pan, X. C.; Guo, X. B.; Zhang, K. M. Evaluating the air quality impacts of the 2008 Beijing Olympic Games: on-road emission factors and black carbon profiles. *Atmos Environ* 2009, *43*, 4535-4543.

134. China. http://en.wikipedia.org/wiki/China (accessed 13 April 2016).

135. Zhang, Y.; Zhang, Y.; Liu, H.; Wang, Y.; Deng, J. Design and application of a novel atmospheric particle sampler. *Environ Monitor China* 2014, *30*, 176-180.

136. NIOSH method 5040 elemental carbon (diesel particulate) NIOSH manual of analytical methods. http://www.cdc.gov/niosh/docs/2003-154/pdfs/5040.pdf (accessed 2 February).

137. Jayarathne, T.; Stockwell, C. E.; Yokelson, R. J.; Nakao, S.; Stone, E. A. Emissions of fine particle fluoride from biomass burning. *Environ Sci Technol* 2014, *48*, 12636-12644.

138. Majestic, B. J.; Schauer, J. J.; Shafer, M. M.; Turner, J. R.; Fine, P. M.; Singh, M.; Sioutas, C. Development of a wet-chemical method for the speciation of iron in atmospheric aerosols. *Environ Sci Technol* 2006, *40*, 2346-2351.

139. Stookey, L. L. Ferrozine - a new spectrophotometric reagent for iron. *Anal Chem* 1970, *42*, 779-781.

140. Schaug, J.; Rambaek, J. P.; Steinnes, E.; Henry, R. C. Multivariate-analysis of trace-element data from moss samples used to monitor atmospheric deposition. *Atmos Environ* 1990, *24*, 2625-2631.

141. Elliott, A. C.; Woodward, W. A. IBM SPSS by example: a practical guide to statistical data analysis. SAGE Publications: 2015.

142. List of major power stations in Guangdong. https://en.wikipedia.org/wiki/List_of_major_power_stations_in_Guangdong (accessed 1 March 2016).

143. Arimoto, R.; Duce, R. A.; Savoie, D. L.; Prospero, J. M.; Talbot, R.; Cullen, J. D.; Tomza, U.; Lewis, N. F.; Jay, B. J. Relationships among aerosol constituents from Asia and the North Pacific during PEM-West A. *J Geophys Res-Atmos* 1996, *101*, 2011-2023.

144. Yao, X. H.; Chan, C. K.; Fang, M.; Cadle, S.; Chan, T.; Mulawa, P.; He, K. B.; Ye, B. M. The water-soluble ionic composition of PM2.5 in Shanghai and Beijing, China. *Atmos Environ* 2002, *36*, 4223-4234.

145. Reimann, C.; De Caritat, P. Intrinsic flaws of element enrichment factors (EFs) in environmental geochemistry. *Environ Sci Technol* 2000, *34*, 5084-5091.

146. Buat-Menard, P.; Chesselet, R. Variable influence of the atmospheric flux on the trace metal chemistry of oceanic suspended matter. *Earth Planet Sci Lett* 1979, *42*, 399-411.

147. Cheung, K.; Daher, N.; Kam, W.; Shafer, M. M.; Ning, Z.; Schauer, J. J.; Sioutas, C. Spatial and temporal variation of chemical composition and mass closure of ambient coarse particulate matter (PM10-2.5) in the Los Angeles area. *Atmos Environ* 2011, *45*, 2651-2662.

148. Clements, N.; Eav, J.; Xie, M. J.; Hannigan, M. P.; Miller, S. L.; Navidi, W.; Peel, J. L.; Schauer, J. J.; Shafer, M. M.; Milford, J. B. Concentrations and source insights for trace elements in fine and coarse particulate matter. *Atmos Environ* 2014, *89*, 373-381.

149. Jiang, S. Y. N.; Yang, F. H.; Chan, K. L.; Ning, Z. Water solubility of metals in coarse PM and PM2.5 in typical urban environment in Hong Kong. *Atmos Pollut Res* 2014, *5*, 236-244.

150. Majestic, B. J.; Schauer, J. J.; Shafer, M. M. Application of synchrotron radiation for measurement of iron red-ox speciation in atmospherically processed aerosols. *Atmos Chem Phys* 2007, *7*, 2475-2487.

151. Cartledge, B. T.; Marcotte, A. R.; Herckes, P.; Anbar, A. D.; Majestic, B. J. The impact of particle size, relative humidity, and sulfur dioxide on iron solubility in simulated atmospheric marine aerosols. *Environ Sci Technol* 2015, *49*, 7179-7187.

152. Oakes, M.; Ingall, E. D.; Lai, B.; Shafer, M. M.; Hays, M. D.; Liu, Z. G.; Russell, A. G.; Weber, R. J. Iron solubility related to particle sulfur content in source emission and ambient fine particles. *Environ Sci Technol* 2012, *46*, 6637-6644.

153. Stumm, W.; Morgan, J. J. *Aquatic chemistry : an introduction emphasizing chemical equilibria in natural waters*. 2d ed.; Wiley: New York, 1981; p xiv, 780 p.

154. Pehkonen, S. O.; Siefert, R.; Erel, Y.; Webb, S.; Hoffmann, M. R. Photoreduction of iron oxyhydroxides in the presence of important atmospheric organic-compounds. *Environ Sci Technol* 1993, *27*, 2056-2062.

155. Barbas, J. T.; Sigman, M. E.; Buchanan, A. C.; Chevis, E. A. Photolysis of substituted naphthalenes on Sio2 and Al2o3. *Photochem Photobiol* 1993, *58*, 155-158.

156. Paris, R.; Desboeufs, K. V. Effect of atmospheric organic complexation on iron-bearing dust solubility. *Atmos Chem Phys* 2013, *13*, 4895-4905.

157. Chen, J. M.; Tan, M. G.; Li, Y. L.; Zhang, Y. M.; Lu, W. W.; Tong, Y. P.; Zhang, G. L.; Li, Y. A lead isotope record of shanghai atmospheric lead emissions in total suspended particles during the period of phasing out of leaded gasoline. *Atmos Environ* 2005, *39*, 1245-1253.

158. Lee, C. S. L.; Li, X. D.; Zhang, G.; Li, J.; Ding, A. J.; Wang, T. Heavy metals and Pb isotopic composition of aerosols in urban and suburban areas of Hong Kong and Guangzhou, South China - Evidence of the long-range transport of air contaminants. *Atmos Environ* 2007, *41*, 432-447.

159. Zhu, L. M.; Tang, J. W.; Lee, B.; Zhang, Y.; Zhang, F. F. Lead concentrations and isotopes in aerosols from Xiamen, China. *Mar Pollut Bull* 2010, *60*, 1946-1955.

160. Thurston, G. D.; Ito, K.; Lall, R. A source apportionment of U.S. fine particulate matter air pollution. *Atmos Environ* 2011, *45*, 3924-3936.

161. Clayton, J. L.; Koncz, I. Petroleum geochemistry of the Zala Basin, Hungary. *Aapg Bull* 1994, *78*, 1-22.

162. Mueller, D.; Uibel, S.; Takemura, M.; Klingelhoefer, D.; Groneberg, D. A. Ships, ports and particulate air pollution - an analysis of recent studies. *J Occup Med Toxicol* 2011, *6*, 1-6.

163. Zhang, R.; Jing, J.; Tao, J.; Hsu, S. C.; Wang, G.; Cao, J.; Lee, C. S. L.; Zhu, L.; Chen, Z.; Zhao, Y.; Shen, Z. Chemical characterization and source apportionment of PM2.5 in Beijing: seasonal perspective. *Atmos Chem Phys* 2013, *13*, 7053-7074.

164. Garg, B. D.; Cadle, S. H.; Mulawa, P. A.; Groblicki, P. J.; Laroo, C.; Parr, G. A. Brake wear particulate matter emissions. *Environ Sci Technol* 2000, *34*, 4463-4469.

165. Oakes, M.; Weber, R. J.; Lai, B.; Russell, A.; Ingall, E. D. Characterization of iron speciation in urban and rural single particles using XANES spectroscopy and micro X-ray fluorescence measurements: investigating the relationship between speciation and fractional iron solubility. *Atmos Chem Phys* 2012, *12*, 745-756.

166. Pope, C. A.; Dockery, D. W. Acute health-effects of Pm10 pollution on symptomatic and asymptomatic children. *Am Rev Respir Dis* 1992, *145*, 1123-1128.

167. Prophete, C.; Maciejczyk, P.; Salnikow, K.; Gould, T.; Larson, T.; Koenig, J.; Jaques, P.; Sioutas, C.; Lippmann, M.; Cohen, M. Effects of select PM-associated metals on alveolar macrophage phosphorylated ERK1 and-2 and iNOS expression during ongoing alteration in iron homeostasis. *J Toxicol Environ Hlth* 2006, *69*, 935-951.

168. Aisch, G.; Fairfield, H. Delhi's air is often more polluted than Beijing's. http://www.nytimes.com/interactive/2015/02/05/world/asia/delhis-air-more-polluted-than-beijings.html (accessed 16 June 2016).

169. Chelani, A. B. Statistical characteristics of ambient PM2.5 concentration at a traffic site in Delhi: source identification using persistence analysis and nonparametric wind regression. *Aerosol Air Qual Res* 2013, *13*, 1768–1778.

170. Kumar, S. S.; Sharma, K. Ambient air quality status of Jaipur city, Rajasthan, India. *Int Res J Environment Sci* 2016, *5*, 43-48.

171. EPA The National Ambient Air Quality Standards for Particle Pollution https://www3.epa.gov/airquality/particlepollution/2012/decfsstandards.pdf (accessed 16 June 2016).

172. Air pollution in India: real-time air quality index visual map. http://aqicn.org/city/delhi/dwarka/ (accessed 16 June 2016).

173. Central Pollution Control Board (CPCB): National air quality index. http://164.100.160.234:9000/ (accessed 16 June 2016).

174. Rizwan, S. A.; Nongkynrih, B.; Gupta, S. K. Air pollution in Delhi: its magnitude and effects on health. *Indian J Community Med* 2013, *38*, 4-8.

175. Kumar, A.; Anand, S. Status of vehicular pollution in NCT of Delhi. *Int J Adv Res Manage Social Sci* 2012, *1*, 85-100.

Appendix A

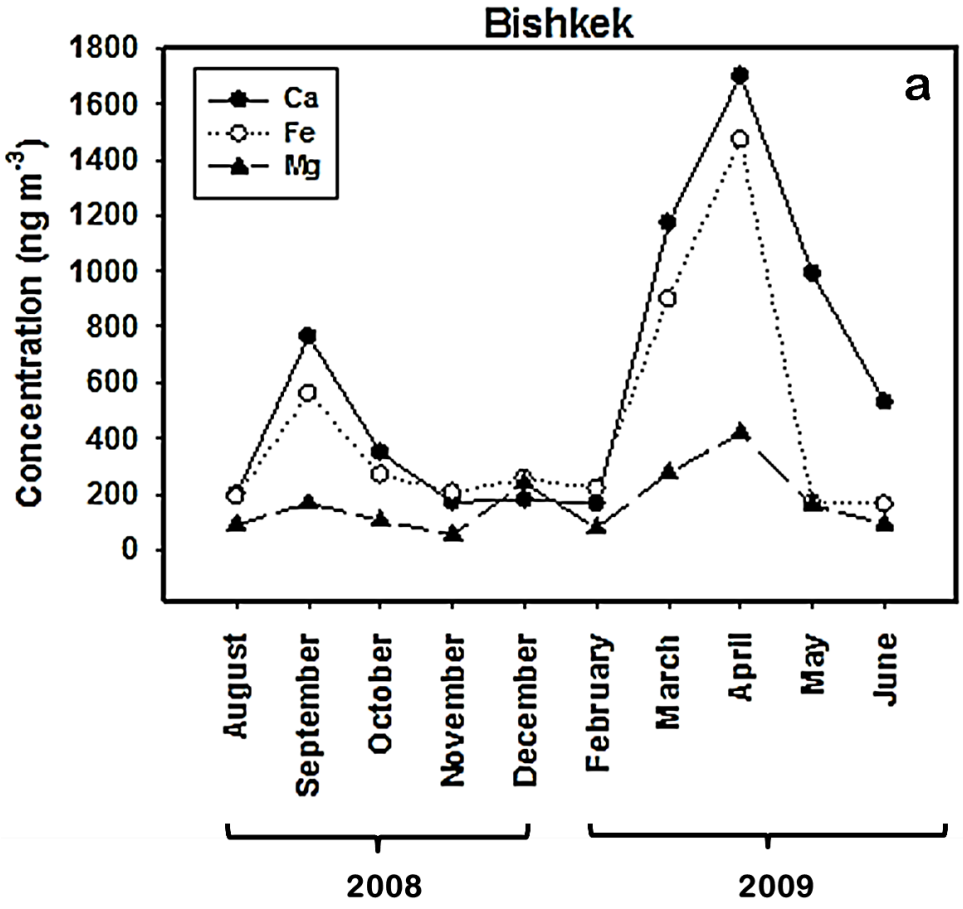

Figure A1 (a): Variation by month of selected PM_{10} elements during dust events at the Bishkek site.

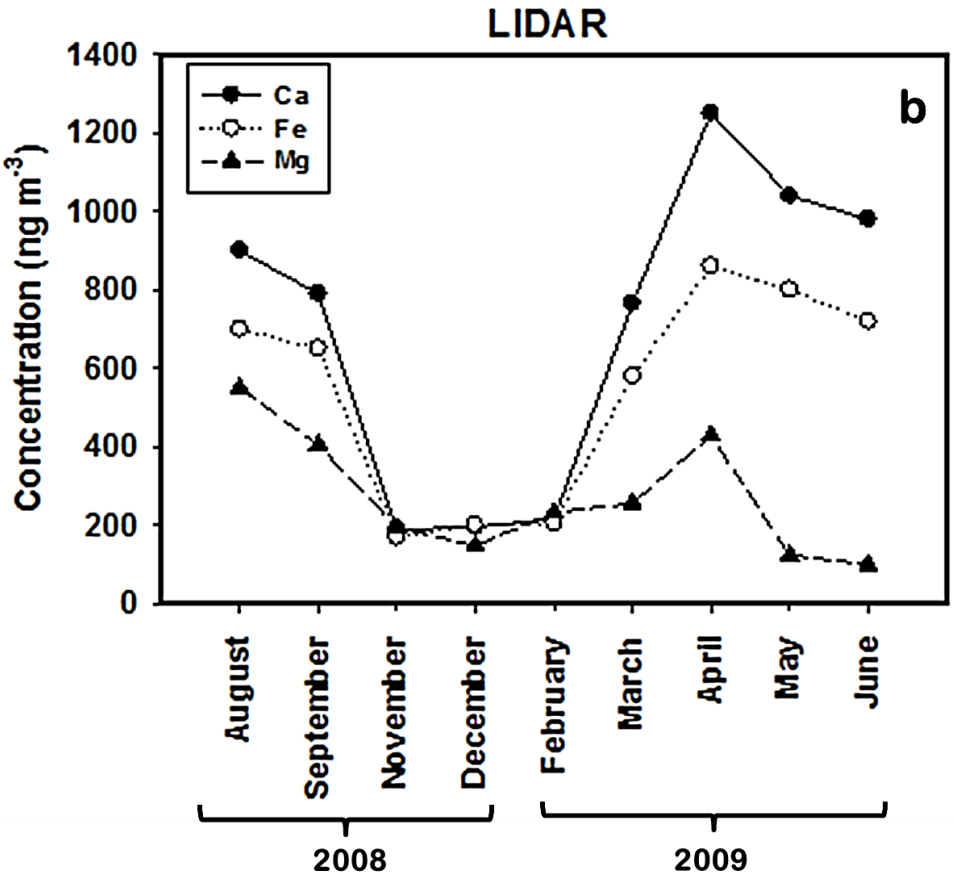

Figure A1 (b): Variation by month of selected PM_{10} elements during dust events at the LIDAR site.

Appendix B

Figure B1: Map showing the location of the PU and LG sampling sites in Shenzhen (shown as red stars) relative to the location of power plants in Guangdong Province, China.

Table B1: Principal component loadings of selected elements and ions for PU and LG sites in Shenzhen during controlled periods.

Element	PC1: Combustion source	PC2: Residual Oil Combustion & Secondary Aerosols	PC3: Sea Spray
Fe	*0.574*	-	-0.415
Pb	**0.905**	-	-
Zn	**0.929**	-	-
Sb	-	-0.229	-
OC	*0.567*	0.641	-
K^+	**0.882**	-	0.339
Al	*0.747*	0.314	-
NH_4^+	-	*0.737*	*0.556*
SO_4^{2-}	0.224	*0.675*	*0.651*
Cl^-	-	-	*0.627*
V	-	**0.924**	-
Ni	-	**0.925**	-
Na^+	*0.620*	-	*0.664*
Se	*0.714*	0.309	-
Mg^{+2}	-	-	**0.887**
Eigen Value	4.68	3.47	2.30
% of Variance	31	23	15

Note: Variables with loading factors above 0.8 are in bold font and variables with loading factors between 0.5 and 0.7 are underlined and italicized. Blank values indicate loading factors <0.200.

Table B2: Principal component loadings of selected elements and ions for PU and LG sites in Shenzhen during uncontrolled periods.

Element	PC1: Secondary Aerosols	PC2: Undetermined	PC3: Sea Spray	PC4: Residual Oil Combustion	PC5: Combustion Emission
Pb	-	0.384	-	-	**0.810**
OC	0.232	-	-	-	**0.868**
Se	-	**0.862**	-	-0.255	0.228
Cl^-	-	-	*0.750*	0.288	0.374
Mg^{+2}	-0.274	-0.454	*0.722*	-	-
Zn	-	-	-	-	-
Fe	0.443	-	-	-	-
Al	-	**0.909**	-	-	-
K^+	*0.699*	*0.583*	0.217	-	-
NH_4^+	**0.908**	-	-	-	-
SO_4^{2-}	**0.899**	-	-	-	0.205
Sb	*0.794*	-0.380	-	-	-
Na^+	0.233	0.436	**0.807**	-	-
V	-	-0.319	-	**0.836**	-
Ni	-	-	-	**0.927**	-
Eigen value	3.17	2.81	1.85	1.84	1.73
% of Variance	21	19	12	12	11

Note: Variables with loading factors above 0.8 are in bold font and variables with loading factors between 0.5 and 0.7 are underlined and italicized. Blank values indicate loading factors <0.200.